Prediction and Prevention of Tripped Rollovers

Final Report

Prepared by:

Gridsada Phanomchoeng
Rajesh Rajamani

Department of Mechanical Engineering
University of Minnesota

CTS 12-33

Technical Report Documentation Page

1. Report No.	2.	3. Recipients Accession No.	
CTS 12-33			
4. Title and Subtitle Prediction and Prevention of Tripped Rollovers		5. Report Date December 2012 6.	
7. Author(s) Gridsada Phanomchoeng and Rajesh Rajamani		8. Performing Organization Report No.	
9. Performing Organization Name and Address Department of Mechanical Engineering University of Minnesota 111 Church Street SE Minneapolis, MN 55455		10. Project/Task/Work Unit No. CTS Project #2011019 11. Contract (C) or Grant (G) No.	
12. Sponsoring Organization Name and Address Intelligent Transportation Systems Institute Center for Transportation Studies University of Minnesota 200 Transportation and Safety Building 511 Washington Ave. SE Minneapolis, MN 55455		13. Type of Report and Period Covered Final Report 14. Sponsoring Agency Code	
15. Supplementary Notes http://www.its.umn.edu/Publications/ResearchReports/			

16. Abstract (Limit: 250 words)

Vehicle rollovers account for a significant fraction of highway traffic fatalities, causing more than 10,000 deaths in the U.S. each year. While active rollover prevention systems have been developed by several automotive manufacturers, the currently available systems address only untripped rollovers. This project focuses on the development of a new real-time rollover index that can detect both tripped and un-tripped rollovers.

A new methodology is developed for estimation of unknown inputs in a class of nonlinear dynamic systems. The methodology is based on nonlinear observer design and dynamic model inversion to compute the unknown inputs from output measurements. The developed approach can enable observer design for a large class of differentiable nonlinear systems with a globally (or locally) bounded Jacobian.

The developed nonlinear observer is then applied for rollover index estimation. The rollover index estimation algorithm is evaluated through simulations with an industry standard software, CARSIM, and with experimental tests on a $1/8^{th}$ scaled vehicle. The simulation and experimental results show that the developed nonlinear observer can reliably estimate vehicle states, unknown normal tire forces, and rollover index for predicting both un-tripped and tripped rollovers. The final chapter of this report evaluates the feasibility of rollover prevention for tripped rollovers using currently available actuation systems on passenger sedans.

17. Document Analysis/Descriptors	18. Availability Statement		
Rollover accidents, Rolling, Estimation theory, Nonlinear systems	No restrictions. Document available from: National Technical Information Services, Alexandria, Virginia 22312		
19. Security Class (this report) Unclassified	20. Security Class (this page) Unclassified	21. No. of Pages 95	22. Price

Prediction and Prevention of Tripped Rollovers

Final Report

Prepared by:

Gridsada Phanomchoeng
Rajesh Rajamani

Department of Mechanical Engineering
University of Minnesota

December 2012

Published by:

Intelligent Transportation Systems Institute
Center for Transportation Studies
University of Minnesota
200 Transportation and Safety Building
511 Washington Ave. S.E.
Minneapolis, Minnesota 55455

Acknowledgments

The authors wish to acknowledge those who made this research possible. The study was funded by the Intelligent Transportation Systems (ITS) Institute, a program of the University of Minnesota's Center for Transportation Studies (CTS). Financial support was provided by the United States Department of Transportation's Research and Innovative Technologies Administration (RITA).

Table of Contents

List of Figures

List of Tables

Executive Summary

Vehicle rollovers account for a significant fraction of highway traffic fatalities, causing more than 10,000 deaths in the U.S. each year. An active rollover prevention system is a vehicle stability control system that prevents rollovers. In such systems, reliable detection of the danger of an impending rollover is necessary. A rollover index is a real-time indicator used for this purpose. A traditional rollover index can detect only untripped rollovers that happen due to high lateral acceleration from sharp turns. It cannot detect tripped rollovers that happen due to tripping from external inputs such as forces when a vehicle strikes a curb or a road bump.

While active rollover prevention systems have been developed by several automotive manufacturers, the currently available systems address only untripped rollovers. This project focuses on the development of a new rollover index that can detect both tripped and untripped rollovers.

A methodology is developed for estimation of unknown inputs in a class of nonlinear systems. The methodology is based on nonlinear observer design and dynamic model inversion to compute the unknown inputs from output measurements. The observer design utilizes the mean value theorem to express the nonlinear estimation error dynamics as a convex combination of known matrices with time varying coefficients. The observer gains are then obtained by solving linear matrix inequalities (LMIs). The developed approach can enable observer design for a large class of differentiable nonlinear systems with a globally (or locally) bounded Jacobian.

The developed nonlinear observer is then applied for rollover index estimation. The rollover index estimation algorithm is evaluated through simulations with an industry standard software, CARSIM, and with experimental tests on a $1/8^{th}$ scaled vehicle. In order to verify that the scaled vehicle experiments can represent a full-sized vehicle, the Buckingham π theorem is used to show dynamic similarity. The simulation and experimental results show that the developed nonlinear observer can reliably estimate vehicle states, unknown normal tire forces, and rollover index for predicting both un-tripped and tripped rollovers.

The final chapter of this report evaluates the feasibility of rollover prevention for tripped rollovers using currently available actuation systems on passenger sedans. Active brake torque distribution and semi-active suspensions are evaluated for their ability to prevent tripped rollovers using the rollover index estimation algorithm developed in this project. Simulations with CARSIM show that the rollover index can play a key role in preventing a rollover with both the brake torque control and semi-active suspension actuation systems.

Chapter 1. Introduction

1.1. Active Rollover Prevention

Rollovers occur in one of two ways, namely tripped or un-tripped [1]. The two types of rollovers are shown in Figure 1.1. A tripped rollover happens due to tripping from external inputs. An example of this rollover happens when a vehicle leaves the roadway and slides sideways, digging its tires into soft soil or striking an object such as a curb or guardrail. On the other hand, an un-tripped rollover happens due to high lateral acceleration from a sharp turn and not due to external tripping. An example of un-tripped rollover is when a vehicle makes a collision avoidance maneuver or a cornering maneuver with high speed.

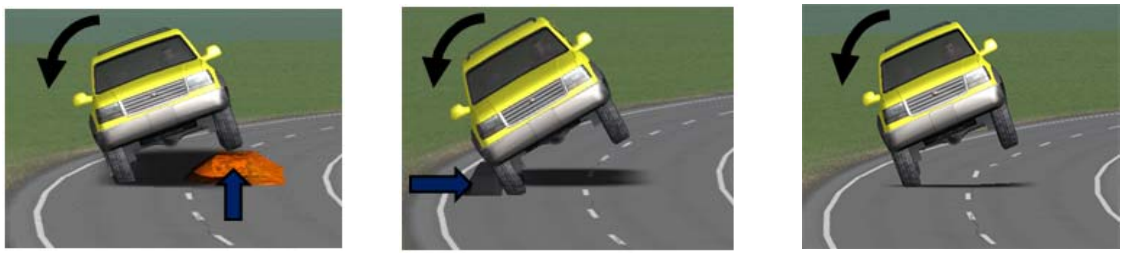

Rollover from vertical inputs Roll from lateral inputs

a) Tripped Rollover b) Un-Tripped Rollover

Figure 1.1: Types of Rollovers

Rollover accidents are dangerous. According to NHTSA's records (http://www.safercar.gov), although there were nearly 11 million crashes in 2002, only 3% involved a rollover. However, there were more than 10,000 deaths in rollover crashes in 2002. Thus, rollovers caused nearly 33% of all deaths from passenger vehicle crashes. In addition, NHTSA data also shows that 95% of single-vehicle rollovers are tripped while un-tripped rollover occurs less than 5% of the time.

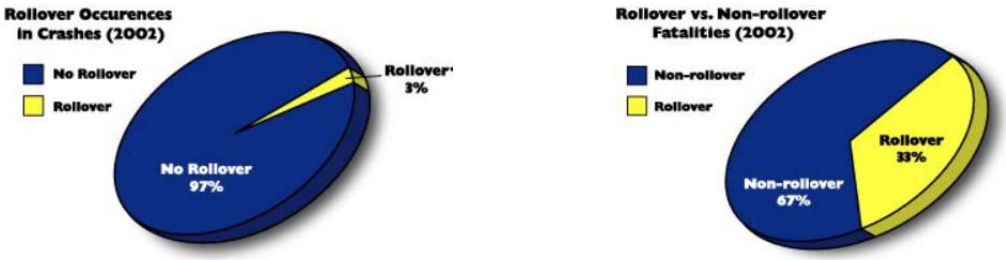

Figure 1.2: NHTSA Rollover Record (http://www.safercar.gov)

Several types of actuation systems can be used for rollover prevention. The differential braking system has received the most attention from researchers. It is used to prevent rollovers by reducing the yaw rate of the vehicle and the speed of the vehicle. By reducing yaw rate and speed, the vehicle propensity to rollover is reduced. Also, steer-by-wire systems and active suspensions can potentially be used to prevent rollovers.

Active rollover prevention systems have already by developed by several automotive manufacturers and are based on modifications of the electronic stability control systems. These

systems utilize lateral accelerometers to detect rollover and can detect and prevent only untripped rollovers [2]. There are no assistance systems available to prevent tripped rollovers.

1.2. Rollover Index and Unknown Disturbance Inputs for Tripped Rollovers

The quick detection of the danger of a vehicle rollover is necessary for initiating a rollover prevention action. To detect vehicle rollover, the concept of a static rollover threshold or the static stability factor (SSF) [3] was studied and used first, but it is not effective for dynamic situations. After that the concept of a rollover index was introduced. Rollover Index is a real time variable used to detect wheel lift off conditions. Many researchers have tried to develop a rollover index to more accurately predict vehicle rollover for un-tripped rollovers. Reference [4] has used the concept of a rollover index based on Time-To-Rollover (TTR) to estimate the time until rollover occurs. References [2], [5], and [6] have described a rollover index using a model-based roll angle estimator. Reference [7] has combined a rollover index with influential factors such as the vehicle's center of gravity and energy of rollover. Even though there are many types of rollover indices, they are derived from the same basic model as shown in Figure 1.3. The basic concept of the rollover index is described by equation (1.1):

$$R = \frac{F_{zr} - F_{zl}}{F_{zr} + F_{zl}}, \quad -1 \le R \le 1 \tag{1.1}$$

where F_{zr} and F_{zl} are the right and left vertical tire force of the vehicle respectively, m_u is unsprung mass, m_s is spung mass, a_y is lateral acceleration, ϕ is roll angle, and $\dot{\phi}$ is roll rate. A vehicle is considered to roll over when R equals 1 or -1. This is when wheel lift-off occurs. For example, when $F_{zl} = 0$, $R = 1$ and the left wheels lift off. Likewise, when $F_{zr} = 0$, $R = -1$ and the right wheels lift off. It should be noted that when a vehicle is traveling straight, F_{zr} equals to F_{zl} and $R = 0$ [22].

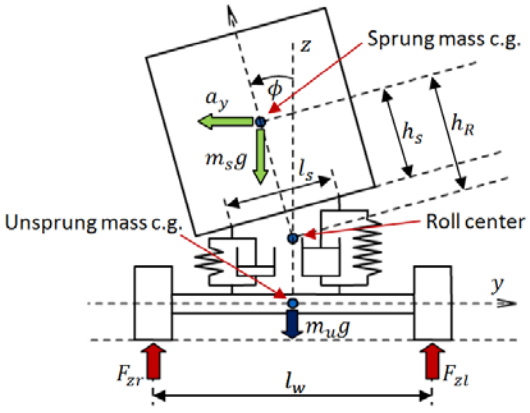

Figure 1.3: Un-Tripped Rollover Model

The definition of R in equation (1.1) cannot be implemented in real-time because the vertical tire forces F_{zr} and F_{zl} cannot be measured. Using the 1-degree of freedom model in Figure 1.3, the summation and difference of tire forces $F_{zr} + F_{zl}$ and $F_{zr} - F_{zl}$ can be estimated for the untripped scenario. An implementable version of the rollover index R can then be calculated in

terms of ϕ and a_y. Such an example of a traditional rollover index calculated using a one degree of freedom is shown below in equation (1.2) [22]:

$$R = \frac{F_{zr} - F_{zl}}{F_{zr} - F_{zl}} = \frac{2m_s a_y h_R}{mgl_w} + \frac{2m_s h_R tan\phi}{ml_w} \tag{1.2}$$

where $m = m_s + m_u$, h_R is c.g. height, m_u is unsprung mass, m_s is spung mass, a_y is lateral acceleration, and ϕ is roll angle.

This type of rollover index is used for detection un-tripped rollovers only. It is a function of lateral acceleration and roll angle as shown in equation (1.2). Some papers have proposed a modification of the above rollover index that uses only lateral acceleration [8], [9], since roll angle is expensive to measure. The stability control with this rollover index may arbitrarily reduce lateral acceleration capability of the vehicle. Also, it still fails to detect rollovers when rollovers are induced by vertical road inputs or other external inputs.

In order to detect tripped rollovers, which happens due to tripping from external inputs, a new rollover index should include the influence of road and other external inputs. Figure 1.4 shows a vehicle rollover model that includes the influence of road inputs, z_{rr} and z_{rl}, and an unknown lateral force input, F_{lat}, at an arbitrary height, h_{lat}, from the roll center. The figure also shows the normal forces on the tires, F_{zr} and F_{zl}.

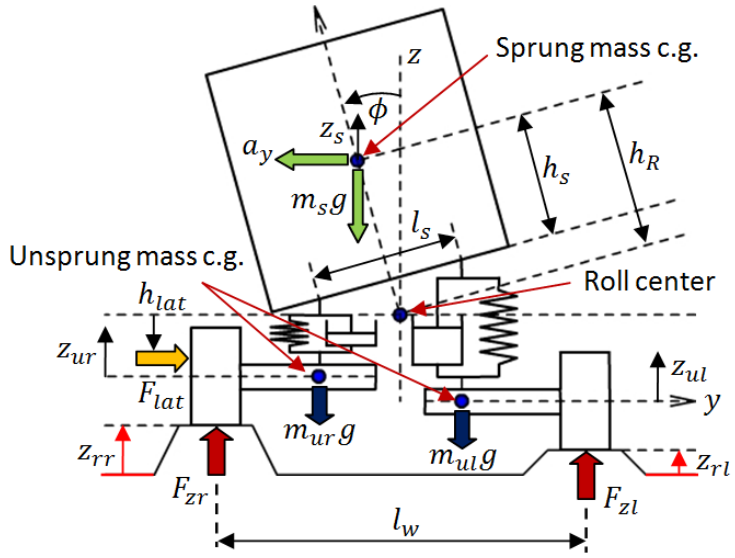

Figure 1.4: Un-Tripped and Tripped Rollover Model

To derive a rollover index in this case, multi-degrees of freedom in the model are needed. When the influence of road inputs is included, the suspension forces are defined by

$$F_{sr} = -k\left(z_s - \frac{l_s}{2}sin\phi - z_{ur}\right) - d\left(\dot{z}_s - \frac{l_s}{2}\dot{\phi}cos\phi - \dot{z}_{ur}\right), \tag{1.3}$$

$$F_{sl} = -k\left(z_s + \frac{l_s}{2}sin\phi - z_{ul}\right) - d\left(\dot{z}_s + \frac{l_s}{2}\dot{\phi}cos\phi - \dot{z}_{ul}\right) \tag{1.4}$$

where k is suspension stiffness, d is suspension damping, z_{ur} and z_{ul} are left and right unsprung mass positions, and z_s is sprung mass position. z_s includes the static displacement due to weight and the vertical displacements due to road inputs.

The difference and the summation of F_{sr} and F_{sl} are given by

$$F_{sr} - F_{sl} = kl_s sin\phi + dl_s\dot{\phi}cos\phi + k(z_{ur} - z_{ul}) + d(\dot{z}_{ur} - \dot{z}_{ul}), \tag{1.5}$$

$$F_{sr} + F_{sl} = -2kz_s - 2d\dot{z}_s + k(z_{ur} + z_{ul}) + d(\dot{z}_{ur} + \dot{z}_{ul}). \tag{1.6}$$

With moment balance at the roll center, $F_{zr} - F_{zl}$ is given by

$$F_{zr} - F_{zl} = \frac{l_s}{l_w}(F_{sr} - F_{sl}) + \frac{2}{l_w}F_{lat}h_{lat} \tag{1.7}$$

Also, vertical force balance yields

$$\begin{gathered} F_{zr} + F_{zl} = mg + F_{sr} + F_{sl} \\ F_{zr} + F_{zl} = mg - 2kz_s - 2d\dot{z}_s + k(z_{ur} + z_{ul}) + d(\dot{z}_{ur} + \dot{z}_{ul}) \end{gathered} \tag{1.8}$$

Therefore, an example of the rollover index for tripped rollovers computed directly from the model of Figure 1.4 is given by

$$\begin{aligned} R = \frac{F_{zr} - F_{zl}}{F_{zr} + F_{zl}} = \frac{l_s}{l_w}\frac{kl_s sin\phi + dl_s\dot{\phi}cos\phi + k(z_{ur} - z_{ul}) + d(\dot{z}_{ur} - \dot{z}_{ul})}{(mg - 2kz_s - 2d\dot{z}_s + k(z_{ur} + z_{ul}) + d(\dot{z}_{ur} + \dot{z}_{ul}))} \\ + \frac{2}{l_w}\frac{F_{lat}h_{lat}}{(mg - 2kz_s - 2d\dot{z}_s + k(z_{ur} + z_{ul}) + d(\dot{z}_{ur} + \dot{z}_{ul}))} \end{aligned} \tag{1.9}$$

where left and right unsprung mass positions, z_{ur} and z_{ul}, depend on road inputs, z_{rr} and z_{rl}. The equations of motion of z_{ur} and z_{ul} are given by

$$m_{ur}\ddot{z}_{ur} = -F_{sr} + k_t(z_{ur} - z_{rr}) - m_{ur}g, \tag{1.10}$$

$$m_{ul}\ddot{z}_{ul} = -F_{sl} + k_t(z_{ul} - z_{rl}) - m_{ul}g \tag{1.11}$$

where k_t is the vertical tire stiffness, m_{ur} and m_{ul} are right unsprung mass and left unsprung mass, respectively.

In order to compute the rollover index in equation (1.9), many variables need to be measured. However, some variables such as unknown road inputs, vertical displacements of unsprung masses and sprung mass, and the unknown lateral force input cannot be directly measured by

sensors. Therefore, it is necessary to develop an approach for estimating the new rollover index without knowing these variables.

1.3. Tripped Rollover Index Estimation

In order to predict tripped and un-tripped rollovers as described in section 1.2, many variables need to be measured. However, some variables such as unknown road inputs, vertical displacements of unsprung masses and sprung mass, and the unknown lateral force input cannot be directly measured by sensors. Therefore, algorithms to estimate the rollover index for tripped and un-tripped rollovers are developed.

Two different algorithms are considered in this project based on the types of sensors available:

1) Using accelerometers, gyroscope, and suspension compression measurement
2) Using accelerometers, and roll angle measurement

The first algorithm is based on an approach to estimate unknown disturbance inputs in a nonlinear system using dynamic model inversion and a modified version of the mean value theorem. In this case, the vehicle dynamics involve both complex nonlinearities and unknown disturbance inputs. The dynamics of a vehicle in this case can be written into the state space form shown in equation (1.12).

$$\begin{aligned} \dot{x} &= \bar{A}x + \eta(x,u) + \bar{B}\mu, \\ z &= \bar{E}x, \\ y &= Cx + \Psi(x) \end{aligned} \tag{1.12}$$

where $u \in R^P$ are the known control inputs, $\mu \in R^P$ are the unknown inputs, $y \in R^m$ and $z \in R^q$ are the output measurements. $\bar{A} \in R^{n\times n}$, $\bar{B} \in R^{n\times p}$, $\bar{E} \in R^{q\times n}$, and $C \in R^{m\times n}$ are appropriate matrices. The functions $\eta(x,u)$: $R^n \times R^p \to R^n$,and $\Psi(x)$: $R^n \to R^m$ are nonlinear.

To deal with this type of system, a new unknown inputs nonlinear observer to estimate both unknown disturbance inputs and state variables has been developed. The developed observer design for this problem is presented in chapters 2, 3 and 4. Then, the application of the unknown inputs nonlinear observer for rollover prevention and corresponding experimental results will be presented in chapter 5.

The second algorithm relies on an algebraic formulation of the new rollover index. The new rollover index utilizes roll angle measurement and vertical accelerometers in addition to a lateral accelerometer and is able to predict rollover in spite of unknown external inputs acting on the system. The details of this new rollover index are also presented in chapter 5.

Chapter 6 of the report focuses on showing the feasibility of rollover prevention using the developed rollover prediction algorithm from previous chapters and using either brake torque distribution or semi-active suspension actuation systems.

Chapter 2. The Bounded Jacobian Approach to Nonlinear Observer Desdign

2.1. Introduction

This chapter presents a new observer design technique for a nonlinear system with a globally (or locally) bounded Jacobian. The developed approach can enable observer design for a large class of differentiable nonlinear systems. Its advantage is that it enables easy observer design for a much wider range of operating conditions compared to linear or Lipschitz observer design methods. A major limitation of the existing results for Lipschitz nonlinear systems is that they work only for adequately small values of the Lipschitz constant. When the equivalent Lipschitz constant has to be chosen large due to the inherent non-Lipschitz nature of the nonlinearity (such as in the case of aerodynamic drag force in vehicle systems), most existing observer design results fail to provide a solution. This section develops a solution methodology that works well without requiring a small Lipschitz constant bound for the nonlinear function. The basic idea in this section is to use the mean value theorem (McLeod (1965) and Korobkov (2001)) to express the nonlinear error dynamics as a convex combination of values of the derivatives of the nonlinear function. The observer gain guaranteeing the convergence of the proposed observer can then be easily computed by LMIs.

2.2. Problem Statement for Nonlinear Observer

This section presents an efficient methodology for designing observers for the class of nonlinear systems described by

$$\begin{aligned} \dot{x} &= Ax + \Phi(x) + g(y,u) \\ y &= Cx \end{aligned} \tag{2.1}$$

where $x \in R^n$ is the state vector, $u \in R^p$ is the input vector, and $y \in R^m$ is the output measurement vector. $A \in R^{n\times n}$ and $C \in R^{m\times n}$ are appropriate matrices. The functions $\Phi(x)\colon R^n \to R^n$, and $g(y,u)\colon R^m \times R^p \to R^n$ are nonlinear. In additional, $\Phi(x)$ is assumed to be differentiable.

The observer will be assumed to be of the form,

$$\dot{\hat{x}} = A\hat{x} + \Phi(\hat{x}) + g(y,u) + L(y - C\hat{x}). \tag{2.2}$$

The estimation error introductions are then seen to be given by

$$\begin{aligned}\dot{\tilde{x}} &= (A - LC)\tilde{x} + \big(\Phi(x) - \Phi(\hat{x})\big) \\ \dot{\tilde{x}} &= (A - LC)\tilde{x} + \widetilde{\Phi}\end{aligned} \tag{2.3}$$

where $\tilde{x} = x - \hat{x}$, $\widetilde{\Phi} = \Phi(x) - \Phi(\hat{x})$.

Let the Lyapunov function candidate for observer design be defined as

$$V = \tilde{x}^T P \tilde{x} \tag{2.4}$$

where $P > 0$ and $P \in R^{n \times n}$.

Then, its derivative is

$$\dot{V} = \tilde{x}^T[(A - LC)^T P + P(A - LC)]\tilde{x} + \tilde{x}^T P\widetilde{\Phi} + \widetilde{\Phi}^T P\tilde{x}. \tag{2.5}$$

2.3. Mean Value Theorem for Bounded Jacobian Systems

In this sub-section, we present mathematical tools which are used subsequently to develop the design for the observer gain in the next section. First, we present the mean value theorem for scalars and the mean value theorem for vector functions. Then, we define the canonical basis for writing a vector function with a composition form. Lastly, we present a new modified form of the mean value theorem for vector functions.

Lemma 1: Scalar Mean Value Theorem

Let $f(x)$: $R \to R$ be a function continuous on $[a, b] \subset R$ and differentiable on (a, b). For x_1,$x_2 \in [a, b,]$, there exist numbers $c \in (a, b)$ such that

$$f(x_2) - f(x_1) = \left.\frac{df}{dx}\right|_{x=c} \times (x_2 - x_1). \tag{2.6}$$

The equation (2.6) can also be rewritten as

$$\begin{gathered} f(x_2) - f(x_1) = \left(\delta_1 \left.\frac{df}{dx}\right|_{x=c_1} + \delta_2 \left.\frac{df}{dx}\right|_{x=c_1}\right)(x_2 - x_1), \\ \delta_1, \delta_2 > 0, \qquad \delta_1 + \delta_2 = 1 \end{gathered} \tag{2.7}$$

where $c_1, c_2 \in (a, b)$ and δ_1 and δ_2 are parameters that vary with the value of x_1 and x_2. The proof of this lemma is presented in [10].

Lemma 2: Mean Value Theorem for a Vector Function, [11]

Let $f(x)\colon R^n \to R^n$ be a function continuous on $[a,b] \in R^n$ and differentiable on a convex hull of the set (a,b) with a Lipschitz continuous gradient ∇f. For $s_1, s_2 \in [a,b]$, there exists $c \in (a,b)$ such that

$$f(s_2) - f(s_1) = \nabla f(c)(s_2 - s_1). \tag{2.8}$$

However, we cannot directly use the mean value theorem of equation (2.8), since c is a varying parameter that continuously changes with the values of s_1 and s_2. Thus $\nabla f(c)$ is an unknown and changing matrix. We need to modify the mean value theorem before it can be utilized.

Lemma 3: Canonical Basis, [12]

Let a vector function be defined by:

$$f(x)\colon R^n \to R^q. \tag{2.9}$$

Then,

$$f(x) = \left[f_1(x), f_2(x), \dots, f_q(x)\right]^T \tag{2.10}$$

where $f_i(x)\colon R^n \to R$ is the i$^{\text{th}}$ component of $f(x)$ and $x \in R^n$.

Let the canonical basis of the vectorial space R^s for all $s \geq 1$ defined by:

$$E_s = \{e_s(i) | e_s(i) = (0,\dots,0,1,0,\dots,0)^T, \qquad i = 1,2,\dots,s\}. \tag{2.11}$$

The vectorial space R^q is generated by the canonical basis E_q. Therefore, $f(x)$ can be written as:

$$f(x) = \sum_{i=1}^{q} e_q(i) f_i(x). \tag{2.12}$$

Now, we are ready to state and prove a modified form of the mean value theorem for a vector function.

Theorem 1: Modified Mean Value Theorem for a Vector Function

Let $f(x)\colon R^n \to R^n$ be a function continuous on $[a,b] \in R^n$ and differentiable on convex hull of the set (a,b). For $s_1, s_2 \in [a,b]$, there exist δ_{ij}^{max} and δ_{ij}^{min} for $i = 1,\dots,n$ and $j = 1,\dots,n$ such that:

$$f(s_2) - f(s_1) = \left[\left(\sum_{i,j=1}^{n,n} H_{ij}^{max}\delta_{ij}^{max}\right) + \left(\sum_{i,j=1}^{n,n} H_{ij}^{min}\delta_{ij}^{min}\right)\right](s_2 - s_1), \tag{2.13}$$
$$\delta_{ij}^{max}, \delta_{ij}^{min} \geq 0, \qquad \delta_{ij}^{max} + \delta_{ij}^{min} = 1$$

where 1) $h_{ij}^{max} \geq max\left(\partial f_i/\partial x_j\right)$ and $h_{ij}^{min} \leq min\left(\partial f_i/\partial x_j\right)$ for $\forall x \in (a,b)$,
2) $H_{ij}^{max} = e_n(i)e_n^T(j)h_{ij}^{max}$and $H_{ij}^{min} = e_n(i)e_n^T(j)h_{ij}^{min}$.

Proof: Lemma 2 shows that

$$f(s_2) - f(s_1) = \nabla f(c)(s_2 - s_1) = \begin{bmatrix} \partial f_1/\partial x_1 & \partial f_1/\partial x_2 & \dots & \partial f_1/\partial x_n \\ \partial f_2/\partial x_1 & \partial f_2/\partial x_2 & \cdots & \partial f_2/\partial x_n \\ \vdots & \vdots & \vdots & \vdots \\ \partial f_n/\partial x_1 & \partial f_n/\partial x_2 & \cdots & \partial f_n/\partial x_n \end{bmatrix}([s_2 - s_1]). \quad (2.14)$$

Lemma 1 shows that each derivative function can be replaced with a convex combination of 2 values of the derivative of the function. Hence, the derivative function, $\partial f_i(c)/\partial x_j$, can be replaced with

$$\begin{aligned} &\frac{\partial f_i}{\partial x_j}(c) = \delta_{ij}^{max}\frac{\partial f_i}{\partial x_j}(\Omega) + \delta_{ij}^{min}\frac{\partial f_i}{\partial x_j}(\lambda), \\ &\delta_{ij}^{max}, \delta_{ij}^{min} \geq 0, \qquad \delta_{ij}^{max} + \delta_{ij}^{min} = 1 \end{aligned} \quad (2.15)$$

where $\Omega = (\Omega_1, \Omega_2, \dots, \Omega_n)$ and $\lambda = (\lambda_1, \lambda_2, \dots, \lambda_n)$. $c, \Omega, \lambda \in (a,b)$.

To satisfy lemma 1, the values of $\partial f_i(\Omega)/\partial x_j$ and $\partial f_i(\lambda)/\partial x_j$ need to be chosen such that

$$\frac{\partial f_i}{\partial x_j}(\Omega) = h_{ij}^{max} \geq max\left(\frac{\partial f_i}{\partial x_j}\right), \text{and } \frac{\partial f_i}{\partial x_j}(\lambda) = h_{ij}^{min} \leq min\left(\frac{\partial f_i}{\partial x_j}\right). \quad (2.16)$$

Note: One can easily show that if either $h_{ij}^{max} < max\left(df_i/dx_j\right)$ or $h_{ij}^{min} > min\left(df_i/dx_j\right)$ for $\forall x \in (a,b)$, then there are no $\delta_{ij}^{max}$and δ_{ij}^{min} that will satisfy equation (2.15) with the constraints $\delta_{ij}^{max}, \delta_{ij}^{min} \geq 0$ and $\delta_{ij}^{max} + \delta_{ij}^{min} = 1$.

Then, the equation (2.15) can be rewritten as

$$\begin{aligned} &\frac{\partial f_i}{\partial x_j}(c) = \delta_{ij}^{max}h_{ij}^{max} + \delta_{ij}^{min}h_{ij}^{min}, \\ &\delta_{ij}^{max}, \delta_{ij}^{min} \geq 0, \qquad \delta_{ij}^{max} + \delta_{ij}^{min} = 1 \end{aligned} \quad (2.17)$$

where $h_{ij}^{max} \geq max\left(\partial f_i/\partial x_j\right)$ and $h_{ij}^{min} \leq min\left(\partial f_i/\partial x_j\right)$. Note: $\delta_{ij}^{max}, \delta_{ij}^{min}$ are parameters that vary with the value of s_1 and s_2. Hence, the equation (2.14) can be rewritten as

$$f(s_2)-f(s_1)=\begin{bmatrix}\delta_{11}^{max}h_{11}^{max} & \delta_{12}^{max}h_{12}^{max} & \dots & \delta_{1n}^{max}h_{1n}^{max}\\ \delta_{21}^{max}h_{21}^{max} & \delta_{22}^{max}h_{22}^{max} & \dots & \delta_{2n}^{max}h_{2n}^{max}\\ \vdots & \vdots & \vdots & \vdots\\ \delta_{n1}^{max}h_{n1}^{max} & \delta_{n2}^{max}h_{n2}^{max} & \dots & \delta_{nn}^{max}h_{nn}^{max}\end{bmatrix}([s_2-s_1])$$
$$+\begin{bmatrix}\delta_{11}^{min}h_{11}^{min} & \delta_{12}^{min}h_{12}^{min} & \dots & \delta_{1n}^{min}h_{1n}^{min}\\ \delta_{21}^{min}h_{21}^{min} & \delta_{22}^{min}h_{22}^{min} & \dots & \delta_{2n}^{min}h_{2n}^{min}\\ \vdots & \vdots & \vdots & \vdots\\ \delta_{n1}^{min}h_{n1}^{min} & \delta_{n2}^{min}h_{n2}^{min} & \dots & \delta_{nn}^{min}h_{nn}^{min}\end{bmatrix}([s_2-s_1]). \tag{2.18}$$

Use the canonical basis from lemma 3. Then $f(s_2)-f(s_1)$ can be written as

$$f(s_2)-f(s_1)=\left[\left(\sum_{i,j=1}^{n,n}H_{ij}^{max}\delta_{ij}^{max}\right)+\left(\sum_{i,j=1}^{n,n}H_{ij}^{min}\delta_{ij}^{min}\right)\right](s_2-s_1), \tag{2.19}$$
$$\delta_{ij}^{max},\delta_{ij}^{min}\geq 0,\qquad \delta_{ij}^{max}+\delta_{ij}^{min}=1$$

where $H_{ij}^{max}=e_n(i)e_n^T(j)h_{ij}^{max}$ and $H_{ij}^{min}=e_n(i)e_n^T(j)h_{ij}^{min}$.

Illustrative Example for Theorem 1

The following is a 2 dimensional example of the application of the modified mean value theorem for a higher-dimensional function. Let $f(s)\colon R^2\to R^2$ be define by:

$$f(s)=[f_1(s)\quad f_2(s)]^T. \tag{2.20}$$

If we set $s_1=[s_{11},s_{12}]^T$ and $s_2=[s_{21},s_{22}]^T$, then

$$f(s_2)-f(s_1)=\nabla f(c)(s_2-s_1)$$
$$=\begin{bmatrix}\begin{bmatrix}max\left(\frac{\partial f_1}{\partial x_1}\right) & 0\\ 0 & 0\end{bmatrix}\delta_{11}^{max}+\begin{bmatrix}min\left(\frac{\partial f_1}{\partial x_1}\right) & 0\\ 0 & 0\end{bmatrix}\delta_{11}^{min}\\ +\begin{bmatrix}0 & max\left(\frac{\partial f_1}{\partial x_2}\right)\\ 0 & 0\end{bmatrix}\delta_{12}^{max}+\begin{bmatrix}0 & min\left(\frac{\partial f_1}{\partial x_2}\right)\\ 0 & 0\end{bmatrix}\delta_{12}^{min}\\ +\begin{bmatrix}0 & 0\\ max\left(\frac{\partial f_2}{\partial x_1}\right) & 0\end{bmatrix}\delta_{21}^{max}+\begin{bmatrix}0 & 0\\ min\left(\frac{\partial f_2}{\partial x_1}\right) & 0\end{bmatrix}\delta_{21}^{min}\\ +\begin{bmatrix}0 & 0\\ 0 & max\left(\frac{\partial f_2}{\partial x_2}\right)\end{bmatrix}\delta_{22}^{max}+\begin{bmatrix}0 & 0\\ 0 & min\left(\frac{\partial f_2}{\partial x_2}\right)\end{bmatrix}\delta_{22}^{min}\end{bmatrix}\times\left(\begin{bmatrix}s_{21}\\ s_{22}\end{bmatrix}-\begin{bmatrix}s_{11}\\ s_{12}\end{bmatrix}\right) \tag{2.21}$$

or

$$f(s_2) - f(s_1) = \begin{bmatrix} H_{11}^{max}\delta_{11}^{max} + H_{11}^{min}\delta_{11}^{min} \\ +H_{12}^{max}\delta_{12}^{max} + H_{12}^{min}\delta_{12}^{min} \\ +H_{21}^{max}\delta_{21}^{max} + H_{21}^{min}\delta_{21}^{min} \\ +H_{22}^{max}\delta_{22}^{max} + H_{22}^{min}\delta_{22}^{min} \end{bmatrix} \times \left(\begin{bmatrix} s_{21} \\ s_{22} \end{bmatrix} - \begin{bmatrix} s_{11} \\ s_{12} \end{bmatrix} \right), \quad (2.22)$$
$$\delta_{ij}^{max}, \delta_{ij}^{min} \geq 0, \qquad \delta_{ij}^{max} + \delta_{ij}^{min} = 1$$

where $H_{ij}^{max} = e_n(i)e_n^T(j)h_{ij}^{max}$, $H_{ij}^{min} = e_n(i)e_n^T(j)h_{ij}^{min}$, $h_{ij}^{max} \geq max\left(\partial f_i/\partial x_j\right)$ and $h_{ij}^{min} \leq min\left(\partial f_i/\partial x_j\right)$.

2.4. Nonlinear Observer

Theorem 2: Bounded Jacobian Observer for General Problems [13]

For the class of systems and observer forms described in equations (2.1) and (2.2), if an observer gain matrix L can be chosen such that

$$\begin{gathered} P\left(A + \bar{H}_{ij}^{max}\right) + \left(A + \bar{H}_{ij}^{max}\right)^T P - C^T L^T P - PLC < 0 \\ P\left(A + \bar{H}_{ij}^{min}\right) + \left(A + \bar{H}_{ij}^{min}\right)^T P - C^T L^T P - PLC < 0 \\ P > 0 \\ \forall i = 1, \dots, n \text{ , and } \forall j = 1, \dots, n \end{gathered} \quad (2.23)$$

where,

1) $h_{ij}^{max} \geq max\left(\partial\Phi_i/\partial x_j\right)$ and $h_{ij}^{min} \leq min\left(\partial\Phi_i/\partial x_j\right)$,
2) $H_{ij}^{max} = e_n(i)e_n^T(j)h_{ij}^{max}$ and $H_{ij}^{min} = e_n(i)e_n^T(j)h_{ij}^{min}$,
3) $z_H = n \times n$ is the state scaling factor, n being dimension of the state vector,
4) $\bar{H}_{ij}^{max} = z_H H_{ij}^{max}$ and $\bar{H}_{ij}^{min} = z_H H_{ij}^{min}$,

then this choice of L leads to asymptotically stable estimates by the observer (2.2) for the system (2.1).

Proof: The derivative of the Lyapunov function is

$$\dot{V} = \tilde{x}^T[(A - LC)^T P + P(A - LC)]\tilde{x} + \tilde{x}^T P\tilde{\Phi} + \tilde{\Phi}^T P\tilde{x}. \quad (2.24)$$

The nonlinear terms can be rewritten using theorem 1 as

$$\begin{aligned} \tilde{\Phi} &= [\Phi(x) - \Phi(\hat{x})\,] \\ &= \left[\left(\sum_{i,j=1}^{n,n} H_{ij}^{max}\delta_{ij}^{max}\right) + \left(\sum_{i,j=1}^{n,n} H_{ij}^{min}\delta_{ij}^{min}\right)\right][x - \hat{x}], \\ &\quad \delta_{ij}^{max}, \delta_{ij}^{min} \geq 0, \qquad \delta_{ij}^{max} + \delta_{ij}^{min} = 1. \end{aligned} \quad (2.25)$$

To simplify the form of the final result, we need to scale $\sum_{i,j=1}^{n,n}\left(\delta_{ij}^{max}+\ \delta_{ij}^{min}\right)$ to one. In the general problem, if all the terms in $\partial\Phi_i/\partial x_j$ are to be considered and not zero, then the scaling factors, z_H is computed by

$$\sum_{i,j=1}^{n,n}\left(\delta_{ij}^{max}+\ \delta_{ij}^{min}\right)=n\times n=z_H,\ \frac{\sum_{i,j=1}^{n,n}\left(\delta_{ij}^{max}+\ \delta_{ij}^{min}\right)}{z_H}=1 \tag{2.26}$$

Rewrite equation (2.25) as

$$\begin{gathered}\widetilde{\Phi}=\left[\left(\sum_{i,j=1}^{n,n}\bar{H}_{ij}^{max}\bar{\delta}_{ij}^{max}\right)+\left(\sum_{i,j=1}^{n,n}\bar{H}_{ij}^{min}\bar{\delta}_{ij}^{min}\right)\right][x-\hat{x}],\\ \bar{\delta}_{ij}^{max},\bar{\delta}_{ij}^{min}\geq 0,\bar{\delta}_{ij}^{max}+\ \bar{\delta}_{ij}^{min}=1/z_H,\sum_{i,j=1}^{n,n}\left(\bar{\delta}_{ij}^{max}+\ \bar{\delta}_{ij}^{min}\right)=1,\end{gathered} \tag{2.27}$$

where,

1) $\bar{H}_{ij}^{max}=z_H H_{ij}^{max}$ and $\bar{H}_{ij}^{min}=z_H H_{ij}^{min}$,
2) $\bar{\delta}_{ij}^{max}=\delta_{ij}^{max}/z_H$ and $\bar{\delta}_{ij}^{min}=\delta_{ij}^{min}/z_H$.

Then, the derivative of the Lyapunov function becomes

$$\dot{V}=\tilde{x}^T\begin{bmatrix}(A-LC)^TP+P(A-LC)\\ +\left[\left(\sum_{i,j=1}^{n,n}\bar{H}_{ij}^{max}\bar{\delta}_{ij}^{max}\right)^{\mathrm{T}}+\left(\sum_{i,j=1}^{n,n}\bar{H}_{ij}^{min}\bar{\delta}_{ij}^{min}\right)^{\mathrm{T}}\right]P\\ +P\left[\left(\sum_{i,j=1}^{n,n}\bar{H}_{ij}^{max}\bar{\delta}_{ij}^{max}\right)+\left(\sum_{i,j=1}^{n,n}\bar{H}_{ij}^{min}\bar{\delta}_{ij}^{min}\right)\right]\end{bmatrix}\tilde{x} \tag{2.28}$$

$$\dot{V}=\tilde{x}^T\begin{bmatrix}\left((A-LC)+\left(\sum_{i,j=1}^{n,n}\bar{H}_{ij}^{max}\bar{\delta}_{ij}^{max}\right)+\left(\sum_{i,j=1}^{n,n}\bar{H}_{ij}^{min}\bar{\delta}_{ij}^{min}\right)\right)^T P\\ +P\left((A-LC)+\left(\sum_{i,j=1}^{n,n}\bar{H}_{ij}^{max}\bar{\delta}_{ij}^{max}\right)+\left(\sum_{i,j=1}^{n,n}\bar{H}_{ij}^{min}\bar{\delta}_{ij}^{min}\right)\right)\end{bmatrix}\tilde{x} \tag{2.29}$$

Since $\sum_{i,j=1}^{n,n}\left(\bar{\delta}_{ij}^{max}+\ \bar{\delta}_{ij}^{min}\right)=1$, equation (2.29) can be rewritten as

$$\dot{V} = \tilde{x}^T \begin{bmatrix} \sum_{i,j=1}^{n,n} \bar{\delta}_{ij}^{max} \{(A-LC)^T P + \bar{H}_{ij}^{max^T} P\} \\ + \sum_{i,j=1}^{n,n} \bar{\delta}_{ij}^{min} \{(A-LC)^T P + \bar{H}_{ij}^{min^T} P\} \\ + \sum_{i,j=1}^{n,n} \bar{\delta}_{ij}^{max} \{P(A-LC) + P\bar{H}_{ij}^{max}\} \\ + \sum_{i,j=1}^{n,n} \bar{\delta}_{ij}^{min} \{P(A-LC) + P\bar{H}_{ij}^{min}\} \end{bmatrix} \tilde{x}. \tag{2.30}$$

$$\dot{V} = \tilde{x}^T M \tilde{x} = \tilde{x}^T \begin{bmatrix} \sum_{i,j=1}^{n,n} \bar{\delta}_{ij}^{max} \{\left(A + \bar{H}_{ij}^{max} - LC\right)^T P + P\left(A + \bar{H}_{ij}^{max} - LC\right)\} \\ + \sum_{i,j=1}^{n,n} \bar{\delta}_{ij}^{min} \{\left(A + \bar{H}_{ij}^{min} - LC\right)^T P + P\left(A + \bar{H}_{ij}^{min} - LC\right)\} \end{bmatrix} \tilde{x}. \tag{2.31}$$

Hence we need

$$M < 0 \tag{2.32}$$

where $\bar{\delta}_{ij}^{max}$, $\bar{\delta}_{ij}^{min} \geq 0$. However, it is not possible to directly solve equation (2.32) for L and P because $\bar{\delta}_{ij}^{max}$, $\bar{\delta}_{ij}^{min}$ are time varying coefficients. Hence, we transform equation (2.32) to equations (2.33) and (2.34).

$$P\left(A + \bar{H}_{ij}^{max}\right) + \left(A + \bar{H}_{ij}^{max}\right)^T P - C^T L^T P - PLC < 0, \tag{2.33}$$

$$P\left(A + \bar{H}_{ij}^{min}\right) + \left(A + \bar{H}_{ij}^{min}\right)^T P - C^T L^T P - PLC < 0, \tag{2.34}$$

for $\forall i = 1, \dots, n$, and $\forall j = 1, \dots, n$.

Then if equation (2.33) and (2.34) are satisfied, equation (2.32) will automatically be satisfied.

Corollary to Theorem 2: Bounded Jacobian Observer for Sparse Problems

For the class of systems and observer forms described in equations (2.1) and (2.2), if an observer gain matrix L can be chosen such that

$$\begin{gathered} P\left(A + \bar{H}_{ij}^{max}\right) + \left(A + \bar{H}_{ij}^{max}\right)^T P - C^T L^T P - PLC < 0 \\ P\left(A + \bar{H}_{ij}^{min}\right) + \left(A + \bar{H}_{ij}^{min}\right)^T P - C^T L^T P - PLC < 0 \\ P > 0 \\ \forall i = 1, \dots, n \text{ , and } \forall j = 1, \dots, n \end{gathered} \tag{2.35}$$

where,

1) $h_{ij}^{max} \geq max\left(\partial\Phi_i/\partial x_j\right)$ and $h_{ij}^{min} \leq min\left(\partial\Phi_i/\partial x_j\right)$,
2) $H_{ij}^{max} = e_n(i)e_n^T(j)h_{ij}^{max}$ and $H_{ij}^{min} = e_n(i)e_n^T(j)h_{ij}^{min}$,
3) 3) $\bar{z}_H = n \times n - w_H$ is the state scaling factor, n being dimension of the state vector, w_H being the number of terms in $\partial\Phi_i/\partial x_j$ that equals zero,
4) $\bar{H}_{ij}^{max} = \bar{z}_H H_{ij}^{max}$ and $\bar{H}_{ij}^{min} = \bar{z}_H H_{ij}^{min}$.

then this choice of L leads to asymptotically stable estimates by the observer (2.2) for the system (2.1).

Proof: The proof of the Corollary follows along the same lines as the proof of theorem 2, except for the definition of the scaling factor $\bar{z}_H$.

In the general problem, if all of terms in $\partial\Phi_i/\partial x_j$ are not zero, then $\sum_{i,j=1}^{n,n}\left(\delta_{ij}^{max} + \delta_{ij}^{min}\right) = n \times n = z_H$. However, if in some problem, there exist $\partial\Phi_i/\partial x_j = 0$, then $\sum_{i,j=1}^{n,n}\left(\delta_{ij}^{max} + \delta_{ij}^{min}\right)$ is less than z_H. We need to define a new scaling factor, $\bar{z}_H$.

$$\sum_{i,j=1}^{n,n}\left(\delta_{ij}^{max} + \delta_{ij}^{min}\right) = n \times n - w_H = \bar{z}_H \tag{2.36}$$

where w_H is number of terms in $\partial\Phi_i/\partial x_j$ that equals zero. Now, we use $\bar{z}_H$ instead of z_H to complete the proof.

2.5. Conclusions

In this chapter, a new observer design technique is developed for a nonlinear system with a globally (or locally) bounded Jacobian. The approach is developed in order to deal with differentiable nonlinear systems. The observer gains in the developed approach can be obtained by solving LMIs.

Chapter 3. The Extended Bounded Jacobian Approach to Observer Design for Nonlinear Systems with Nonlinear Measurement Equation

This chapter extends the result in chapter 2 and presents how the technique can be applied for a nonlinear system with a nonlinear measurement model.

3.1. Problem Statement for Nonlinear Observer

This chapter presents an efficient methodology for designing observers for the class of nonlinear systems described by

$$\begin{aligned} \dot{x} &= Ax + \Phi(x) + g(y,u), \\ y &= Cx + \Psi(x) \end{aligned} \tag{3.1}$$

where $x \in R^n$ is the state vector, $u \in R^p$ is the input vector, and $y \in R^m$ is the output measurement vector. $A \in R^{n\times n}$ and $C \in R^{m\times n}$are appropriate matrices. The functions $\Phi(x)$: $R^n \to R^n$, $\Psi(x)$: $R^n \to R^m$, and $g(y,u)$: $R^m \times R^p \to R^n$ are nonlinear. In addition, $\Phi(x)$ and $\Psi(x)$ are assumed to be differentiable.

The observer will be assumed to be of the form

$$\begin{aligned} \dot{\hat{x}} &= A\hat{x} + \Phi(\hat{x}) + g(y,u) + L(y - \hat{y}) \\ \hat{y} &= C\hat{x} + \Psi(\hat{x}). \end{aligned} \tag{3.2}$$

The estimation error introductions are then seen to be given by

$$\dot{\tilde{x}} = (A - LC)\tilde{x} + \tilde{\Phi} - L\tilde{\Psi} \tag{3.3}$$

where $\tilde{x} = x - \hat{x}$, $\tilde{\Phi} = \Phi(x) - \Phi(\hat{x})$, and $\tilde{\Psi} = \Psi(x) - \Psi(\hat{x})$.

Let the Lyapunov function candidate for observer design be defined as

$$V = \tilde{x}^T P \tilde{x}. \tag{3.4}$$

where $P > 0$ and $P \in R^{n\times n}$. Then, its derivative is

$$\dot{V} = \tilde{x}^T[(A - LC)^T P + P(A - LC)]\tilde{x} + \tilde{x}^T P\tilde{\Phi} + \tilde{\Phi}^{\mathrm{T}} P\tilde{x} - \tilde{x}^T PL\tilde{\Psi} - \tilde{\Psi}^{\mathrm{T}} L^T P\tilde{x}. \tag{3.5}$$

3.2. Mean Value Theorem for Bounded Jacobian Systems

The mathematical tools which are used subsequently to develop the observer gain in the next section are the same as one in the chapter 2 section 2.3. So, we will not repeat them again.

3.3. Nonlinear Observer

Theorem 3: Bounded Jacobian Observer for General Problem

For the class of systems and observer forms described in equations (3.1) and (3.2), if an observer gain matrix L can be chosen such that

$$\begin{gathered}
P\left(A+\bar{H}_{ij}^{max}\right)+\left(A+\bar{H}_{ij}^{max}\right)^{T}P-\left(C+\bar{G}_{kj}^{max}\right)^{T}L^{T}P-PL\left(C+\bar{G}_{kj}^{max}\right)<0 \\
P\left(A+\bar{H}_{ij}^{max}\right)+\left(A+\bar{H}_{ij}^{max}\right)^{T}P-\left(C+\bar{G}_{kj}^{min}\right)^{T}L^{T}P-PL\left(C+\bar{G}_{kj}^{min}\right)<0 \\
P\left(A+\bar{H}_{ij}^{min}\right)+\left(A+\bar{H}_{ij}^{min}\right)^{T}P-\left(C+\bar{G}_{kj}^{max}\right)^{T}L^{T}P-PL\left(C+\bar{G}_{kj}^{max}\right)<0 \\
P\left(A+\bar{H}_{ij}^{min}\right)+\left(A+\bar{H}_{ij}^{min}\right)^{T}P-\left(C+\bar{G}_{kj}^{min}\right)^{T}L^{T}P-PL\left(C+\bar{G}_{kj}^{min}\right)<0 \\
P>0 \\
\forall i=1,\dots,n\,,\forall j=1,\dots,n \text{ and } \forall k=1,\dots,m
\end{gathered} \tag{3.6}$$

where,

1) $h_{ij}^{max}\geq max\left(\partial\Phi_i/\partial x_j\right)$ and $h_{ij}^{min}\leq min\left(\partial\Phi_i/\partial x_j\right)$,
2) $H_{ij}^{max}=e_n(i)e_n^T(j)h_{ij}^{max}$ and $H_{ij}^{min}=e_n(i)e_n^T(j)h_{ij}^{min}$,
3) $z_H=n\times n$ is the state scaling factor, n being dimension of the state vector,
4) $\bar{H}_{ij}^{max}=z_H H_{ij}^{max}$ and $\bar{H}_{ij}^{min}=z_H H_{ij}^{min}$,
5) $g_{kj}^{max}\geq max\left(\partial\Psi_k/\partial x_j\right)$ and $g_{kj}^{min}\leq min\left(\partial\Psi_k/\partial x_j\right)$,
6) $G_{kj}^{max}=e_n(k)e_n^T(j)g_{kj}^{max}$and $G_{kj}^{min}=e_n(k)e_n^T(j)g_{kj}^{min}$,
7) $z_G=m\times n$ is the output scaling factor, m being dimension of the output vector,
8) $\bar{G}_{kj}^{max}=z_G G_{kj}^{max}$ and $\bar{G}_{kj}^{min}=z_G G_{kj}^{min}$,

then this choice of L leads to asymptotically stable estimates by the observer (3.2) for the system (3.1).

Proof: The derivative of the Lyapunov function is

$$\dot{V}=\tilde{x}^T[(A-LC)^TP+P(A-LC)]\tilde{x}+\tilde{x}^TP\tilde{\Phi}+\tilde{\Phi}^{\mathrm{T}}P\tilde{x}-\tilde{x}^TPL\tilde{\Psi}-\tilde{\Psi}^{\mathrm{T}}L^TP\tilde{x}. \tag{3.7}$$

$$\dot{V}=\tilde{x}^T[(A-LC)^TP+P(A-LC)]\tilde{x}+\tilde{x}^TP\tilde{\Phi}+\tilde{\Phi}^{\mathrm{T}}P\tilde{x}-\tilde{x}^TPL\tilde{\Psi}-\tilde{\Psi}^{\mathrm{T}}L^TP\tilde{x}. \tag{3.1}$$

The nonlinear terms can be rewritten using theorem 1 as

$$\begin{aligned}\widetilde{\Phi} &= [\Phi(x) - \Phi(\hat{x})\,] \\ &= \left[\left(\sum_{i,j=1}^{n,n} H_{ij}^{max}\delta_{ij}^{max}\right) + \left(\sum_{i,j=1}^{n,n} H_{ij}^{min}\delta_{ij}^{min}\right)\right][x - \hat{x}], \\ &\qquad \delta_{ij}^{max}, \delta_{ij}^{min} \geq 0, \qquad \delta_{ij}^{max} + \delta_{ij}^{min} = 1\end{aligned} \tag{3.8}$$

$$\begin{aligned}\widetilde{\Psi} &= [\Psi(x) - \Psi(\hat{x})\,] \\ &= \left[\left(\sum_{k,j=1}^{m,n} G_{kj}^{max}\gamma_{kj}^{max}\right) + \left(\sum_{k,j=1}^{m,n} G_{kj}^{min}\gamma_{kj}^{min}\right)\right][x - \hat{x}], \\ &\qquad \gamma_{kj}^{max}, \gamma_{kj}^{min} \geq 0, \qquad \gamma_{kj}^{max} + \gamma_{kj}^{min} = 1\end{aligned} \tag{3.9}$$

To simplify the form of the final result, we need to scale $\sum_{i,j=1}^{n,n}\left(\delta_{ij}^{max} + \delta_{ij}^{min}\right)$ and $\sum_{k,j=1}^{m,n}\left(\gamma_{kj}^{max} + \gamma_{kj}^{min}\right)$ to one. In the general problem, if all the terms in $\partial\Phi_i/\partial x_j$ and $\partial\Psi_k/\partial x_j$ are to be considered and not zero, then the scaling factors, z_H and z_G are computed by

$$\begin{aligned}&\sum_{i,j=1}^{n,n}\left(\delta_{ij}^{max} + \delta_{ij}^{min}\right) = n \times n = z_H, \quad \frac{\sum_{i,j=1}^{n,n}\left(\delta_{ij}^{max} + \delta_{ij}^{min}\right)}{z_H} = 1 \\ &\sum_{k,j=1}^{m,n}\left(\gamma_{kj}^{max} + \gamma_{kj}^{min}\right) = m \times n = z_G, \quad \frac{\sum_{k,j=1}^{m,n}\left(\gamma_{kj}^{max} + \gamma_{kj}^{min}\right)}{z_G} = 1\end{aligned} \tag{3.10}$$

Rewrite equation (3.8) and (3.9) as

$$\begin{aligned}&\widetilde{\Phi} = \left[\left(\sum_{i,j=1}^{n,n} \bar{H}_{ij}^{max}\bar{\delta}_{ij}^{max}\right) + \left(\sum_{i,j=1}^{n,n} \bar{H}_{ij}^{min}\bar{\delta}_{ij}^{min}\right)\right][x - \hat{x}], \\ &\bar{\delta}_{ij}^{max}, \bar{\delta}_{ij}^{min} \geq 0, \bar{\delta}_{ij}^{max} + \bar{\delta}_{ij}^{min} = 1/z_H, \sum_{i,j=1}^{n,n}\left(\bar{\delta}_{ij}^{max} + \bar{\delta}_{ij}^{min}\right) = 1,\end{aligned} \tag{3.11}$$

$$\begin{aligned}&\widetilde{\Psi} = \left[\left(\sum_{k,j=1}^{m,n} \bar{G}_{kj}^{max}\bar{\gamma}_{kj}^{max}\right) + \left(\sum_{k,j=1}^{m,n} \bar{G}_{kj}^{min}\bar{\gamma}_{kj}^{min}\right)\right][x - \hat{x}], \\ &\bar{\gamma}_{kj}^{max}, \bar{\gamma}_{kj}^{min} \geq 0, \ \bar{\gamma}_{kj}^{max} + \bar{\gamma}_{kj}^{min} = 1/z_G, \sum_{k,j=1}^{m,n}\left(\bar{\gamma}_{kj}^{max} + \bar{\gamma}_{kj}^{min}\right) = 1\end{aligned} \tag{3.12}$$

where,

1) $\bar{H}_{ij}^{max} = z_H H_{ij}^{max}$ and $\bar{H}_{ij}^{min} = z_H H_{ij}^{min}$,
2) $\bar{\delta}_{ij}^{max} = \delta_{ij}^{max}/z_H$ and $\bar{\delta}_{ij}^{min} = \delta_{ij}^{min}/z_H$,
3) $\bar{G}_{kj}^{max} = z_G G_{kj}^{max}$ and $\bar{G}_{kj}^{min} = z_G G_{kj}^{min}$,
4) $\bar{\gamma}_{kj}^{max} = \gamma_{kj}^{max}/z_G$, and $\bar{\gamma}_{kj}^{min} = \gamma_{kj}^{min}/z_G$.

Then, the derivative of the Lyapunov function becomes

$$\dot{V} = \tilde{x}^T \begin{bmatrix} (A-LC)^T P + P(A-LC) \\ -\left[\left(\sum_{k,j=1}^{m,n} \bar{G}_{kj}^{max} \bar{\gamma}_{kj}^{max}\right)^{\mathrm{T}} + \left(\sum_{k,j=1}^{m,n} \bar{G}_{kj}^{min} \bar{\gamma}_{kj}^{min}\right)^{\mathrm{T}}\right] L^T P \\ -PL\left[\left(\sum_{k,j=1}^{m,n} \bar{G}_{kj}^{max} \bar{\gamma}_{kj}^{max}\right) + \left(\sum_{k,j=1}^{m,n} \bar{G}_{kj}^{min} \bar{\gamma}_{kj}^{min}\right)\right] \\ +\left[\left(\sum_{i,j=1}^{n,n} \bar{H}_{ij}^{max} \bar{\delta}_{ij}^{max}\right)^{\mathrm{T}} + \left(\sum_{i,j=1}^{n,n} \bar{H}_{ij}^{min} \bar{\delta}_{ij}^{min}\right)^{\mathrm{T}}\right] P \\ +P\left[\left(\sum_{i,j=1}^{n,n} \bar{H}_{ij}^{max} \bar{\delta}_{ij}^{max}\right) + \left(\sum_{i,j=1}^{n,n} \bar{H}_{ij}^{min} \bar{\delta}_{ij}^{min}\right)\right] \end{bmatrix} \tilde{x} \qquad (3.13)$$

Since $\sum_{i,j=1}^{n,n}\left(\bar{\delta}_{ij}^{max}+\bar{\delta}_{ij}^{min}\right)=1$, equation (3.13) can be rewritten as

$$\dot{V}=\tilde{x}^{T}\begin{bmatrix}\sum_{i,j=1}^{n,n}\bar{\delta}_{ij}^{max}\{(A-LC)^{T}P+\bar{H}_{ij}^{max^{T}}P \\ -\left(\sum_{k,j=1}^{m,n}\bar{G}_{kj}^{max}\bar{\gamma}_{kj}^{max}\right)^{\mathrm{T}}L^{T}P-\left(\sum_{k,j=1}^{m,n}\bar{G}_{kj}^{min}\bar{\gamma}_{kj}^{min}\right)^{\mathrm{T}}L^{T}P\} \\ +\sum_{i,j=1}^{n,n}\bar{\delta}_{ij}^{min}\{(A-LC)^{T}P+\bar{H}_{ij}^{min^{T}}P \\ -\left(\sum_{k,j=1}^{m,n}\bar{G}_{kj}^{max}\bar{\gamma}_{kj}^{max}\right)^{\mathrm{T}}L^{T}P-\left(\sum_{k,j=1}^{m,n}\bar{G}_{kj}^{min}\bar{\gamma}_{kj}^{min}\right)^{\mathrm{T}}L^{T}P\} \\ +\sum_{i,j=1}^{n,n}\bar{\delta}_{ij}^{max}\{P(A-LC)+P\bar{H}_{ij}^{max} \\ -PL\left(\sum_{k,j=1}^{m,n}\bar{G}_{kj}^{max}\bar{\gamma}_{kj}^{max}\right)-PL\left(\sum_{k,j=1}^{m,n}\bar{G}_{kj}^{min}\bar{\gamma}_{kj}^{min}\right)\} \\ +\sum_{i,j=1}^{n,n}\bar{\delta}_{ij}^{min}\{P(A-LC)+P\bar{H}_{ij}^{min} \\ -PL\left(\sum_{k,j=1}^{m,n}\bar{G}_{kj}^{max}\bar{\gamma}_{kj}^{max}\right)-PL\left(\sum_{k,j=1}^{m,n}\bar{G}_{kj}^{min}\bar{\gamma}_{kj}^{min}\right)\}\end{bmatrix}\tilde{x}. \qquad (3.14)$$

$$\dot{V} = \tilde{x}^T M \tilde{x} = \tilde{x}^T \left[\begin{array}{l} \sum_{i,j=1}^{n,n} \bar{\delta}_{ij}^{max} \{ (A-LC)^T P + \bar{H}_{ij}^{max^T} P + P(A-LC) + P\bar{H}_{ij}^{max} \\ \quad - \left(\sum_{k,j=1}^{m,n} \bar{G}_{kj}^{max} \bar{\gamma}_{kj}^{max} \right)^{\mathrm{T}} L^T P - \left(\sum_{k,j=1}^{m,n} \bar{G}_{kj}^{min} \bar{\gamma}_{kj}^{min} \right)^{\mathrm{T}} L^T P \\ \quad - PL \left(\sum_{k,j=1}^{m,n} \bar{G}_{kj}^{max} \bar{\gamma}_{kj}^{max} \right) - PL \left(\sum_{k,j=1}^{m,n} \bar{G}_{kj}^{min} \bar{\gamma}_{kj}^{min} \right) \} \\ + \sum_{i,j=1}^{n,n} \bar{\delta}_{ij}^{min} \{ (A-LC)^T P + \bar{H}_{ij}^{min^T} P + P(A-LC) + P\bar{H}_{ij}^{min} \\ \quad - \left(\sum_{k,j=1}^{m,n} \bar{G}_{kj}^{max} \bar{\gamma}_{kj}^{max} \right)^{\mathrm{T}} L^T P - \left(\sum_{k,j=1}^{m,n} \bar{G}_{kj}^{min} \bar{\gamma}_{kj}^{min} \right)^{\mathrm{T}} L^T P \\ \quad - PL \left(\sum_{k,j=1}^{m,n} \bar{G}_{kj}^{max} \bar{\gamma}_{kj}^{max} \right) - PL \left(\sum_{k,j=1}^{m,n} \bar{G}_{kj}^{min} \bar{\gamma}_{kj}^{min} \right) \} \end{array} \right] \tilde{x}. \quad (3.15)$$

Hence we need

$$M < 0 \quad (3.16)$$

where $\bar{\delta}_{ij}^{max}$, $\bar{\delta}_{ij}^{min} \geq 0$. However, it is not possible to directly solve equation (3.16) for L and P because $\bar{\delta}_{ij}^{max}$, $\bar{\delta}_{ij}^{min}$ are time varying coefficients. Hence, we transform equation (3.16) to equations (3.17) and (3.18).

$$\left[\left(\begin{array}{c} (A-LC)^T P + \bar{H}_{ij}^{max^T} P + P(A-LC) + P\bar{H}_{ij}^{max} \\ - \left(\sum_{k,j=1}^{m,n} \bar{G}_{kj}^{max} \bar{\gamma}_{kj}^{max} \right)^{\mathrm{T}} L^T P - \left(\sum_{k,j=1}^{m,n} \bar{G}_{kj}^{min} \bar{\gamma}_{kj}^{min} \right)^{\mathrm{T}} L^T P \\ - PL \left(\sum_{k,j=1}^{m,n} \bar{G}_{kj}^{max} \bar{\gamma}_{kj}^{max} \right) - PL \left(\sum_{k,j=1}^{m,n} \bar{G}_{kj}^{min} \bar{\gamma}_{kj}^{min} \right) \end{array} \right) \right] < 0 \quad (3.17)$$

$$\left[\left(\begin{array}{c}(A-LC)^T P+\bar{H}_{ij}^{min^T} P+P(A-LC)+P\bar{H}_{ij}^{min} \\ -\left(\sum_{k,j=1}^{m,n} \bar{G}_{kj}^{max} \bar{\gamma}_{kj}^{max}\right)^{\mathrm{T}} L^T P-\left(\sum_{k,j=1}^{m,n} \bar{G}_{kj}^{min} \bar{\gamma}_{kj}^{min}\right)^{\mathrm{T}} L^T P \\ -PL\left(\sum_{k,j=1}^{m,n} \bar{G}_{kj}^{max} \bar{\gamma}_{kj}^{max}\right)-PL\left(\sum_{k,j=1}^{m,n} \bar{G}_{kj}^{min} \bar{\gamma}_{kj}^{min}\right)\end{array}\right)\right]<0 \tag{3.18}$$

Since $\sum_{k,j=1}^{m,n}\left(\bar{\gamma}_{kj}^{max}+\bar{\gamma}_{kj}^{min}\right)=1$, equation (3.17) and (3.18) can be rewritten as

$$\left[\left(\begin{array}{l}\sum_{k,j=1}^{m,n} \bar{\gamma}_{kj}^{max}\left(\left(A+\bar{H}_{ij}^{max}\right)^T P-C^{\mathrm{T}} L^T P-\bar{G}_{kj}^{max^T} L^T P\right) \\ +\sum_{k,j=1}^{m,n} \bar{\gamma}_{kj}^{min}\left(\left(A+\bar{H}_{ij}^{max}\right)^T P-C^{\mathrm{T}} L^T P-\bar{G}_{kj}^{min^T} L^T P\right) \\ +\sum_{k,j=1}^{m,n} \bar{\gamma}_{kj}^{max}\left(P\left(A+\bar{H}_{ij}^{max}\right)-PLC-PL\bar{G}_{kj}^{max}\right) \\ +\sum_{k,j=1}^{m,n} \bar{\gamma}_{kj}^{min}\left(P\left(A+\bar{H}_{ij}^{max}\right)-PLC-PL\bar{G}_{kj}^{min}\right)\end{array}\right)\right]<0 \tag{3.19}$$

$$\left[\left(\begin{array}{l}\sum_{k,j=1}^{m,n} \bar{\gamma}_{kj}^{max}\left(\left(A+\bar{H}_{ij}^{min}\right)^T P-C^{\mathrm{T}} L^T P-\bar{G}_{kj}^{max^T} L^T P\right) \\ +\sum_{k,j=1}^{m,n} \bar{\gamma}_{kj}^{min}\left(\left(A+\bar{H}_{ij}^{min}\right)^T P-C^{\mathrm{T}} L^T P-\bar{G}_{kj}^{min^T} L^T P\right) \\ +\sum_{k,j=1}^{m,n} \bar{\gamma}_{kj}^{max}\left(P\left(A+\bar{H}_{ij}^{min}\right)-PLC-PL\bar{G}_{kj}^{max}\right) \\ +\sum_{k,j=1}^{m,n} \bar{\gamma}_{kj}^{min}\left(P\left(A+\bar{H}_{ij}^{min}\right)-PLC-PL\bar{G}_{kj}^{min}\right)\end{array}\right)\right]<0 \tag{3.20}$$

where $\bar{\gamma}_{kj}^{max}, \bar{\gamma}_{kj}^{min} \geq 0$. Further, rearrange equation (3.19) and (3.20) as

$$\left[\left(\begin{array}{l}\sum_{k,j=1}^{m,n}\bar{\gamma}_{kj}^{max}\{\left(A+\bar{H}_{ij}^{max}\right)^{T}P+P\left(A+\bar{H}_{ij}^{max}\right)\\ -C^{\mathrm{T}}L^{T}P-\bar{G}_{kj}^{max^{T}}L^{T}P-PLC-PL\bar{G}_{kj}^{max}\}\\ +\sum_{k,j=1}^{m,n}\bar{\gamma}_{kj}^{min}\{\left(A+\bar{H}_{ij}^{max}\right)^{T}P+P\left(A+\bar{H}_{ij}^{max}\right)\\ -C^{\mathrm{T}}L^{T}P-\bar{G}_{kj}^{min^{T}}L^{T}P-PLC-PL\bar{G}_{kj}^{min}\}\end{array}\right)\right]<0 \quad (3.21)$$

$$\left[\left(\begin{array}{l}\sum_{k,j=1}^{m,n}\bar{\gamma}_{kj}^{max}\{\left(A+\bar{H}_{ij}^{min}\right)^{T}P+P\left(A+\bar{H}_{ij}^{min}\right)\\ -C^{\mathrm{T}}L^{T}P-\bar{G}_{kj}^{max^{T}}L^{T}P-PLC-PL\bar{G}_{kj}^{max}\}\\ +\sum_{k,j=1}^{m,n}\bar{\gamma}_{kj}^{min}\{\left(A+\bar{H}_{ij}^{min}\right)^{T}P+P\left(A+\bar{H}_{ij}^{min}\right)\\ -C^{\mathrm{T}}L^{T}P-\bar{G}_{kj}^{min^{T}}L^{T}P-PLC-PL\bar{G}_{kj}^{min}\}\end{array}\right)\right]<0 \quad (3.22)$$

However, it is still not possible to solve equation (3.19) and (3.20) for L and P because $\bar{\gamma}_{kj}^{max}, \bar{\gamma}_{kj}^{min}$ are time varying coefficients. Hence, to overcome this problem, we transform the problem in equations (3.19) and (3.20) to equations (3.23)-(3.26) which do not involve $\bar{\gamma}_{kj}^{max}$, and $\bar{\gamma}_{kj}^{min}$.

$$P\left(A+\bar{H}_{ij}^{max}\right)+\left(A+\bar{H}_{ij}^{max}\right)^{T}P-\left(C+\bar{G}_{kj}^{max}\right)^{T}L^{T}P-PL\left(C+\bar{G}_{kj}^{max}\right)<0, \quad (3.23)$$

$$P\left(A+\bar{H}_{ij}^{max}\right)+\left(A+\bar{H}_{ij}^{max}\right)^{T}P-\left(C+\bar{G}_{kj}^{min}\right)^{T}L^{T}P-PL\left(C+\bar{G}_{kj}^{min}\right)<0, \quad (3.24)$$

$$P\left(A+\bar{H}_{ij}^{min}\right)+\left(A+\bar{H}_{ij}^{min}\right)^{T}P-\left(C+\bar{G}_{kj}^{max}\right)^{T}L^{T}P-PL\left(C+\bar{G}_{kj}^{max}\right)<0, \quad (3.25)$$

$$P\left(A+\bar{H}_{ij}^{min}\right)+\left(A+\bar{H}_{ij}^{min}\right)^{T}P-\left(C+\bar{G}_{kj}^{min}\right)^{T}L^{T}P-PL\left(C+\bar{G}_{kj}^{min}\right)<0, \quad (3.26)$$

for $\forall i=1,\dots,n$, $\forall j=1,\dots,n$, and $\forall j=1,\dots,m$.

If equations (3.23)-(3.26) are satisfied, then equation (3.16) is automatically satisfied.

Corollary to Theorem 3: Bounded Jacobian Observer for Sparse Problems

For the class of systems and observer forms described in equations (3.1) and (3.2), if an observer gain matrix L can be chosen such that

$$
\begin{gathered}
P\left(A+\bar{H}_{ij}^{max}\right)+\left(A+\bar{H}_{ij}^{max}\right)^{T}P-\left(C+\bar{G}_{kj}^{max}\right)^{T}L^{T}P-PL\left(C+\bar{G}_{kj}^{max}\right)<0 \\
P\left(A+\bar{H}_{ij}^{max}\right)+\left(A+\bar{H}_{ij}^{max}\right)^{T}P-\left(C+\bar{G}_{kj}^{min}\right)^{T}L^{T}P-PL\left(C+\bar{G}_{kj}^{min}\right)<0 \\
P\left(A+\bar{H}_{ij}^{min}\right)+\left(A+\bar{H}_{ij}^{min}\right)^{T}P-\left(C+\bar{G}_{kj}^{max}\right)^{T}L^{T}P-PL\left(C+\bar{G}_{kj}^{max}\right)<0 \\
P\left(A+\bar{H}_{ij}^{min}\right)+\left(A+\bar{H}_{ij}^{min}\right)^{T}P-\left(C+\bar{G}_{kj}^{min}\right)^{T}L^{T}P-PL\left(C+\bar{G}_{kj}^{min}\right)<0 \\
P>0 \\
\forall i=1,\dots,n\,,\forall j=1,\dots,n \text{ and } \forall k=1,\dots,m
\end{gathered}
\tag{3.27}
$$

Where,

1) $h_{ij}^{max} \geq max\left(\partial\Phi_i/\partial x_j\right)$ and $h_{ij}^{min} \leq min\left(\partial\Phi_i/\partial x_j\right)$,
2) $H_{ij}^{max} = e_n(i)e_n^T(j)h_{ij}^{max}$ and $H_{ij}^{min} = e_n(i)e_n^T(j)h_{ij}^{min}$,
3) $\bar{z}_H = n \times n - w_H$ is the state scaling factor, n being dimension of the state vector, w_H being the number of terms in $\partial\Phi_i/\partial x_j$ that equals zero,
4) $\bar{H}_{ij}^{max} = \bar{z}_H H_{ij}^{max}$ and $\bar{H}_{ij}^{min} = \bar{z}_H H_{ij}^{min}$,
5) $g_{kj}^{max} \geq max\left(\partial\Psi_k/\partial x_j\right)$ and $g_{kj}^{min} \leq min\left(\partial\Psi_k/\partial x_j\right)$,
6) $G_{kj}^{max} = e_n(k)e_n^T(j)g_{kj}^{max}$and $G_{kj}^{min} = e_n(k)e_n^T(j)g_{kj}^{min}$,
7) $\bar{z}_G = m \times n - w_G$, is the state scaling factor, m being dimension of the output vector, w_G being the number of terms in $\partial\Psi_i/\partial x_j$ that equals zero,
8) $\bar{G}_{kj}^{max} = \bar{z}_G G_{kj}^{max}$ and $\bar{G}_{kj}^{min} = \bar{z}_G G_{kj}^{min}$,

then this choice of L leads to asymptotically stable estimates by the observer (3.2) for the system (3.1).

Proof: The proof of the Corollary follows along the same lines as the proof of theorem 3, except for the definition of the scaling factor $\bar{z}_H$ and $\bar{z}_G$.

In the general problem, if all of terms in $\partial\Phi_i/\partial x_j$ are not zero, then $\sum_{i,j=1}^{n,n}\left(\delta_{ij}^{max} + \delta_{ij}^{min}\right) = n \times n = z_H$ or if all of terms in $\partial\Psi_k/\partial x_j$ are not zero, then $\sum_{k,j=1}^{m,n}\left(\gamma_{kj}^{max} + \gamma_{kj}^{min}\right) = m \times n = z_G$. However, in some problems, if there exist $\partial\Phi_i/\partial x_j = 0$ or $\partial\Psi_k/\partial x_j = 0$, then $\sum_{i,j=1}^{n,n}\left(\delta_{ij}^{max} + \delta_{ij}^{min}\right)$ is less than z_H or $\sum_{k,j=1}^{m,n}\left(\gamma_{kj}^{max} + \gamma_{kj}^{min}\right)$ is less that z_G. We can then define new scaling factors, $\bar{z}_H$ and $\bar{z}_G$ as follows:

$$
\sum_{i,j=1}^{n,n}\left(\delta_{ij}^{max} + \delta_{ij}^{min}\right) = n \times n - w_H = \bar{z}_H \tag{3.28}
$$

$$
\sum_{k,j=1}^{m,n}\left(\gamma_{kj}^{max} + \gamma_{kj}^{min}\right) = m \times n - w_G = \bar{z}_G \tag{3.29}
$$

where w_H is the number of terms in $\partial\Phi_i/\partial x_j$ that equals zero and w_G is the number of terms in $\partial\Psi_k/\partial x_j$ that equals zero. Now, the use of $\bar{z}_H$ and $\bar{z}_G$ instead of z_H and z_G can be used to complete the proof.

3.4. Conclusions

In this chapter, a new observer design technique is developed for a nonlinear system with a locally or globally bounded Jacobian and a nonlinear output measurement equation. The results developed in chapters 2 and 3 will be extended to address disturbance estimation for nonlinear systems in chapter 4.

Chapter 4. Novel Unknown Inputs Nonlinear Observer

4.1. Introduction

This chapter extends the result in chapter 2 and chapter 3 and presents an observer design technique for an unknown inputs nonlinear system with a globally (or locally) bounded Jacobian. This observer can applied for an unknown inputs nonlinear system with nonlinear measurement model. The approach utilized is to use measurements and state estimates to express the unknown inputs and use the mean value theorem to express the nonlinear error dynamics as a convex combination of known matrices with time varying coefficients. The observer gains are then obtained by solving linear matrix inequalities. The developed approach can enable observer design for a large class of differentiable nonlinear systems with a globally (or locally) bounded Jacobian. The developed theory is used successfully in the design of observers for vehicle systems involving complex nonlinearities and unknown inputs. The use of the observer design technique is illustrated for estimation of roll angle and rollover index in chapter 5.

4.2. Problem Statement for Unknown Inputs Nonlinear Observer

This section presents an efficient methodology for designing observers for the class of nonlinear systems described by

$$\dot{x} = \bar{A}x + \eta(x,u) + \bar{B}\mu \tag{4.1}$$

$$z = Ex \tag{4.2}$$

$$y = Cx + \Psi(x) \tag{4.3}$$

where $u \in R^P$ are the known control inputs, $\mu \in R^P$ are the unknown inputs, $y \in R^m$ and $z \in R^q$ are the output measurements. $\bar{A} \in R^{n\times n}$, $\bar{B} \in R^{n\times p}$, $E \in R^{q\times n}$, and $C \in R^{m\times n}$ are appropriate matrices. The functions $\eta(x,u)$: $R^n \times R^p \to R^n$,and $\Psi(x)$: $R^n \to R^m$ are nonlinear. In addition, $\eta(x,u)$ and $\Psi(x)$ are assumed to be differentiable nonlinear functions with globally (or locally) bounded Jacobian.

The objective of this estimation problem is to quantitatively estimate the unknown inputs $\mu(t)$ and to estimate the state vector $x(t)$, given the output measurements $y(t)$ and $z(t)$. The approach to estimate unknown inputs will first be described in the section 4.3 and subsequently the nonlinear observer design technique will be described in the section 4.4.

The overall approach to the estimation problem is as follows:

1) The unknown inputs are estimated assuming that full state measurement is available. The algebraic relation between the unknown inputs, the states and outputs is developed.
2) Using the algebraic relation between the unknown inputs and states, a modified state introductions equations are developed which do not depend on the unknown inputs.
3) Stable observer design for the new modified nonlinear introductions ensures that the state and unknown inputs can both be estimated.

4.3. Unknown Input Estimation

To make the presentation easy to follow, we will consider single input nonlinear systems first. Then, we will extend the results to multi-input nonlinear systems.

4.3.1. Single Input Nonlinear Systems

Consider equations (4.1)-(4.3) when $p = 1$ (p is number of unknown inputs, μ) and $q = 1$ (q is number of output measurements, z).

Let the relative degree from μ to z be r_μ. Hence

$$E\bar{A}^i\bar{B} = 0, \qquad 0 \le i < r_\mu - 1 \tag{4.4}$$

$$E\bar{A}^{r_\mu - 1}\bar{B} \neq 0. \tag{4.5}$$

Define the relative degree $\boldsymbol{r_\eta}$ from the nonlinear function $\boldsymbol{\eta(x,u)}$ to $\boldsymbol{z}$ as the number of times the output $\boldsymbol{z}$ must be differentiated before the nonlinear function $\boldsymbol{\eta(x,u)}$ is encountered. In order words, $\boldsymbol{r_\eta}$ is defined as a whole number such that

$$E\bar{A}^i\eta(x,u) = 0, \qquad 0 \le i < r_\eta - 1 \tag{4.6}$$

$$E\bar{A}^{r_\eta - 1}\eta(x,u) \neq 0. \tag{4.7}$$

Theorem 4: Let the relative degrees from the input r_μ and from the nonlinearity r_η be such that $r_\eta \ge r_\mu$. Then the estimated unknown input is given by

$$\hat{\mu} = (E\bar{A}^{r_\mu - 1}\bar{B})^{-1}\left[z_f^{(r_\mu)} - E\bar{A}^{r_\mu}x - E\bar{A}^{r_\mu - 1}\eta(x,u)\right], \tag{4.8}$$

where we assume that the state variables, $\boldsymbol{x}$, are known, and the filtered derivatives of the output $\boldsymbol{z}$ are given by

$$\frac{d}{dt}\begin{bmatrix} z_f \\ \dot{z}_f \\ \vdots \\ z_f^{(r-1)} \end{bmatrix} = \begin{bmatrix} -\frac{1}{\tau} & 0 & 0 & 0 \\ -\frac{1}{\tau^2} & -\frac{1}{\tau} & \ddots & 0 \\ \ddots & \ddots & \ddots & 0 \\ -\frac{1}{\tau^{r-1}} & \cdots & -\frac{1}{\tau^2} & -\frac{1}{\tau} \end{bmatrix}\begin{bmatrix} z_f \\ \dot{z}_f \\ \vdots \\ z_f^{(r-1)} \end{bmatrix} + \begin{bmatrix} \frac{1}{\tau} \\ \frac{1}{\tau^2} \\ \vdots \\ \frac{1}{\tau^{r-1}} \end{bmatrix} z. \tag{4.9}$$

Proof: Since the relative degree of the system from the output z to the unknown input μ is r_μ, it follows that

$$z^{(r_\mu)} = (E\bar{A}^{r_\mu}x) + \left(E\bar{A}^{r_\mu - 1}\eta(x,u)\right) + E\bar{A}^{r_\mu - 1}\bar{B}\mu. \tag{4.10}$$

Since $\boldsymbol{E\bar{A}^{r_\mu - 1}\bar{B} \neq 0}$, it therefore follows that the unknown input is given by

$$\mu = (E\bar{A}^{r_\mu - 1}\bar{B})^{-1}\left[z^{(r_\mu)} - E\bar{A}^{r_\mu}x - E\bar{A}^{r_\mu - 1}\eta(x,u)\right] \tag{4.11}$$

Since z is measured but the r_μth derivative of the output z is not unavailable, we therefore use the following estimator for the unknown input.

$$\hat{\mu} = (E\bar{A}^{r_\mu - 1}\bar{B})^{-1}\left[z_f^{(r_\mu)} - E\bar{A}^{r_\mu}x - E\bar{A}^{r_\mu - 1}\eta(x,u)\right] \tag{4.12}$$

where $z_f^{(r)}$ is obtained from the r_μth order filter given in equation (4.9). Then, as the filter constant $\tau \to 0$, $\hat{\mu} \to \mu$ as $t \to \infty$.

4.3.2. Multi-Input Nonlinear System

Consider equations (4.1)-(4.3) when $p > 1$ (p is number of unknown inputs) and $q > 1$ (q is number of output measurements, z).

Let the vector relative degree of the system from the outputs z to the input μ be $[r_{\mu 1} \quad r_{\mu 2} \quad \cdots \quad r_{\mu q}]$. Let the relative degree from each of the outputs to the nonlinearity be $r_{\eta 1}, r_{\eta 2}, \ldots, r_{\eta(q-1)}$ and $r_{\eta q}$. Assume that $r_{\eta 1} \geq r_{\mu 1}, r_{\eta 2} \geq r_{\mu 2}, \ldots, r_{\eta(q-1)} \geq r_{\mu q}$ and $r_{\eta q} \geq r_{\mu q}$. It follows that

$$z_i^{(r_{\mu i})} = (E_i\bar{A}^{r_{\mu i}}x) + \left(E_i\bar{A}^{r_{\mu i}-1}\eta(x,u)\right) + E_i\bar{A}^{r_{\mu i}-1}\bar{B}\mu, \qquad i = 1,2,\ldots,q \tag{4.13}$$

Hence

$$\begin{bmatrix} z_1^{r_{\mu 1}} \\ z_2^{r_{\mu 2}} \\ \vdots \\ z_q^{r_{\mu q}} \end{bmatrix} = \begin{bmatrix} E_1\bar{A}^{r_{\mu 1}}x \\ E_2\bar{A}^{r_{\mu 2}}x \\ \vdots \\ E_q\bar{A}^{r_{\mu q}}x \end{bmatrix} + \begin{bmatrix} E_1\bar{A}^{r_{\mu 1}-1} \\ E_2\bar{A}^{r_{\mu 2}-1} \\ \vdots \\ E_q\bar{A}^{r_{\mu q}-1} \end{bmatrix}\eta(x,u) + \begin{bmatrix} E_1\bar{A}^{r_{\mu 1}-1}\bar{B} \\ E_2\bar{A}^{r_{\mu 2}-1}\bar{B} \\ \vdots \\ E_q\bar{A}^{r_{\mu q}-1}\bar{B} \end{bmatrix}\mu. \tag{4.14}$$

It therefore follows that the unknown inputs are given by

$$\begin{bmatrix} \mu_1 \\ \mu_2 \\ \vdots \\ \mu_q \end{bmatrix} = \begin{bmatrix} E_1\bar{A}^{r_{\mu 1}-1}\bar{B} \\ E_2\bar{A}^{r_{\mu 2}-1}\bar{B} \\ \vdots \\ E_q\bar{A}^{r_{\mu q}-1}\bar{B} \end{bmatrix}^{-1} \left\{ \begin{bmatrix} z_1^{r_{\mu 1}} \\ z_2^{r_{\mu 2}} \\ \vdots \\ z_q^{r_{\mu q}} \end{bmatrix} - \begin{bmatrix} E_1\bar{A}^{r_{\mu 1}}x \\ E_2\bar{A}^{r_{\mu 2}}x \\ \vdots \\ E_q\bar{A}^{r_{\mu q}}x \end{bmatrix} - \begin{bmatrix} E_1\bar{A}^{r_{\mu 1}-1} \\ E_2\bar{A}^{r_{\mu 2}-1} \\ \vdots \\ E_q\bar{A}^{r_{\mu q}-1} \end{bmatrix}\eta(x,u) \right\}. \tag{4.15}$$

Theorem 5: The estimated unknown inputs are given by

$$\begin{bmatrix}\hat{\mu}_1\\ \hat{\mu}_2\\ \vdots\\ \hat{\mu}_q\end{bmatrix}=\begin{bmatrix}E_1\bar{A}^{r_{\mu 1}-1}\bar{B}\\ E_2\bar{A}^{r_{\mu 2}-1}\bar{B}\\ \vdots\\ E_q\bar{A}^{r_{\mu q}-1}\bar{B}\end{bmatrix}^{-1}\left\{\begin{bmatrix}z_{1f}^{r_{\mu 1}}\\ z_{2f}^{r_{\mu 2}}\\ \vdots\\ z_{qf}^{r_{\mu q}}\end{bmatrix}-\begin{bmatrix}E_1\bar{A}^{r_{\mu 1}}x\\ E_2\bar{A}^{r_{\mu 2}}x\\ \vdots\\ E_q\bar{A}^{r_{\mu q}}x\end{bmatrix}-\begin{bmatrix}E_1\bar{A}^{r_{\mu 1}-1}\\ E_2\bar{A}^{r_{\mu 2}-1}\\ \vdots\\ E_q\bar{A}^{r_{\mu q}-1}\end{bmatrix}\eta(x,u)\right\} \tag{4.16}$$

where we assume that the state variables, x, are known and

$$\frac{d}{dt}\begin{bmatrix}z_{if}\\ \dot{z}_{if}\\ \vdots\\ z_{if}^{(r-1)}\end{bmatrix}=\begin{bmatrix}-\frac{1}{\tau} & 0 & 0 & 0\\ -\frac{1}{\tau^2} & -\frac{1}{\tau} & \ddots & 0\\ \ddots & \ddots & \ddots & 0\\ -\frac{1}{\tau^{r-1}} & \cdots & -\frac{1}{\tau^2} & -\frac{1}{\tau}\end{bmatrix}\begin{bmatrix}z_{if}\\ \dot{z}_{if}\\ \vdots\\ z_{if}^{(r-1)}\end{bmatrix}+\begin{bmatrix}\frac{1}{\tau}\\ \frac{1}{\tau^2}\\ \vdots\\ \frac{1}{\tau^{r-1}}\end{bmatrix}z_i,\qquad i=1,2,\dots,q \tag{4.17}$$

Proof: Follows along the same lines as the proof for Theorem 4.

4.4. Unknown Inputs Nonlinear Observer

In section 4.4, we have shown that the estimated unknown inputs, $\hat{\mu}$, can be estimated by using equation (4.16). So, we can substitute the unknown inputs, μ, by using equation (4.16). Then, the new dynamic equation for the nonlinear system is given by

$$\dot{x}=\bar{A}x+\eta(x,u)+\bar{B}\begin{bmatrix}E_1\bar{A}^{r_{\mu 1}-1}\bar{B}\\ E_2\bar{A}^{r_{\mu 2}-1}\bar{B}\\ \vdots\\ E_q\bar{A}^{r_{\mu q}-1}\bar{B}\end{bmatrix}^{-1}\left\{\begin{bmatrix}z_{1f}^{r_{\mu 1}}\\ z_{2f}^{r_{\mu 2}}\\ \vdots\\ z_{qf}^{r_{\mu q}}\end{bmatrix}-\begin{bmatrix}E_1\bar{A}^{r_{\mu 1}}x\\ E_2\bar{A}^{r_{\mu 2}}x\\ \vdots\\ E_q\bar{A}^{r_{\mu q}}x\end{bmatrix}-\begin{bmatrix}E_1\bar{A}^{r_{\mu 1}-1}\\ E_2\bar{A}^{r_{\mu 2}-1}\\ \vdots\\ E_q\bar{A}^{r_{\mu q}-1}\end{bmatrix}\eta(x,u)\right\} \tag{4.18}$$

Rearrange equation (4.18), as

$$\begin{aligned}\dot{x}&=Ax+\Phi(x,u)+g(z_f),\\ A&=\bar{A}-\bar{B}\begin{bmatrix}E_1\bar{A}^{r_{\mu 1}-1}\bar{B}\\ E_2\bar{A}^{r_{\mu 2}-1}\bar{B}\\ \vdots\\ E_q\bar{A}^{r_{\mu q}-1}\bar{B}\end{bmatrix}^{-1}\begin{bmatrix}E_1\bar{A}^{r_{\mu 1}}\\ E_2\bar{A}^{r_{\mu 2}}\\ \vdots\\ E_q\bar{A}^{r_{\mu q}}\end{bmatrix},\\ \Phi(x,u)&=\eta(x,u)-\bar{B}\begin{bmatrix}E_1\bar{A}^{r_{\mu 1}-1}\bar{B}\\ E_2\bar{A}^{r_{\mu 2}-1}\bar{B}\\ \vdots\\ E_q\bar{A}^{r_{\mu q}-1}\bar{B}\end{bmatrix}\begin{bmatrix}E_1\bar{A}^{r_{\mu 1}-1}\\ E_2\bar{A}^{r_{\mu 2}-1}\\ \vdots\\ E_q\bar{A}^{r_{\mu q}-1}\end{bmatrix}\eta(x,u),\end{aligned} \tag{4.19}$$

$$g(z_f) = \bar{B}\begin{bmatrix} E_1\bar{A}^{r_{\mu 1}-1}\bar{B} \\ E_2\bar{A}^{r_{\mu 2}-1}\bar{B} \\ \vdots \\ E_q\bar{A}^{r_{\mu q}-1}\bar{B} \end{bmatrix}^{-1}\begin{bmatrix} z_{1f}^{r_{\mu 1}} \\ z_{2f}^{r_{\mu 2}} \\ \vdots \\ z_{qf}^{r_{\mu q}} \end{bmatrix}$$

where z_f is the derivative of the output z.

4.4.1. Nonlinear Observer

We have substituted for the unknown inputs, μ by using equation (4.16). Now, we need to design a nonlinear observer for a nonlinear system described by

$$\begin{aligned} \dot{x} &= Ax + \Phi(x,u) + g(z_f), \\ y &= Cx + \Psi(x). \end{aligned} \tag{4.20}$$

Note: Φ and Ψ are assumed to be differentiable and z_f is the derivative of the output z.

The observer for this problem will be assumed to be of the form

$$\begin{aligned} \dot{\hat{x}} &= A\hat{x} + \Phi(\hat{x}) + g(y,u) + L(y-\hat{y}), \\ \hat{y} &= C\hat{x} + \Psi(\hat{x}). \end{aligned} \tag{4.21}$$

Since the nonlinear system described by equation (4.20) is the same as that described by equation (3.1) in chapter 3, we can directly apply Theorem 3 or Corollary to Theorem 3 to design an observer. The Corollary to Theorem 3 will be repeated as follows:

Corollary to Theorem 3: Bounded Jacobian Observer for Sparsely Nonlinear Systems

For the class of systems and observer forms described in equations (4.20) and (4.21), if an observer gain matrix L can be chosen such that

$$\begin{gathered} P\left(A+\bar{H}_{ij}^{max}\right)+\left(A+\bar{H}_{ij}^{max}\right)^T P-\left(C+\bar{G}_{kj}^{max}\right)^T L^T P-PL\left(C+\bar{G}_{kj}^{max}\right)<0 \\ P\left(A+\bar{H}_{ij}^{max}\right)+\left(A+\bar{H}_{ij}^{max}\right)^T P-\left(C+\bar{G}_{kj}^{min}\right)^T L^T P-PL\left(C+\bar{G}_{kj}^{min}\right)<0 \\ P\left(A+\bar{H}_{ij}^{min}\right)+\left(A+\bar{H}_{ij}^{min}\right)^T P-\left(C+\bar{G}_{kj}^{max}\right)^T L^T P-PL\left(C+\bar{G}_{kj}^{max}\right)<0 \\ P\left(A+\bar{H}_{ij}^{min}\right)+\left(A+\bar{H}_{ij}^{min}\right)^T P-\left(C+\bar{G}_{kj}^{min}\right)^T L^T P-PL\left(C+\bar{G}_{kj}^{min}\right)<0 \\ P>0 \\ \forall i=1,\ldots,n\,,\forall j=1,\ldots,n \text{ and } \forall k=1,\ldots,m \end{gathered} \tag{4.22}$$

where,

1) $h_{ij}^{max} \geq max\left(\partial\Phi_i/\partial x_j\right)$ and $h_{ij}^{min} \leq min\left(\partial\Phi_i/\partial x_j\right)$,
2) $H_{ij}^{max} = e_n(i)e_n^T(j)h_{ij}^{max}$ and $H_{ij}^{min} = e_n(i)e_n^T(j)h_{ij}^{min}$,

3) $\bar{z}_H = n \times n - w_H$ is the state scaling factor, n being dimension of the state vector, w_H being the number of terms in $\partial\Phi_i/\partial x_j$ that equals zero,
4) $\bar{H}_{ij}^{max} = \bar{z}_H H_{ij}^{max}$ and $\bar{H}_{ij}^{min} = \bar{z}_H H_{ij}^{min}$,
5) $g_{kj}^{max} \geq max\left(\partial\Psi_k/\partial x_j\right)$ and $g_{kj}^{min} \leq min\left(\partial\Psi_k/\partial x_j\right)$,
6) $G_{kj}^{max} = e_n(k)e_n^T(j)g_{kj}^{max}$ and $G_{kj}^{min} = e_n(k)e_n^T(j)g_{kj}^{min}$,
7) $\bar{z}_G = m \times n - w_G$, is the state scaling factor, m being dimension of the output vector, w_G being the number of terms in $\partial\Psi_i/\partial x_j$ that equals zero,
8) $\bar{G}_{kj}^{max} = \bar{z}_G G_{kj}^{max}$ and $\bar{G}_{kj}^{min} = \bar{z}_G G_{kj}^{min}$,

then this choice of L leads to asymptotically stable estimates by the observer (4.21) for the system (4.20).

4.5. Conclusions

In this chapter, a new observer design technique is developed for an unknown inputs nonlinear system with a locally or globally bounded Jacobian. The approach is developed in order to deal with differentiable nonlinear systems with unknown inputs. The observer gains can be obtained by solving LMIs. The use of the observer design technique is illustrated for estimation of roll angle and rollover index in chapter 5.

Chapter 5. Application of Nonlinear Observer to Rollover Index Estimation for Tripped and Un-Tripped Rollovers

In order to predict tripped and un-tripped rollovers, as described in chapter 1, many variables need to be known. However, some variables such as unknown road inputs, vertical displacements of unsprung masses and sprung mass, and the unknown lateral force input cannot be directly measured by sensors. Therefore, two different algorithms to estimate the rollover index for tripped and un-tripped rollovers have been developed.

The first algorithm is an approach to estimate unknown disturbance inputs in a nonlinear system using dynamic model inversion and a modified version of the mean value theorem, as described in chapter 4. The developed theory is used to estimate vertical tire forces and predict tripped rollovers in situations involving road bumps, potholes, and lateral unknown force inputs.

The second algorithm utilizes a new algebraic formulation of the new rollover index. This algorithm is simple and convenient but can be used only if the roll angle and vertical accelerations at multiple locations on the vehicle body are available as measurements.

5.1. Summary

Accurate detection of the danger of an impending rollover is necessary for active vehicle rollover prevention systems. A real-time rollover index is an indicator used for this purpose. A traditional rollover index utilizes lateral acceleration measurements and can detect only un-tripped rollovers that happen due to high lateral acceleration from a sharp turn. It cannot detect tripped rollovers that happen due to tripping from external inputs such as forces when a vehicle strikes a curb or a road bump. Therefore, this project develops a new rollover index that can detect both tripped and un-tripped rollovers.

5.2. Introduction

Vehicles with increased dimensions and weights are known to be at higher risk of rollover. Normally, rollovers occur in one of two ways, tripped and un-tripped [1]. The two types of rollovers are shown in Figure 5.1. A tripped rollover happens due to tripping from external inputs. An example of this rollover happens when a vehicle leaves the roadway and slides sideways, digging its tires into soft soil or striking an object such as a curb or guardrail. An un-tripped rollover, on the other hand, happens due to high lateral acceleration from a sharp turn and not due to external inputs. An example of an un-tripped rollover is when a vehicle makes a sharp collision avoidance lane change maneuver or a cornering maneuver at high speed, and consequently rolls over.

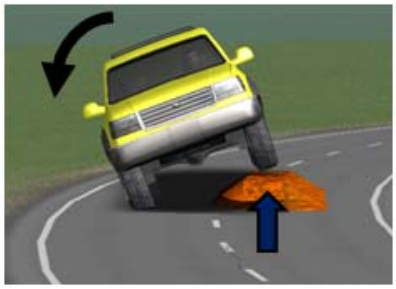

a) Tripped Rollver

b) Un-tripped Rollover

Figure 5.1: Type of Rollover

An active rollover prevention system is a vehicle stability control system that prevents vehicles from un-tripped rollovers. It has been developed by several automotive manufacturers [15], [2], e.g. Ford and Volvo. To the best of the authors' knowledge, there are no assistance systems currently available that directly address tripped rollovers. Several types of actuation systems can be used in rollover prevention. A differential braking system has received the most attention from researchers [16], [17], [18] and is used for preventing rollovers by reducing the yaw rate of a vehicle and its speed. Also, steer-by-wire and active suspension systems can be potentially used to prevent rollovers [7], [19].

In order to make these systems effective in their tasks, accurate detection of the danger of un-tripped and tripped vehicle rollovers is necessary [2]. To detect a vehicle rollover, many researchers have developed a real-time index that provides an indication of the danger of rollover. However, they have focused on developing an indicator only for un-tripped rollovers. There are no currently published papers that have studied how to detect tripped vehicle rollovers with unknown external inputs.

In this chapter, we present a method of estimating vehicle states based on a nonlinear vehicle model. The estimated vehicle states are used to calculate unknown normal tire forces, and a rollover index that can detect both un-tripped and tripped rollovers. The method is suitable for a large range of operating conditions. To begin with, we will introduce the vehicle rollover index in section 5.3. Then the vehicle dynamic model is presented in section 5.4. In section 5.5, we apply the new observer design of chapter 4 to the vehicle problem. After that, in section 5.6, we evaluate the developed estimation algorithm by implementing it in CARSIM, an industry standard vehicle dynamics simulation software. Moreover, we evaluate the estimation algorithm with experimental tests on a $1/8^{th}$ scaled vehicle in section 5.7. An alternate rollover index with additional measurements will be presented in section 5.8. Finally, the conclusions are presented in section 5.9.

5.3. Vehicle Rollover Index

Initially, the concept of a static rollover threshold called the static stability factor (SSF) [3], [20] was studied to detect vehicle rollovers. However, the SSF by itself is not adequate for rollover prediction in dynamic situations. After that the concept of a rollover index has been introduced. A rollover index has also been known by other names such as Roll Safety Factor (RSF) and Load Transfer Ratio (LTR). A rollover index is a real-time variable used for rollover prevention. A simple method of defining the rollover index is based on the use of the real-time difference

in vertical tire loads between left and right sides of the vehicle, as shown in Figure 5-2. The formula of the rollover index is described by equation (5.1) [21].

$$R = \frac{F_{zr} - F_{zl}}{F_{zr} + F_{zl}}, \qquad -1 \le R \le 1 \tag{5.1}$$

where $\boldsymbol{F_{zr}}$ and $\boldsymbol{F_{zl}}$ are the right and left vertical tire forces of a vehicle respectively. When $\boldsymbol{R = 1}$ ($\boldsymbol{F_{zl} = 0}$) or $\boldsymbol{R = -1}$ ($\boldsymbol{F_{zr} = 0}$), the left or right wheels lift off. Thus $\boldsymbol{R}$ should be prevented from approaching $\mathbf{1}$ or $\mathbf{-1}$. It should be noted that when a vehicle is traveling straight, $\boldsymbol{F_{zr}}$ equals to $\boldsymbol{F_{zl}}$ and $\boldsymbol{R = 0}$.

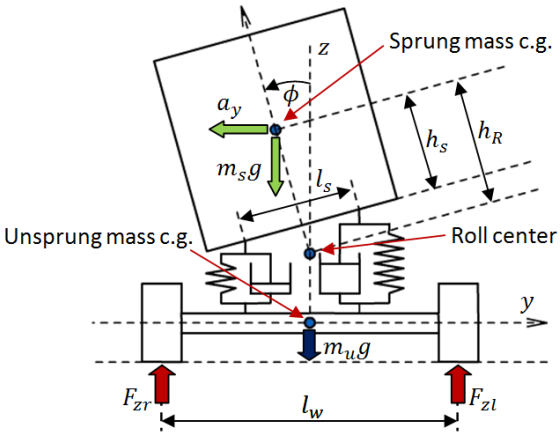

Figure 5.2: Vehicle Model for Un-Tripped Rollovers

The definition of R in equation (5.1) cannot be easily implemented in real-time because the vertical tire forces F_{zr} and F_{zl} cannot be directly measured. Thus, many researchers have tried to derive an estimation of the rollover index based on a 1-degree of freedom model as shown in Figure 5.2. The 1-degree of freedom is the roll angle ϕ of the vehicle body. Such an example of a traditional rollover index calculated using a one degree of freedom is shown below in equation (5.2):

$$R = \frac{F_{zr} - F_{zl}}{F_{zr} + F_{zl}} = \frac{2m_s a_y h_R}{mgl_w} + \frac{2m_s h_R tan\phi}{ml_w} \tag{5.2}$$

where $m = m_s + m_u$, h_R is c.g. height, l_w is track width, m_u is unsprung mass, m_s is spung mass, a_y is lateral acceleration, and ϕ is roll angle.

This type of rollover index is used for detecting un-tripped rollovers only. It is a function of lateral acceleration and roll angle. Some papers have proposed a rollover index that uses only lateral acceleration [8], [9] since roll angle is expensive to measure. The stability control with this rollover index may arbitrarily reduce the lateral acceleration capability of the vehicle. Also, as we shall show, it still fails to detect rollovers when rollovers are induced by vertical road inputs or other external inputs.

In order to detect tripped rollovers, which happen due to tripping from external inputs, a new rollover index should include the influence of road and other external inputs. Figure 5.3 shows a vehicle rollover model that includes the influence of road inputs, z_{rr} and z_{rl}. The figure also shows the normal forces on the vehicle, F_{zr} and F_{zl}.

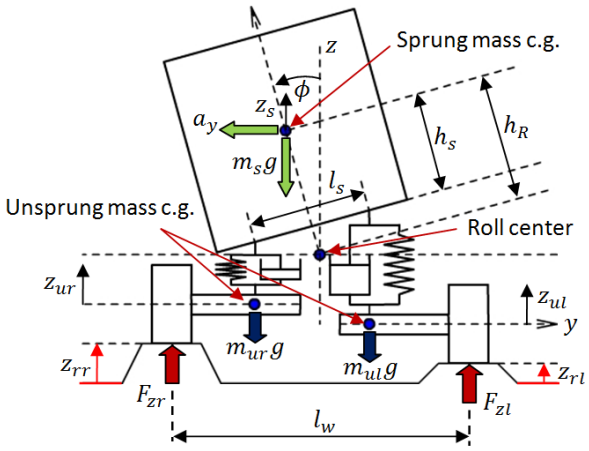

Figure 5.3: Vehicle Model for Un-Tripped and Tripped Rollovers

To derive a rollover index in this case, four-degrees of freedom in the model are needed as described in section 5.4. When the influence of road inputs is included, the normal forces on the vehicle, F_{zr} and F_{zl}, are defined by

$$F_{zr} = -F_{tr} + m_{ur}g + \frac{m_s}{2}g, \tag{5.3}$$

$$F_{zl} = -F_{tl} + m_{ul}g + \frac{m_s}{2}g \tag{5.4}$$

where F_{tr} and F_{tl} are the right and left dynamic vertical tire forces, and m_{ur} and m_{ul}, are right and left unsprung masses.

The right and left dynamic vertical tire forces, F_{tr} and F_{tl}, can be calculated by

$$F_{tr} = k_t(z_{ur} - z_{rr}), \tag{5.5}$$

$$F_{tl} = k_t(z_{ul} - z_{rl}) \tag{5.6}$$

where k_t is vertical tire stiffness, z_{rr} and z_{rl} are right and left unknown road profile inputs, z_{ur} and z_{ul} are right and left unsprung mass positions.

It should be noted that the right and left unsprung mass positions, z_{ur} and z_{ul}, depend on the dynamic motions of the heave z_s (sprung mass position), roll angle ϕ of the vehicle body, and the vertical motion of each side of the unsprung masses, z_{ur} and z_{ul}. Therefore, the measurements of roll angle, ϕ, and lateral acceleration, a_y, alone are not enough to calculate the rollover index for predicting tripped rollover. A lot of additional variables need to be measured or estimated. Moreover, some variables such as unknown road inputs, z_{rr} and z_{rl}, vertical displacements of unsprung masses, and sprung mass, cannot be directly measured by sensors.

Therefore, it is necessary to develop an approach for estimating the normal forces of a vehicle, F_{zr} and F_{zl} using available sensors only.

In the next section, we will present the vehicle dynamic model for un-tripped and tripped rollovers. We will write the model in a form that is suitable for estimating the unknown normal forces of a vehicle, F_{zr} and F_{zl}. Subsequently the rollover index can be calculated.

5.4. Vehicle Dynamics Model [22]

In order to obtain the rollover index for predicting tripped rollovers, a model of a vehicle with 4-degrees of freedom is needed as shown in Figure 5.4. The vehicle body is represented by the sprung mass m_s while the mass due to the axles and tires are represented by unsprung masses m_{ul} and m_{ur}. The springs and dampers between the sprung and unsprung masses represent the vehicle suspension. The vertical tire stiffness of each side of the vehicle is represented by the spring k_t.

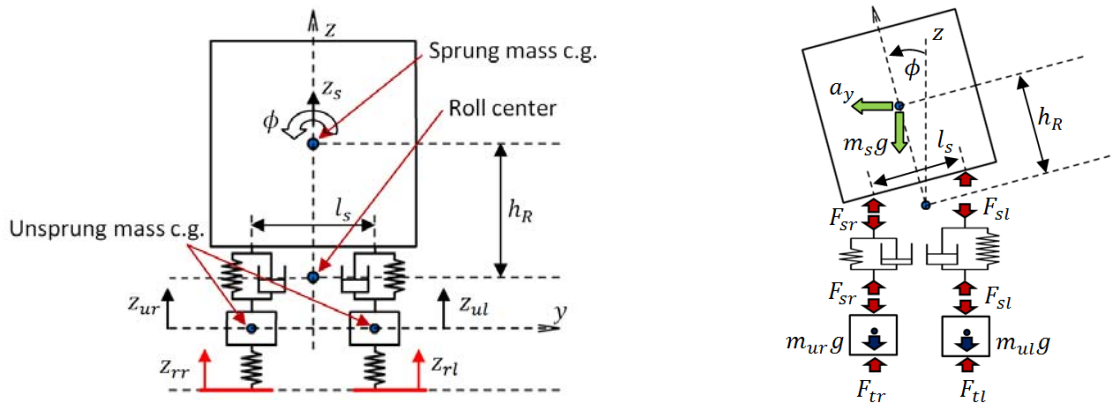

Figure 5.4: Four-Degrees of Freedom Vehicle Model.

The 4-degrees of freedom of the model are the heave z_s, roll angle ϕ of the vehicle body, and the vertical motion of each side of the unsprung masses, z_{ur} and z_{ul}. The variables z_{rr} and z_{rl} are the road profile inputs that excite the system.

The dynamic suspension forces are given by

$$F_{sr} = -k(z_s - z_{ur}) + k\frac{l_s}{2}sin\phi - d(\dot{z}_s - \dot{z}_{ur}) + d\frac{l_s}{2}\dot{\phi}cos\phi, \tag{5.7}$$

$$F_{sl} = -k(z_s - z_{ul}) - k\frac{l_s}{2}sin\phi - d(\dot{z}_s - \dot{z}_{ul}) - d\frac{l_s}{2}\dot{\phi}cos\phi \tag{5.8}$$

where k is suspension stiffness, d is suspension damping. z_s, z_{ur}, and z_{ul} are measured from their equilibrium points.

Then, the dynamic equations of sprung mass heave and sprung mass roll motions are given by (5.9) and (5.10).

$$\ddot{z}_s = -\frac{k}{m_s}(z_s - z_{ur}) - \frac{d}{m_s}(\dot{z}_s - \dot{z}_{ur}) - \frac{k}{m_s}(z_s - z_{ul}) - \frac{d}{m_s}(\dot{z}_s - \dot{z}_{ul}) \tag{5.9}$$

$$\begin{aligned}\ddot{\phi} = {} & \frac{kl_s}{2I}(z_s - z_{ur}) + \frac{dl_s}{2I}(\dot{z}_s - \dot{z}_{ur}) - \frac{kl_s}{2I}(z_s - z_{ul}) - \frac{dl_s}{2I}(\dot{z}_s - \dot{z}_{ul}) \\ & + \left(\frac{m_s g h_R}{I} - \frac{kl_s^2}{2I}\right) sin\phi - \frac{dl_s^2}{2I}\dot{\phi} cos\phi + \frac{m_s a_y h_R}{I} cos\phi\end{aligned} \tag{5.10}$$

where I is moment of inertia, and l_s is distance between right and left suspension. It should be noted that the roll dynamics depend on the lateral dynamics through the lateral acceleration term a_y. By avoiding further expansion of this term in terms of lateral tire forces and lateral dynamic states, a complicated coupled set of equations between roll and lateral dynamics is avoided. Instead, the variable a_y is assumed to be measured.

Assume that $m_{ur} = m_{ul} = m_u$. Then, the dynamic models of the right and left unsprung mass motions are given by

$$\ddot{z}_{ur} = \frac{k}{m_u}(z_s - z_{ur}) - \frac{d}{m_u}(\dot{z}_s - \dot{z}_{ur}) - \frac{kl_s}{2m_u} sin\phi - \frac{dl_s}{2m_u}\dot{\phi} cos\phi - \frac{F_{tr}}{m_u}, \tag{5.11}$$

$$\ddot{z}_{ul} = \frac{k}{m_u}(z_s - z_{ul}) - \frac{d}{m_u}(\dot{z}_s - \dot{z}_{ul}) + \frac{kl_s}{2m_u} sin\phi + \frac{dl_s}{2m_u}\dot{\phi} cos\phi - \frac{F_{tl}}{m_u}. \tag{5.12}$$

The equations (5.3) and (5.4) show that the normal forces on the vehicle, F_{zr} and F_{zl}, can be computed if we know the right and left vertical tire forces, F_{tr} and F_{tl}.

In order to design an observer to estimate the variables used to calculate the rollover index, we need to rewrite equations (5.9)-(5.12) into a state space form. The state space form of equations (5.9)-(5.12) is shown in equation (5.13).

$$\dot{x} = \bar{A}x + \eta(x, u) + \bar{B}\mu \tag{5.13}$$

where u is the vector of known inputs, μ is the vector of unknown inputs,

$$x = [z_s - z_{ur} \quad \dot{z}_s - \dot{z}_{ur} \quad z_s - z_{ul} \quad \dot{z}_s - \dot{z}_{ul} \quad \phi \quad \dot{\phi}]^T,$$

$$\bar{A} = \begin{bmatrix} 0 & 1 & 0 & 0 & 0 & 0 \\ -\frac{k}{m_s} - \frac{k}{m_u} & -\frac{d}{m_s} - \frac{d}{m_u} & -\frac{k}{m_s} & -\frac{d}{m_s} & 0 & 0 \\ 0 & 0 & 0 & 1 & 0 & 0 \\ -\frac{k}{m_s} & -\frac{d}{m_s} & -\frac{k}{m_s} - \frac{k}{m_u} & -\frac{d}{m_s} - \frac{d}{m_u} & 0 & 0 \\ 0 & 0 & 0 & 0 & 0 & 1 \\ \frac{kl_s}{2I} & \frac{dl_s}{2I} & -\frac{kl_s}{2I} & -\frac{dl_s}{2I} & 0 & 0 \end{bmatrix}, \tag{5.14}$$

$$\eta(x,u)=\begin{bmatrix} 0 \\ +\frac{kl_s}{2m_u}sin\phi+\frac{dl_s}{2m_u}\dot{\phi}cos\phi \\ 0 \\ -\frac{kl_s}{2m_u}sin\phi-\frac{dl_s}{2m_u}\dot{\phi}cos\phi \\ 0 \\ +\frac{m_s a_y h_R}{I}cos\phi+\left(\frac{m_s g h_R}{I}-\frac{kl_s^2}{2I}\right)sin\phi-\frac{dl_s^2}{2I}\dot{\phi}cos\phi \end{bmatrix},$$

$$\bar{B}=\begin{bmatrix} 0 & 0 \\ \frac{1}{m_u} & 0 \\ 0 & 0 \\ 0 & \frac{1}{m_u} \\ 0 & 0 \\ 0 & 0 \end{bmatrix}, \mu=\begin{bmatrix} F_{tr} \\ F_{tl} \end{bmatrix}.$$

The available measurements used to estimate variables is shown in equation (5.15) and (5.17).

$$z=Ex+\beta(x,u)+b\mu \tag{5.15}$$

where

$$z=\begin{bmatrix} \ddot{z}_{ur} \\ \ddot{z}_{ul} \end{bmatrix}, E=\begin{bmatrix} \frac{k}{m_u} & \frac{d}{m_u} & 0 & 0 & 0 & 0 \\ 0 & 0 & \frac{k}{m_u} & \frac{d}{m_u} & 0 & 0 \end{bmatrix},$$
$$\beta=\begin{bmatrix} -\frac{kl_s}{2m_u}sin\phi-\frac{dl_s}{2m_u}\dot{\phi}cos\phi \\ +\frac{kl_s}{2m_u}sin\phi+\frac{dl_s}{2m_u}\dot{\phi}cos\phi \end{bmatrix}, b=\begin{bmatrix} -\frac{1}{m_u} & 0 \\ 0 & -\frac{1}{m_u} \end{bmatrix}. \tag{5.16}$$

$$y=Cx+\Psi(x) \tag{5.17}$$

where

$$y=\begin{bmatrix} z_s-z_{ur}-\frac{l_s}{2}sin\phi \\ \dot{\phi} \end{bmatrix}, C=\begin{bmatrix} 1 & 0 & 0 & 0 & 0 & 0 \\ 0 & 0 & 0 & 0 & 0 & 1 \end{bmatrix}, \Psi=\begin{bmatrix} -\frac{l_s}{2}sin\phi \\ 0 \end{bmatrix}. \tag{5.18}$$

It is desired to use an observer based on the above vehicle model to estimate variables. The equations (5.13) and (5.17) show that we have the nonlinear terms, η and Ψ, and the unknown inputs μ included in the dynamic and measurement equations. Also, the relative degree for this problem is zero, $r_\mu=0$. We do not have to differentiate the equation (5.15). The measurements, z, directly relate to the unknown inputs, μ. Thus, the dynamic and measurement equations of this problem are in the appropriate state space form for applying the nonlinear observer described in chapter 8 to solve the problem.

The form of equations (5.13), (5.15), and (5.17) is the same as the form of equations (4.1)-(4.3). So, we can design a nonlinear observer for this problem.

5.5. Observer Design for the Vehicle Problem

In this section, we will apply Theorem 5 and the Corollary to Theorem 3 for the estimation problem. To apply them, first, we need to calculate the matrix A. Then, the observability of the pair of (A, C) needs to be examined. If the pair of (A, C) is detectable, we can apply Corollary to Theorem 3 for observer gains.

Using Theorem 5, the unknown inputs, μ, can be computed by

$$\mu = b^{-1}[z - Ex - \beta(x,u)] \tag{5.19}$$

Substitute equation (5.19) into (5.13).

$$\dot{x} = \bar{A}x + \eta(x,u) + \bar{B}b^{-1}[z - Ex - \beta(x,u)] \tag{5.20}$$

$$\dot{x} = (\bar{A} - \bar{B}b^{-1}E)x + \eta(x,u) - \bar{B}b^{-1}\beta(x,u) + \bar{B}b^{-1}z \tag{5.21}$$

Then, $A, \Phi, g(z_f)$ are given by

$$A = (\bar{A} - \bar{B}b^{-1}E), \qquad \Phi = \eta(x,u) - \bar{B}b^{-1}\beta(x,u), \qquad g(z_f) = \bar{B}b^{-1}z \tag{5.22}$$

However, we found that the pair (A, C) is unobservable. With this system, we cannot directly design an observer for this problem. We need to modify the equations (5.13) and (5.14).

The modified model is given by

$$\dot{x} = \bar{A}x + \eta(x,u) + \bar{B}\mu \tag{5.23}$$

$$x = [z_s - z_{ur} \quad \dot{z}_s - \dot{z}_{ur} \quad z_s - z_{ul} \quad \dot{z}_s - \dot{z}_{ul} \quad \phi \quad \dot{\phi}]^T, \tag{5.24}$$

$$\bar{A} = \begin{bmatrix} 0 & 1 & 0 & 0 & 0 & 0 \\ -\frac{k}{m_s} - \frac{k}{m_u} & -\frac{d}{m_s} - \frac{d}{m_u} & -\frac{k}{m_s} & -\frac{d}{m_s} & 0 & 0 \\ 0 & 0 & 0 & 1 & 0 & 0 \\ -\frac{k}{m_s} & -\frac{d}{m_s} & -\frac{k}{m_s} - \frac{k}{m_u} & -\frac{d}{m_s} - \frac{d}{m_u} & 0 & 0 \\ 0 & 0 & 0 & 0 & 0 & 1 \\ \frac{kl_s}{2I} & \frac{dl_s}{2I} & -\frac{kl_s}{2I} & -\frac{dl_s}{2I} & -a_{65} & -a_{66} \end{bmatrix}, \tag{5.25}$$

$$\eta(x,u)=\begin{bmatrix} 0 \\ +\frac{kl_s}{2m_u}sin\phi+\frac{dl_s}{2m_u}\dot{\phi}cos\phi \\ 0 \\ -\frac{kl_s}{2m_u}sin\phi-\frac{dl_s}{2m_u}\dot{\phi}cos\phi \\ 0 \\ +\frac{m_s a_y h_R}{I}cos\phi+\left(\frac{m_s g h_R}{I}-\frac{kl_s^2}{2I}\right)sin\phi-\frac{dl_s^2}{2I}\dot{\phi}cos\phi+a_{65}\phi+a_{66}\dot{\phi} \end{bmatrix},$$

$$\bar{B}=\begin{bmatrix} 0 & 0 \\ \frac{1}{m_u} & 0 \\ 0 & 0 \\ 0 & \frac{1}{m_u} \\ 0 & 0 \\ 0 & 0 \end{bmatrix}, \mu=\begin{bmatrix} F_{tr} \\ F_{tl} \end{bmatrix}$$

where $a_{65}>0$, $a_{66}>0$.

The modified model is valid for designing an observer since the original model includes stabilized terms, $\left(\frac{m_s g h_R}{I}-\frac{kl_s^2}{2I}\right)sin\phi$ and $-\frac{dl_s^2}{2I}\dot{\phi}cos\phi$. Now, the modified model will be unobservable only when $\phi=0$.

To make the problem easy to solve, the measurement model is given by

$$y=\begin{bmatrix} z_s-z_{ur}-\frac{l_s}{2}sin\phi \\ \dot{\phi} \end{bmatrix}=\begin{bmatrix} 1 & 0 & 0 & 0 & -c_{15} & 0 \\ 0 & 0 & 0 & 0 & 0 & 1 \end{bmatrix}x+\begin{bmatrix} -\frac{l_s}{2}sin\phi+c_{15}\phi \\ 0 \end{bmatrix}. \quad (5.26)$$

where $c_{15}>0$. With this modification, bounds on the Jacobian of the nonlinear function are decreased.

5.5.1. Observer Design Using Corollary to Theorem 3 in Chapter 4

Apply Corollary to Theorem 3 for the problem. The nonlinear function Φ is

$$\Phi=\eta(x,u)-\bar{B}b^{-1}\beta(x,u)$$

$$=\begin{bmatrix} 0 \\ 0 \\ 0 \\ 0 \\ 0 \\ +\frac{m_s a_y h_R}{I}cos\phi+\left(\frac{m_s g h_R}{I}-\frac{kl_s^2}{2I}\right)sin\phi-\frac{dl_s^2}{2I}\dot{\phi}cos\phi+a_{65}\phi+a_{66}\dot{\phi} \end{bmatrix} \quad (5.27)$$

For the nonlinear function in equations (5.27), the scaling factor $\bar{z}_H$ is 2. Since $\Phi_1, \Phi_2, \ldots, \Phi_5 = 0$, and $\frac{\partial \Phi_6}{\partial x_{i=1:4}} = 0$ then $w_H = 34$ and the scaling factor $\bar{z}_H$ is $n \times n - w_H$. ($\bar{z}_H = 6 \times 6 - 34 = 2$). Then, the jacobian of the nonlinear function Φ is computed to find $\bar{H}_{65}^{max}, \bar{H}_{66}^{max}$ and $\bar{H}_{65}^{min}, \bar{H}_{66}^{min}$. (Note: we can choose a_{65}, a_{66} such that $|\bar{H}_{ij}^{max}|$ and $|\bar{H}_{ij}^{min}|$ are small.)

$$\frac{\partial \Phi_6}{\partial \phi} = -\frac{m_s a_y h_R}{I} sin\phi + \left(\frac{m_s g h_R}{I} - \frac{k l_s^2}{2I}\right) cos\phi + \frac{d l_s^2}{2I} \dot{\phi} sin\phi + a_{65} \tag{5.28}$$

$$\frac{\partial \Phi_6}{\partial \dot{\phi}} = -\frac{d l_s^2}{2I} cos\phi + a_{66} \tag{5.29}$$

$$\bar{H}_{65}^{max}(6,5) = 2 \times \max\left(\frac{\partial \Phi_6}{\partial \phi}\right), \qquad \bar{H}_{65}^{min}(6,5) = 2 \times \min\left(\frac{\partial \Phi_6}{\partial \phi}\right) \tag{5.30}$$

$$\bar{H}_{66}^{max}(6,6) = 2 \times \max\left(\frac{\partial \Phi_6}{\partial \dot{\phi}}\right), \qquad \bar{H}_{66}^{min}(6,6) = 2 \times \min\left(\frac{\partial \Phi_6}{\partial \dot{\phi}}\right) \tag{5.31}$$

(The other elements of $\bar{H}^{max}$ and $\bar{H}^{min}$ are zeros.)

The nonlinear function Ψ is

$$\Psi = \begin{bmatrix} -\frac{l_s}{2} sin\phi + c_{15}\phi \\ 0 \end{bmatrix}. \tag{5.32}$$

For the nonlinear function in equation (5.32), the scaling factor $\bar{z}_G$ is 1. Since $\Psi_2 = 0$ and $\frac{\partial \Psi_1}{\partial x_{i=1:4,6}} = 0$ the scaling factor $\bar{z}_G$ is $m \times n - w_G$. ($\bar{z}_G = 2 \times 6 - 11 = 1$). Then, the jacobian of the nonlinear function Ψ is computed to find $\bar{G}_{15}^{max}$ and $\bar{G}_{16}^{min}$. (Note: we can choose a_{65}, a_{66} such that $|\bar{G}_{ij}^{max}|$ and $|\bar{G}_{ij}^{min}|$ are small.)

$$\frac{\partial \Psi_1}{\partial \phi} = -\frac{l_s}{2} + c_{15} \tag{5.33}$$

$$\bar{G}_{15}^{max}(1,5) = 1 \times \max\left(\frac{\partial \Psi_1}{\partial \phi}\right), \qquad \bar{G}_{15}^{min}(1,5) = 1 \times \min\left(\frac{\partial \Psi_1}{\partial \phi}\right) \tag{5.34}$$

(The other elements of $\bar{G}^{max}$ and $\bar{G}^{min}$ are zeros.)

Next, we solve equations (4.22) for the observer gain using the LMI toolbox in Matlab. (Note: The LMI toolbox in Matlab provides only one gain, though theoretically many solutions can exist to the LMI (4.22). If a faster convergence rate is desired, the RHS in equation (4.22) could be replaced by a negative definite matrix instead of zero.)

5.6. Simulation and Simulation Results

5.6.1. Simulation Setup

In this section, we will evaluate the algorithm described in the previous section in simulations by implementing it in CARSIM, an industry standard vehicle dynamics simulation software. The vehicle model from CARSIM chosen for this simulation is a standard SUV.

In the simulation, we simulate the case that the SUV vehicle strikes road bumps during cornering. The curvature of the road is shown on Figure 5.5 and the road bumps are shown on the second row of Figure 5.6. The first bump is applied to the right wheels of the vehicle and the second bump is applied to the left wheels of the vehicle. The magnitude of the first bump is larger than that of the second bump but the displacement rate of the first bump is slower than that of the second bump. The fast displacement rate of the road input causes a lot of change in normal tire forces. The vehicle is set up to make cornering with a vehicle speed of 100 kph. It should be noted that when the vehicle strikes a bump, the wheels of the vehicle still do not lift off the road surface. The lateral acceleration in this case is shown on the first row of Figure 5.6.

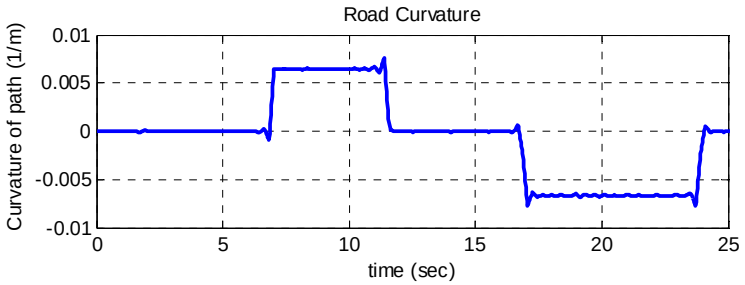

Figure 5.5: Road Curvature

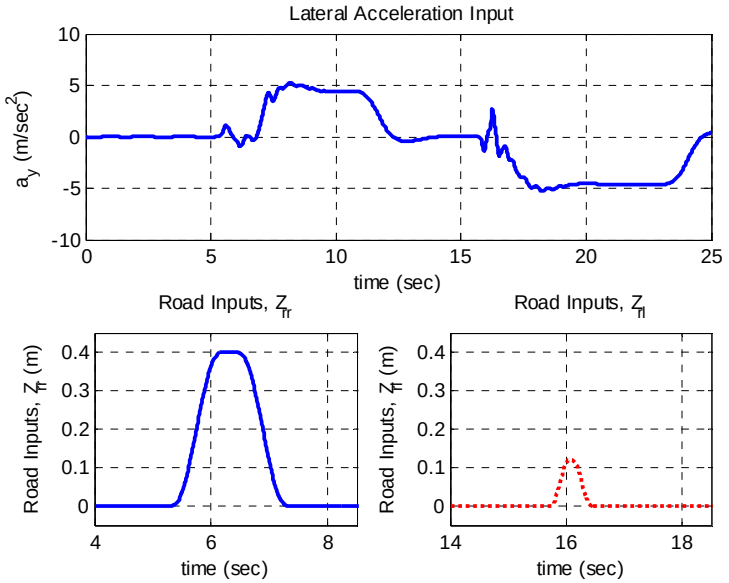

Figure 5.6: Lateral Acceleration and Road Inputs

5.6.2. Simulation Results

For designing an observer for this problem, we assume that

1.$-45 \leq \phi \leq 45\ deg.$,
2. $-1 \leq \dot{\phi} \leq 1$ rad./sec. or $-57.3 \leq \dot{\phi} \leq 57.3$ deg./sec.,
3.$-15 \leq a_y \leq 15$ m/s^2,

4. $\dot{a}_y$ is small.

The feedback measurements that we need to feed to the observer are 1. Right unsprung mass vertical acceleration, $\ddot{z}_{ur}$, 2. Left unsprung mass vertical acceleration, $\ddot{z}_{ul}$, 3. Right suspension compression, $(z_s - z_{ur} + \frac{l_s}{2} sin\phi)$, and 4. roll rate, $\dot{\phi}$.

Then the local bound of the nonlinearity can be found. The observer gain found by using the new observer is $L = \begin{bmatrix} 1.4320 & -109.8388 & 0.8108 & -20.0510 & -0.2167 & 5.2887 \\ 13.5762 & 440.6767 & -13.5380 & -432.6672 & 8.1034 & 113.1697 \end{bmatrix}^T$.

The estimation results are shown on Figure 5.7-Figure 5.10. The results show that the estimated states are very close to the actual values. The estimated states are not exactly equal to the actual values because the vehicle model in CARSIM has many degrees of freedom but our model is only a 3-degrees of freedom model with 6 states. Also, there is a time delay in CARSIM between the front and rear wheels of the vehicle when the vehicle strikes a bump.

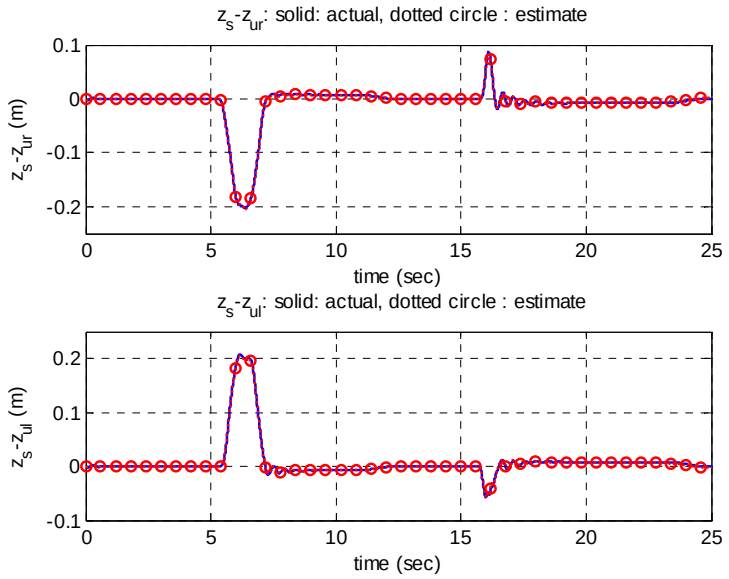

Figure 5.7: Estimation of Right and Left Suspension Compressions

Note: the outputs of the Carsim are right and left suspension compressions, $(z_s - z_{ur} + \frac{l_s}{2} sin\phi)$ and $(z_s - z_{ul} - \frac{l_s}{2} sin\phi)$. However, on Figure 5.7, we compute the actual value of $(z_s - z_{ur})$ and $(z_s - z_{ul})$ from CARSIM and compare the values of them with those from our observer.

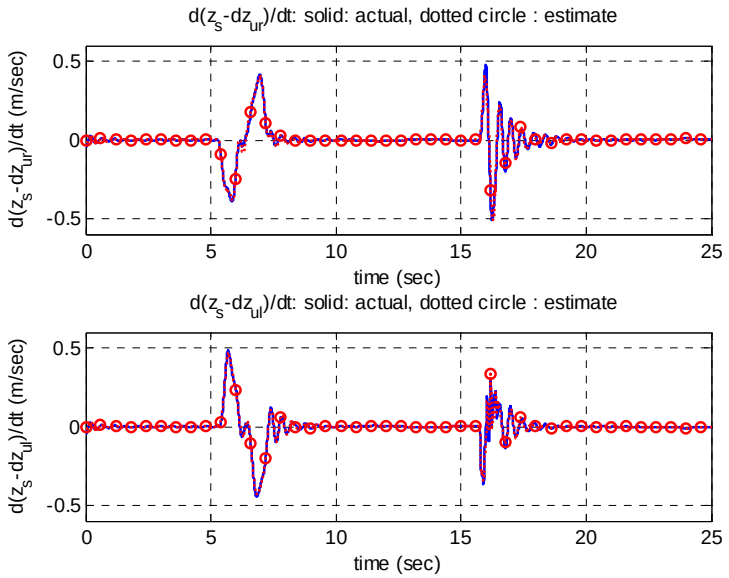

Figure 5.8: Estimation of Right and Left Suspension Compression Rate

Note: the outputs of the Carsim are right and left suspension compression rates, $(\dot{z}_s - \dot{z}_{ur} + \frac{l_s}{2}\dot{\phi}cos\phi)$ and $(\dot{z}_s - \dot{z}_{ul} + \frac{l_s}{2}\dot{\phi}cos\phi)$. However, on Figure 5.8, we compute the actual values of $(\dot{z}_s - \dot{z}_{ur})$ and $(\dot{z}_s - \dot{z}_{ul})$ and compare these values with our observer.

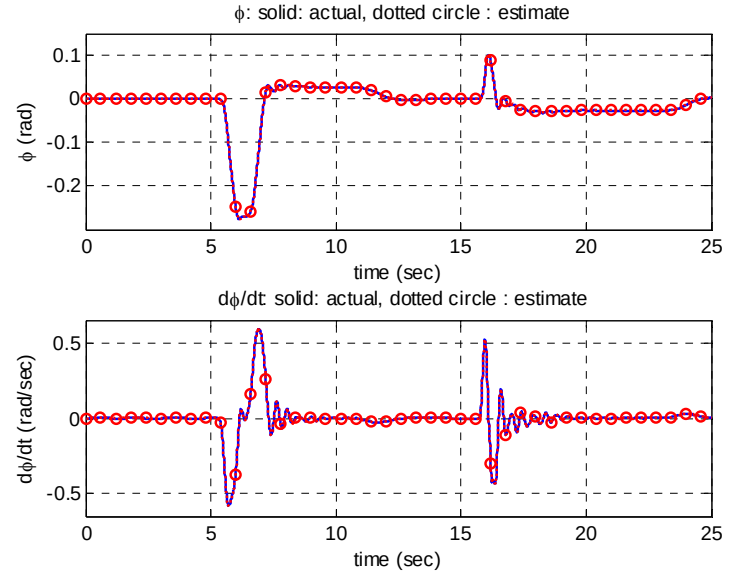

Figure 5.9: Roll Angle and Roll Rate Estimation.

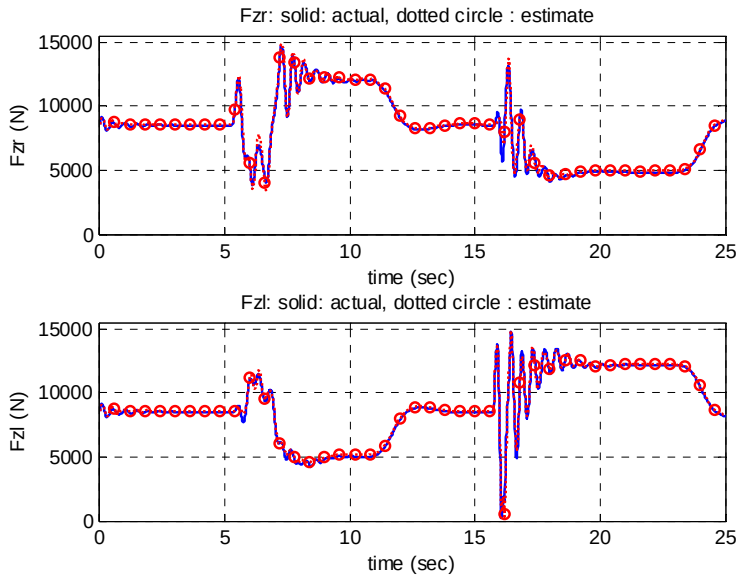

Figure 5.10: Normal Tire Forces Estimation, F_{zr} and F_z

The estimated rollover index is shown on Figure 5.11. The result shows that the estimated and actual rollover indices are extremely close. There are very small errors and these happen because there is a time delay between the front and rear wheels of the vehicle when the vehicle strikes a bump. Since we use only 3-degrees of freedom for observer design, we cannot provide this time delay. However, if we carefully look at the result, we will see that the estimated rollover is good enough to predict un-tripped and tripped rollovers.

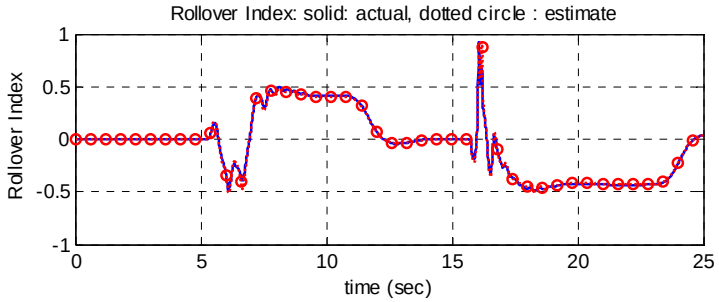

Figure 5.11: Rollover Index Estimation

5.7. The Scaled Vehicle for Experiments

The simulation results in the previous section show that the new rollover index can detect both tripped and un-tripped rollovers. However, we still need to confirm the approach with a test vehicle.

The use of a full-sized vehicle for testing of a control system in this rollover application is challenging due to cost limitations and safety issues. It is estimated that the cost of developing a full-sized instrumented vehicle for testing is more than $100,000 [23]. Most of this cost goes for equipment and instrumentation development. Also, a full-sized vehicle is difficult to operate and involves significant safety issues in this application which involves vehicle rollover.

It is more convenient to use a scaled vehicle to test the roll control system. A scaled radio controlled vehicle is inexpensive and safe for evaluation of rollover maneuvers. Many researchers have studied scaled vehicles for testing of vehicle dynamics and control systems. For instance, references [23], [24], [25], and [26] developed a $1/10^{th}$ scaled vehicle to study lateral vehicle dynamics. Reference [27] developed a $1/8^{th}$ scaled vehicle to study longitudinal vehicle dynamics. References [28], [29], [30], and [31] studied stability control algorithms with a scaled vehicle. Reference [32] studied tire characteristics with scaled tries.

In order to use a scaled vehicle to describe the behavior of a full-sized vehicle, we need to show that they have dynamic similarity. In the next section, we will show that the scaled vehicle we use has dynamic similarity to a full-sized vehicle. Then, we describe the experimental setup to test rollover scenarios and present the experimental results in the following section.

5.7.1. Dynamic Similitude Analysis

Two systems of different size scales are dynamically similar if the solutions to their governing differential equations are identical after accounting for the dimensional scaling of parameters in the equations of motion. There are many approaches to evaluate dynamic similarity. The Buckingham π theorem is a tool that provides us an easy approach to show dynamic similarity. The details of the Buckingham π theorem are discussed in [27], and [33].

This theorem is convenient to apply. It can show dynamic similarity without explicitly knowing the accurate dynamic equations of both systems. We need only know the list of all variables and parameters associated with the system. References [23], [24], [25], and [32] used the Buckingham π theorem to show the lateral dynamic similarity between a full-sized vehicle and a $1/10^{th}$ scaled vehicle. Also, reference [27] showed the longitudinal dynamic similarity between a full-sized vehicle and a $1/13^{th}$ scaled vehicle. Therefore, we use the Buckingham π theorem to show the roll and vertical vehicle dynamics similarity between our scaled vehicle and a full-sized vehicle.

The Buckingham π theorem shows that if the values of the dimensionless π groups of variables and parameters are maintained, then the solution to any differential equation, regardless of its order or nonlinearity, can be made invariant with respect to dimensional scaling [26]. To apply the Buckingham π theorem to the roll and vertical vehicle dynamics, we need the list of all variables and parameters associated with these dynamics. We limit the number of variables and parameters to those used in the 4-degrees of freedom model as described in section 5.4. Therefore, the roll angle will be a function primarily dependent on the scaled parameters,

$$\phi = F\left(m_s, m_u, I_{xx}, k, d, l_s, h_R, k_t, a_y, \ddot{z}_s, \ddot{z}_{ul}, \ddot{z}_{ur}\right). \tag{5.35}$$

The parameters and variables of the vehicle dynamic model in equation (5.35) and their units are given in Table 5.1.

Table 5.1: Summary of Parameters Associated with the Vehicle Dynamics

		Mass	Length	Time
ϕ, roll angle	dimensionless	0	0	0
m_s, sprung mass	kg	1	0	0
m_u, unsprung mass	kg	1	0	0
I_{xx}, moment of inertia	kg.m^2	1	2	0
k, spring stiffness	kg/sec^2	1	0	-2
d, damper	kg/sec	1	0	-1
l_s, distance between left and right suspensions	m	0	1	0
h_R, c.g. height	m	0	1	0
k_t, tire stiffness	kg/sec^2	1	0	-2
a_y, lateral acceleration	m/sec^2	0	1	-2
$\ddot{z}_s$, sprung mass vertical acceleration	m/sec^2	0	1	-2
$\ddot{z}_{ul}$, left unsprung mass vertical acceleration	m/sec^2	0	1	-2
$\ddot{z}_{ur}$, right unsprung mass vertical acceleration	m/sec^2	0	1	-2

There are 13 parameters ($n = 13$) to represent the vehicle dynamics and 3 basic unit dimensions (j=3): mass (M), length (L), and time (T). We choose the sprung mass (m_s), c.g. height (h_R), and lateral acceleration (a_y) to represent repeating fundamental units in three-dimensional space. So, the remaining 10 unused parameters (k=n-j=10) can be formed as dimensionless π groups by appropriate division or multiplication of the repeating variables m_s, h_R, and a_y. The list of all the π groups is given in Table 5.2.

Table 5.2: π Groups

(m_s, h_R, a_y, ϕ)	$[M]^0[L]^0[LT^{-2}]^0[]$	$\pi_1 = \phi$
(m_s, h_R, a_y, m_u)	$[M]^1[L]^0[LT^{-2}]^0[M]^{-1}$	$\pi_2 = \frac{m_s}{m_u}$
(m_s, h_R, a_y, I_{xx})	$[M]^{-1}[L]^{-2}[LT^{-2}]^0[ML^2]^1$	$\pi_3 = \frac{I_{xx}}{m_s h_R^2}$
(m_s, h_R, a_y, k)	$[M]^{-1}[L]^1[LT^{-2}]^{-1}[MT^{-2}]^1$	$\pi_4 = \frac{k h_R}{a_y m_s}$
(m_s, h_R, a_y, d)	$[M]^{-2}[L]^1[LT^{-2}]^{-1}[MT^{-1}]^2$	$\pi_5 = \frac{d^2 h_R}{a_y {m_s}^2}$
(m_s, h_R, a_y, l_s)	$[M]^0[L]^{-1}[LT^{-2}]^0[L]^1$	$\pi_6 = \frac{l_s}{h_R}$
(m_s, h_R, a_y, k_t)	$[M]^{-1}[L]^1[LT^{-2}]^{-1}[MT^{-2}]^1$	$\pi_7 = \frac{k_t h_R}{a_y m_s}$
$(m_s, h_R, a_y, \ddot{z}_s)$	$[M]^0[L]^0[LT^{-2}]^{-1}[LT^{-2}]^1$	$\pi_8 = \frac{\ddot{z}_s}{a_y}$
$(m_s, h_R, a_y, \ddot{z}_{ul})$	$[M]^0[L]^0[LT^{-2}]^{-1}[LT^{-2}]^1$	$\pi_9 = \frac{\ddot{z}_{ul}}{a_y}$
$(m_s, h_R, a_y, \ddot{z}_{ur})$	$[M]^0[L]^0[LT^{-2}]^{-1}[LT^{-2}]^1$	$\pi_{10} = \frac{\ddot{z}_{ur}}{a_y}$

Note: All of the dimensionless parameters, such as angles form their own π group.

To have the roll and vertical vehicle dynamics of the scaled vehicle the same as those of a full-sized vehicle, we need to tune the scaled vehicle until the values of π groups of the scaled vehicle are close to the values of π groups of a full-sized vehicle. The variables and parameters of the full-sized and scaled vehicle are shown in Table 5.3 and the π groups of them are shown in Table 5.4. The photographs of the scaled vehicle are shown in Figure 5.12.

Figure 5.12: Scaled Test Vehicle: 1:8 (30.5 x 58.5 cm)

Table 5.3: Vehicle Variables and Parameters

Variables and Parameter	Scaled Vehicle	Full-Sized vehicle
m_s (kg)	3	1600
m_u (kg)	0.2	135
I_{xx} (kg.m^2)	0.04	600
k (N/m)	900	90000
d (N.sec/m)	15	3000
l_s (m)	0.2	1.11
h_R (m)	0.18	1
k_t(N/m)	4000	400000

Note: The parameters of the full-sized vehicle are obtained from the software CARSIM.

Table 5.4: Comparison of π Groups

π	Scaled Vehicle	Full-Sized vehicle
π_1	ϕ_s	ϕ_f
π_2	15	11.9
π_3	0.41	0.375
π_4	$54/a_{ys}$	$56.25/a_{yf}$
π_5	$4.5/a_{ys}$	$3.5/a_{yf}$
π_6	1.11	1.11
π_7	$240/a_{ys}$	$250/a_{yf}$
π_8	$\ddot{z}_{ss}/a_{ys}$	$\ddot{z}_{sf}/a_{yf}$
π_9	$\ddot{z}_{uls}/a_{ys}$	$\ddot{z}_{ulf}/a_{yf}$
π_{10}	$\ddot{z}_{urs}/a_{ys}$	$\ddot{z}_{urf}/a_{yf}$

Table 5.4 shows that if the lateral accelerations (a_{ys} and a_{yf}) that cause the scaled and full-sized vehicle to roll over have the same magnitude, then the π group values of the scaled vehicle are close to those of the full-sized vehicle. Also, the resulting vertical accelerations will have the same order.

Based on experiments on the scaled vehicle and simulations of the full-sized vehicle, the lateral accelerations that cause them to roll over are both approximately 7 m/s^2. Then, the dimensionless π groups of them are of the same order and it is reasonable to use the scaled vehicle to study the roll and vertical dynamics of the vehicle.

Note: The dimensional analysis will be correct, only if all variables and parameters associated with the system are involved. In this problem, we assume that only the variables and parameters shown in equation (5.35) are associated with the dynamics. Then, the corresponding π groups are shown on Table 5.4. However, un-modeled dynamics between the full-sized and scaled vehicles could be different and might lead to errors. For example, the scaled vehicle could have significant friction forces which are large compared to other forces on the system. On the full-

sized vehicle, on the other hand, the friction could be negligible. For purposes of this project, we ignore the unmodeled dynamics of the scaled and full vehicles.

5.7.2. Experimental Set Up

The developed rollover index will be validated with the scaled vehicle since the roll and vertical dynamics of it are similar to those of a full-size vehicle. A microcontroller (EM430F6137RF900) from Texas Instruments is used for real-time data acquisition and control of the scaled vehicle speed and steering. The microcontroller is installed on the test vehicle. It samples the data from sensors and wirelessly sends them to a receiver connected to a computer at the baud rate of 66 Hz. Four 3-axis accelerometers (MMA7260Q) from Freescale Semiconductor and a dual axis gyroscope (LPY530AL) from STMicroelectronics are used for this test to measure acceleration and angle rate, respectively. Two accelerometers installed on the left and right size of the sprung mass are used to measure the left and right vertical accelerations. Another two accelerometers are placed on the front left and front right wheels, unsprung masses, for measuring longitudinal, lateral, and left and right vertical accelerations. Also, the dual axis gyroscope placed near the c.g. of the vehicle is used to measure yaw rate and roll rate. In order to measure the suspension defection of the scaled vehicle, a linear potentiometer (LCP12Y-25-10K) from ETI systems is installed parallel to the front right suspension of the scaled vehicle. The photographs of the microcontroller and the sensors are shown in Figure 5.13.

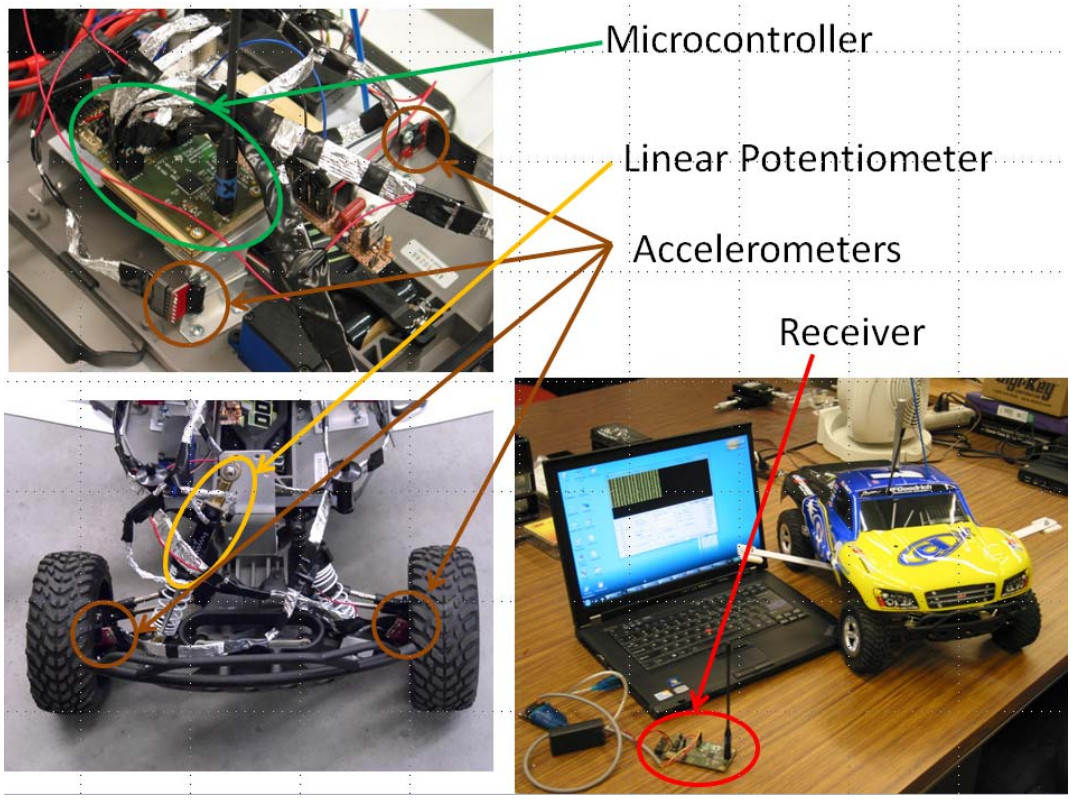

Figure 5.13: Microcontroller and Sensors

To evaluate the rollover index, the scaled vehicle speed and steering inputs are programmed in the microcontroller. So, the identical experiment can be repeated many times. For the first experiment, we set the vehicle to follow the path as shown in Figure 5.14a at a speed of approximately 2.4 meter per second. In this case, the right wheels of the scaled vehicle come close to lifting off from the ground.

For the second experiment, we put an obstacle on the route of the vehicle as shown in Figure 5.14b. The size of the obstacle is 2.54 centimeters in height and 2.54 centimeters in width. Then, we set the vehicle to follow the path at a speed of approximately 2.4 meter per second. In this case, the right wheels of the scaled vehicle fully lift off.

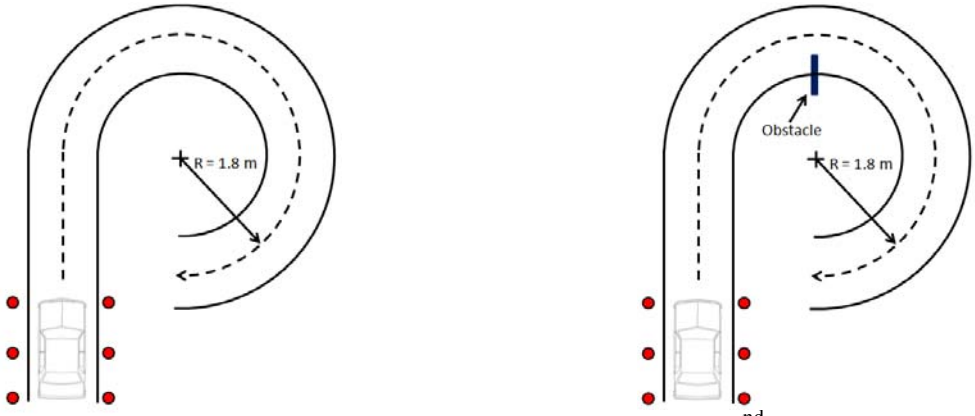

a) 1st experiment b) 2nd experiment

Figure 5.14: The Scaled Vehicle Path

5.7.3. Experimental Results

The measurements of the vehicle longitudinal and lateral accelerations are presented in Figure 5.15. The longitudinal and lateral accelerations in all experiments are similar and of the same order because of the same setting in all experiments. The scaled vehicle starts to accelerate after $t > 7$ sec. Then it starts to corner to the right after $t > 8.5$. The scaled vehicle completes the maneuver after $t > 12.5$ sec.

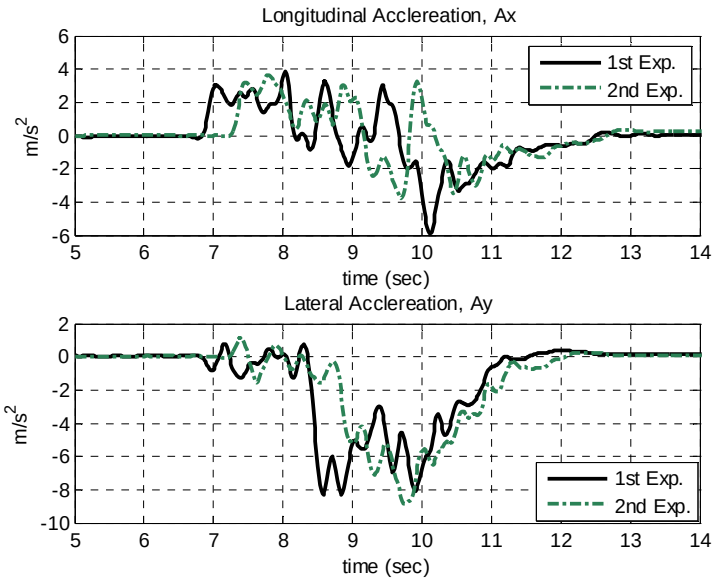

Figure 5.15: Longitudinal and Lateral Acceleration of the Scaled Vehicle

Now, we apply the Corollary to Theorem 3 for the problem. The signals required for the designed observer are 1. lateral acceleration, 2. left and right vertical accelerations of unsprung masses, 3. roll rate, and 4. front right suspension defection. Then, vehicle states and unknown vertical tire forces can be estimated. The results of the experiments are shown in Figure 5.16-Figure 5.19.

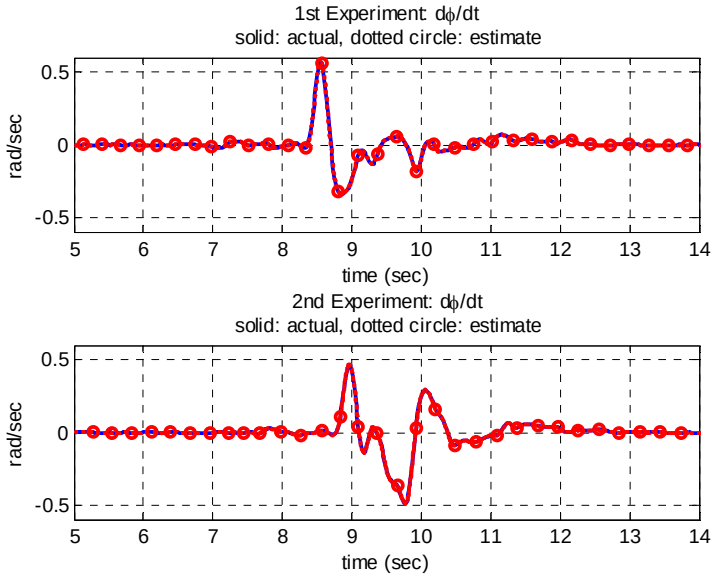

Figure 5.16: Estimation of Roll Rate

Figure 5.16 shows the estimation of roll rate. The figure shows that the estimated roll rates from the first and second experiments match well with the actual roll rates. The magnitude and shape of roll angle and roll rate are reasonable since they look similar to the results that we obtained when we simulate with CARSIM.

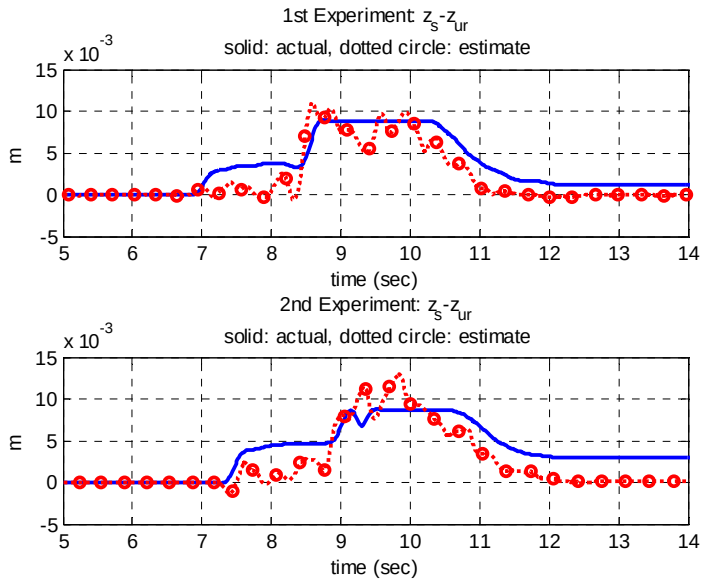

Figure 5.17: Estimation of Right Suspension Defection (z_s-z_{ur}-$l_s sin\phi/2$)

The estimations of front right suspension defection of the first and second experiments are shown in Figure 5.17. The suspension defections from the linear potentiometer needs to be scaled before using it because the suspension of the scaled vehicle are not perpendicular to the sprung mass and unsprung masses. Also, we did not measure the rear right suspension defections. Thus we assume that the rear right suspension defection is proportional to the front right suspension for calculation.

The measurements of front right suspension defection in Figure 5.17 show that the suspensions of the scaled vehicle are nonlinear suspensions. There is a saturation point. Moreover, due to the coulomb friction, there are more than one equilibrium points. When the scaled vehicle rested at the start point ($t < 7sec$), the equilibrium point of the suspension defection was 0 m. During the scaled vehicle acceleration on the straight route ($7 < t < 8.5$), the equilibrium point converged to another value ($\approx 4 \times 10^{-4} m$). During the scaled vehicle making a turn, the suspension defection saturated at about $8.8 \times 10^{-4} m$. After the scaled vehicle completed the maneuver, the equilibrium point moved to another value ($\approx 3 \times 10^{-4} m$). In order to make the computation simple, we ignore the unmodeled dynamics of the friction of the scaled vehicle.

Note: For the second experiment, the second row of Figure 5.17 shows the vehicle strikes the obstacle at $t \approx 9.1$ seconds. This makes the right vertical acceleration larger than the left vertical acceleration. It should be noted that when the right wheels of the scaled vehicle lift off during the time, $t \approx 9.7 - 10$ seconds, the measurements during this period may not be accurate.

Even though the estimations of right suspension defection in Figure 5.17 do not perfectly match to the actual value, the magnitude and shape of them seem reasonable. They try to track the actual value.

Now we need to examine the rollover index. Since, the unknown vertical tire forces can be estimated, the rollover index can be directly calculated from equation (5.1). In order to examine the rollover index from the designed observer, we will compare it with the traditional rollover index as shown in equation (5.2). However, we do not know the actual roll angle of the scaled vehicle since the measurement of roll angle is expensive. So, we assume that the roll angle is small. (Figure 5.18 also confirms that the roll angle is small.) Then, it is appropriate to use rollover index given by equation (5.36) instead of equation (5.2).

$$R_t = \frac{2m_s a_y h_R}{mgl_w} + \frac{2m_s h_R tan\phi}{ml_w} \approx \frac{2m_s a_y h_R}{mgl_w} \tag{5.36}$$

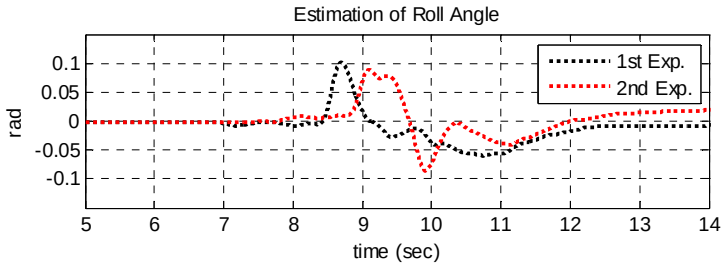

Figure 5.18: Estimation of Roll Angle

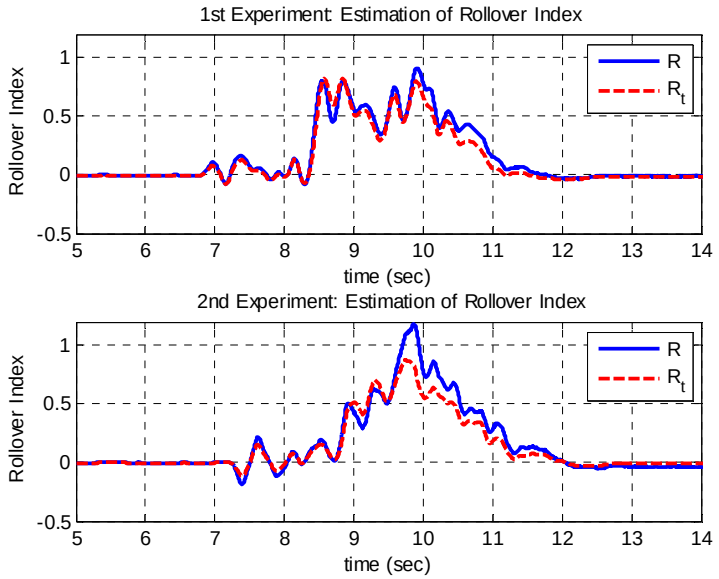

Figure 5.19: Comparison of Rollover Indices of the Scaled Vehicle

The first row of Figure 5.19 shows the rollover indices from the first experiment. In this experiment, the external road input is not applied to the vehicle. So, the difference of vertical accelerations is small between the two cases. Then, the rollover indices from the equations (5.1)

and (5.36) are almost the same. Both rollover indices show that the wheels of the vehicle do not lift off.

Likewise, the second row of Figure 5.19 shows the rollover indices from the second experiment. The scaled vehicle strike the obstacle and its right wheels fully lift off in this case. Thus, there is a difference of vertical accelerations. The traditional rollover index R_t in equation (5.36) shows that the wheels of the vehicle come close to lift off. That fails to detect the wheel lift off condition. However, the rollover index R that is computed by using the developed nonlinear observer shows that the right wheels of the vehicle do lift off. Therefore, the develop rollover index is able to detect both tripped and un-tripped rollovers.

5.8. Alternate Rollover Index with Additional Measurements

If the roll angle, ϕ, and vertical accelerations on the vehicle body (sprung mass) are measured and available, then the rollover R for tripped and un-tripped rollovers can be computed algebraically without needing to use an observer.

5.8.1. New Rollover Index for Tripped and Un-Tripped Rollovers

In this section, a new version of the rollover index computed algebraically from available measurements is presented. The new rollover index can be computed without knowing any of the following variables: the road input disturbances, z_{rr} and z_{rl}, the vertical displacements of unsprung masses, z_{ur} and z_{ul}, the vertical displacement of sprung mass, z_s, and the unknown lateral force input, F_{lat}.

In order to obtain the rollover index for predicting tripped rollovers, we need a model of a vehicle with 4-degrees of freedom which is shown in Figure 5.20. The vehicle body is represented by the sprung mass m_s while the mass due to the axles and tires are represented by unsprung masses m_{ul} and m_{ur}. The springs and dampers between the sprung and unsprung masses represent the vehicle suspension. The vertical tire stiffness of each side of the vehicle are represented by the springs k_{tr} and k_{tl}.

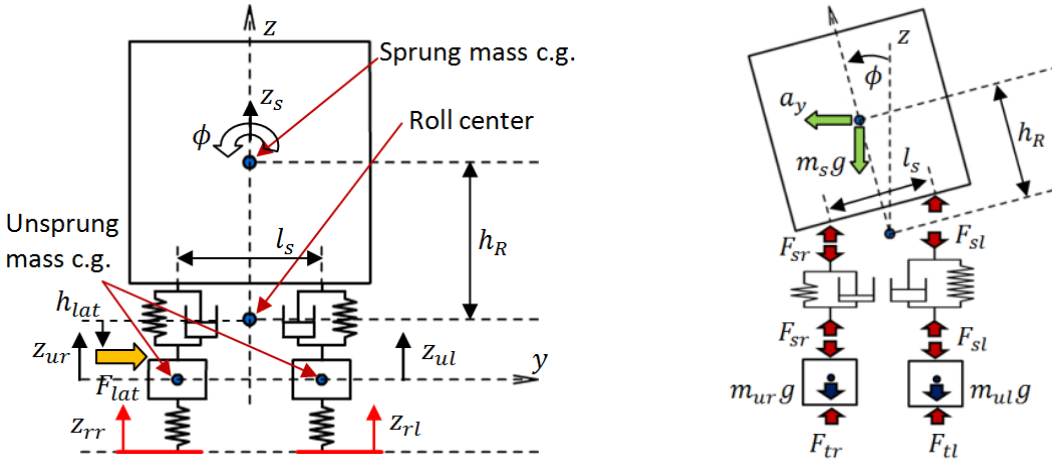

Figure 5.20: Four-Degrees of Freedom Vehicle Model

The 4-degrees of freedom of the model are the heave z_s, roll angle ϕ of the vehicle body, and the vertical motion of each side of the unsprung masses, z_{ur} and z_{ul}. The variables z_{rr} and z_{rl} are the road profile inputs that excite the system.

The external inputs z_{rl}, z_{rr}, and F_{lat} cannot be measured and are unknown. However, outputs that depend on these unknown inputs are available for measurement. For example, vertical and lateral accelerations of the vehicle can be measured using accelerometers placed on the vehicle body. These vertical and lateral accelerations can be related to the unknown inputs and to the states of the system using algebraic equations. This section develops equations for the external disturbance inputs z_{rl}, z_{rr}, and F_{lat} using measured accelerometers signals and measured states of the vehicle model.

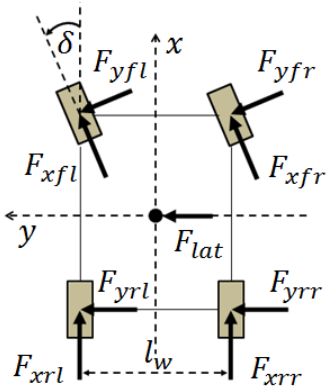

Figure 5.21: Lateral Vehicle Dynamics

Consider the vehicle lateral dynamics as shown in Figure 5.21. The measurement of lateral acceleration a_y involves the influence of the lateral tire forces and the unknown external lateral force F_{lat}. The measured lateral acceleration a_y is given by

$$a_y = \frac{(F_{yr} + F_{xf}\sin(\delta) + F_{yf}\cos(\delta) + F_{lat})}{m} \tag{5.37}$$

where $m = m_s + m_u$, F_{xf} is the longitudinal tire forces of the front wheels, F_{yf} and F_{yr} are the lateral tire forces of the front and rear wheels respectively, δ is steering angle, and F_{lat} is the unknown external lateral force.

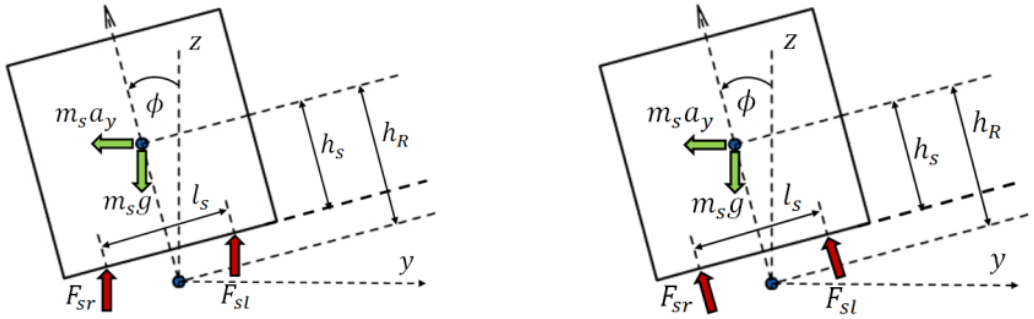

a) Suspension forces are always vertical.

b) Suspension forces are perpendicular to the sprung mass.

Figure 5.22: Suspension Forces Direction

5.8.2. Derivation of Rollover Index

Assume that the suspension forces always act vertically. Then, the sprung mass roll motion is given by equation (5.38).

$$(I_{xx} + m_s h_R^2)\ddot{\phi} = \frac{l_s}{2}(F_{sl} - F_{sr}) + m_s a_y h_R cos\phi + m_s g h_R sin\phi - (F_{sl} + F_{sr})(h_R - \quad (5.38)$$

5.38)

which leads to

$$(I_{xx} + m_s h_R^2)\ddot{\phi} = \frac{l_s}{2}(F_{sl} - F_{sr}) + m_s a_y h_R cos\phi + m_s g h_s sin\phi. \quad (5.39)$$

where I_{xx} is roll moment of inertia.

However, if we assume that the suspension forces always act perpendicular to the sprung mass. The sprung mass roll motion is then given by equation (5.40).

$$(I_{xx} + m_s h_R^2)\ddot{\phi} = \frac{l_s}{2}(F_{sl} - F_{sr}) + m_s a_y h_R cos\phi + m_s g h_R sin\phi \quad (5.40)$$

Thus the major difference between equations (5.39) and (5.40) is the coefficient h_s instead of h_R in the gravity term. Both models are quite similar. Since h_s and h_R will be never be perfectly known, the difference between the 2 models is not great importance. To keep the presentation simple, we will use the sprung mass roll motion as described by equation (5.40).

In this case, the vertical dynamics of sprung mass translation is given by equation (5.41).

$$m_s \ddot{z}_s = F_{sr} + F_{sl} - m_s g, \quad (5.41)$$

The dynamic models of the unsprung mass motions are given by

$$m_{ur}\ddot{z}_{ur} = -F_{sr} + F_{tr} - m_{ur} g, \quad (5.42)$$
$$m_{ul}\ddot{z}_{ul} = -F_{sl} + F_{tl} - m_{ul} g \quad (5.43)$$

where F_{tr} and F_{tl} are left and right vertical tire forces respectively.

From unsprung mass equations, the vertical tire forces are seen to be given by

$$F_{tr} = m_{ur}\ddot{z}_{ur} + F_{sr} + m_{ur}g, \tag{5.44}$$
$$F_{tl} = m_{ul}\ddot{z}_{ul} + F_{sl} + m_{ul}g \tag{5.45}$$

Since the vertical tire forces F_{tr} and F_{tl} equal to the normal forces F_{zr} and F_{zl}, the rollover index can be written as

$$R = \frac{F_{zr} - F_{zl}}{F_{zr} + F_{zl}} = \frac{F_{tr} - F_{tl}}{F_{tr} + F_{tl}} = \frac{m_{ur}\ddot{z}_{ur} + F_{sr} + m_{ur}g - m_{ul}\ddot{z}_{ul} - F_{sl} - m_{ul}g}{m_{ur}\ddot{z}_{ur} + F_{sr} + m_{ur}g + m_{ul}\ddot{z}_{ul} + F_{sl} + m_{ul}g}. \tag{5.46}$$

If $m_{ur} = m_{ul} = m_u$, then the rollover index becomes

$$R = \frac{m_u(\ddot{z}_{ur} - \ddot{z}_{ul}) + F_{sr} - F_{sl}}{m_u(\ddot{z}_{ur} + \ddot{z}_{ul}) + F_{sr} + F_{sl} + 2m_u g} \tag{5.47}$$

where F_{sr} and F_{sl} are computed from equations (5.7) and (5.8). However, F_{sr} and F_{sl} are unknown and cannot measured or easily estimated. We need to eliminate these unknown parameters.

To determine suspension forces F_{sr} and F_{sl}, we consider equations (5.40) and (5.41).

$$\begin{gathered} m_s\ddot{z}_s = F_{sr} + F_{sl} - m_s g \\ (F_{sr} + F_{sl}) = m_s\ddot{z}_s + m_s g \end{gathered} \tag{5.48}$$

$$\begin{gathered} (I_{xx} + m_s h_R^2)\ddot{\phi} = \frac{l_s}{2}(F_{sl} - F_{sr}) + m_s a_y h_R cos\phi + m_s g h_R sin\phi \\ (F_{sl} - F_{sr}) = \frac{2}{l_s}\left[(I_{xx} + m_s h_R^2)\ddot{\phi} - m_s a_y h_R cos\phi - m_s g h_R sin\phi\right] \end{gathered} \tag{5.49}$$

$\ddot{z}_s$ can be measured by using an accelerometer and ϕ can be obtained by a tilt angle sensor. An example of a tilt angle sensor is the Crossbow CXTD02. The Crossbow tilt angle sensor consists of two axis in-built accelerometers and signal processing algorithms that enable static tilt angle to be calculated from the accelerometer measurements. An example of an algorithm that can be used for this purpose can be found in [34]. However, $\ddot{\phi}$ is still unknown and cannot be measured.

To measure $\ddot{\phi}$, we need to place two extra accelerometers at the right and left ends on a vehicle sprung mass. The locations of the extra accelerometers are shown on Figure 5.23.

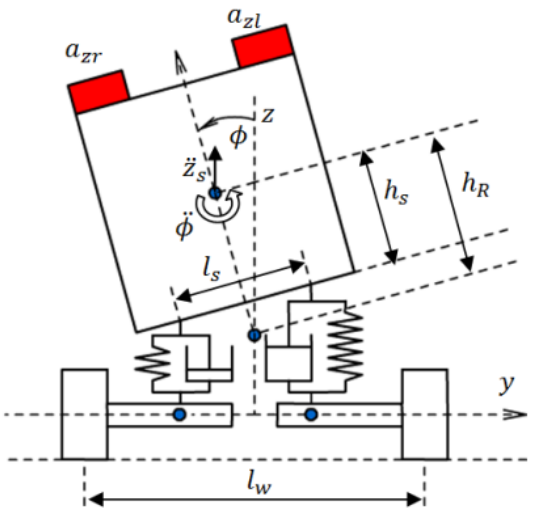

Figure 5.23: Extra Accelerometer Locations

The right accelerometer measurement a_{zr} is given by

$$a_{zr} = \ddot{z}_s cos\phi - \frac{l_s}{2}\ddot{\phi} + (\ddot{y} + v_x r) sin\phi + g cos\phi. \tag{5.50}$$

The left accelerometer measurement a_{zl} is given by

$$a_{zl} = \ddot{z}_s cos\phi + \frac{l_s}{2}\ddot{\phi} + (\ddot{y} + v_x r) sin\phi + g cos\phi. \tag{5.51}$$

It should be noted that the term $(\ddot{y} + v_x r)$ includes the influence of the unknown lateral force F_{lat}.

Subtract equation (5.50) from (5.51).

$$a_{zl} - a_{zr} = l_s \ddot{\phi} \tag{5.52}$$

$$\ddot{\phi} = \frac{a_{zl} - a_{zr}}{l_s} \tag{5.53}$$

With equation (5.53), the equation (5.49) can be rewritten as

$$(F_{sl} - F_{sr}) = \frac{2}{l_s}\left[(I_{xx} + m_s h_R^2)\left(\frac{a_{zr} - a_{zl}}{l_s}\right) - m_s a_y h_R cos\phi - m_s g h_R sin\phi\right]. \tag{5.54}$$

Place equations (5.48) and (5.54) into (5.47).

$$R = \frac{m_u(\ddot{z}_{ur} - \ddot{z}_{ul}) - \frac{2}{l_s^2}(I_{xx} + m_s h_R^2)(a_{zl} - a_{zr})}{m_u(\ddot{z}_{ur} + \ddot{z}_{ul}) + m_s\ddot{z}_s + m_s g + 2m_u g} + \frac{\frac{2}{l_s}m_s a_y h_R cos\phi + \frac{2}{l_s}m_s g h_R sin\phi}{m_u(\ddot{z}_{ur} + \ddot{z}_{ul}) + m_s\ddot{z}_s + m_s g + 2m_u g} \tag{5.55}$$

Then, the rollover index for this case is

$$R = \frac{m_u(\ddot{z}_{ur} - \ddot{z}_{ul}) - \frac{2}{l_s^2}(I_{xx} + m_s h_R^2)(a_{zl} - a_{zr})}{m_u(\ddot{z}_{ur} + \ddot{z}_{ul}) + m_s\ddot{z}_s + mg} + \frac{\frac{2}{l_s}m_s a_y h_R cos\phi + \frac{2}{l_s}m_s g h_R sin\phi}{m_u(\ddot{z}_{ur} + \ddot{z}_{ul}) + m_s\ddot{z}_s + mg} \tag{5.56}$$

$$R = \frac{m_u(\ddot{z}_{ur} - \ddot{z}_{ul}) - \frac{2}{l_s^2}(I_{xx} + m_s h_R^2)(a_{zl} - a_{zr})}{m_u(\ddot{z}_{ur} + \ddot{z}_{ul}) + m_s\ddot{z}_s + mg} + \frac{\frac{2}{l_s}m_s a_y h_R cos\phi + \frac{2}{l_s}m_s g h_R sin\phi}{m_u(\ddot{z}_{ur} + \ddot{z}_{ul}) + m_s\ddot{z}_s + mg} \tag{3.2}$$

where $m = m_s + 2m_u$, $(\ddot{z}_{ur} - \ddot{z}_{ul})$ is difference between unsprung mass accelerations, $(a_{zl} - a_{zr})$ is difference between sprung mass accelerations, a_y is lateral acceleration, ϕ is roll angle. These parameters can be measured and estimated. Since the new rollover index involves the term $(a_{zl} - a_{zr})$ or $\ddot{\phi}$, the new rollover index can handle both unknown external lateral force inputs and unknown road inputs with the same algorithm.

Note: 1. The term involving $sin\phi$ can be ignored at small roll angles. However, it becomes important at large roll angles. In particular, if roll angle is higher for a given lateral acceleration (e.g. for higher c.g. vehicles), then the term $sin\phi$ is important and must be considered in the rollover index calculation. The roll angle may be obtained from a Crossbow tilt angle sensor or a fusion of a tilt sensor and a gyroscope with a simple first order observer [34].

2. Since tripped rollovers happen due to external inputs, rollover can happen, even if the roll angle is small. Thus, only lateral acceleration and roll angle measurements cannot by themselves be used to predict tripped rollovers.

5.8.3. Sensitivity Analysis to Mass Change

The vehicle mass changes due to the increase or decrease of passengers or goods in the vehicle. In this section, we show that the rollover index of equation (5.56) has very little sensitivity to mass change.

In general, the sprung mass is significantly larger than the unsprung mass ($m_s \gg m_u$). For purposes of rough analysis, we can neglect the unsprung mass and also assume that $m_s \approx m$. The equation (5.56) can then be rewritten as

$$R = \frac{-m\frac{2}{l_s^2}\left(\frac{(h_R^2 + l_w^2)}{12} + h_R^2\right)(a_{zl} - a_{zr})}{m(\ddot{z}_s + g)} + \frac{m\left(\frac{2}{l_s}a_y h_R cos\phi + \frac{2}{l_s}g h_R sin\phi\right)}{m(\ddot{z}_s + g)} \tag{5.57}$$

where $I_{xx} = m(h_R^2 + l_w^2)/12$.

Equation (5.57) shows that the rollover index is roughly independent of the vehicle mass, m, since it appears in both the numerator and denominator as a factor. Thus, the developed rollover index has low sensitivity to mass change.

Note: While the rollover index is not sensitive to mass, the equation (5.57) clearly shows that the rollover index is sensitive to the c.g. height, h_R. The c.g. height , h_R, can be estimated by an algorithm, as suggested in [35].

5.8.4. Simulation and Simulation Results

In this section, the rollover indices that are described in the previous section are evaluated in simulations by implementing them in CARSIM, industry standard vehicle dynamics simulation software. The vehicle model from CARSIM chosen for this simulation is a standard SUV. The rollover indices evaluated are

1. The traditional rollover index given by

$$R_1 = \frac{2m_s a_y h_R}{mgl_w} + \frac{2m_s h_R tan\phi}{ml_w}. \tag{5.58}$$

2. The traditional rollover index plus the difference of unsprung mass accelerations given by

$$R_2 = \frac{2m_s a_y h_R}{mgl_w} + \frac{2m_s h_R tan\phi}{ml_w} + \frac{m_u(\ddot{z}_{ur} - \ddot{z}_{ul})}{mg}. \tag{5.59}$$

3. The new rollover index given by

$$R_3 = \frac{m_u(\ddot{z}_{ur} - \ddot{z}_{ul}) - \frac{2}{l_s^2}(I_{xx} + m_s h_R^2)(a_{zl} - a_{zr})}{m_u(\ddot{z}_{ur} + \ddot{z}_{ul}) + m_s\ddot{z}_s + mg} + \frac{\frac{2}{l_s}m_s a_y h_R cos\phi + \frac{2}{l_s}m_s g h_R sin\phi}{m_u(\ddot{z}_{ur} + \ddot{z}_{ul}) + m_s\ddot{z}_s + mg} \tag{5.60}$$

These rollover indices are compared with the actual unimplementable rollover index given by equation (5.1) and denoted by R.

In the first two simulations, we simulate the case that the wheels of the vehicle do not lift off. The first simulation evaluates the case that the input is a step road input. The step road input, $z_{rl} = 0.15\ m$, is applied to the left wheels of the vehicle. The vehicle speed is set at 80 kph. The rollover indices of this simulation are shown in Figure5–24a.

The next simulation evaluates the event that the inputs are a simultaneous step road input and step steering input. The step steering input, $\delta = 1.2\ deg.$, is applied starting at the 1st second. Then, the step road input, $z_{rl} = 0.15\ m$, is applied to the left wheels of the vehicle at the 3rd second. The vehicle speed is set at 80 kph. The rollover indices of this case are shown in Figure5–24b.

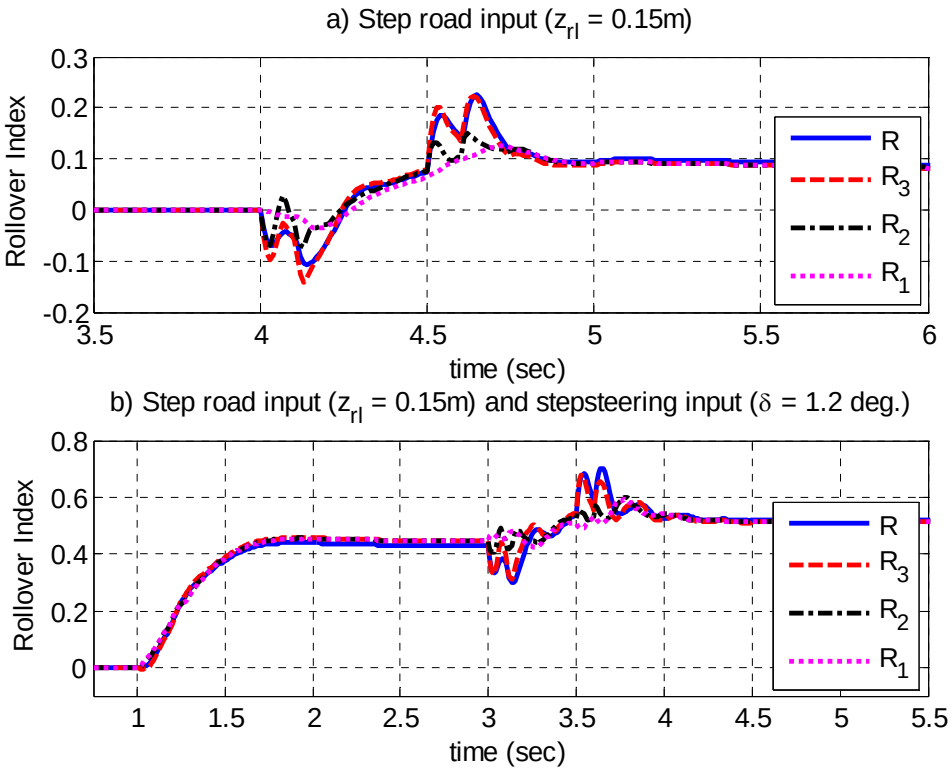

Figure 5.24: Comparison of Rollover Indices

For the last simulation, we simulate the case that the wheels of the vehicle lift off. The vehicle speed is set at 100 kph. The step steering input, $\delta = 1.2\ deg.$, is started to apply at the 1st second. Then the left wheels of the vehicle strike a bump at approximately the 2nd second. This cause the left wheels of the vehicle to lift off for a few seconds. The results of this simulation are shown in Figure5–25.

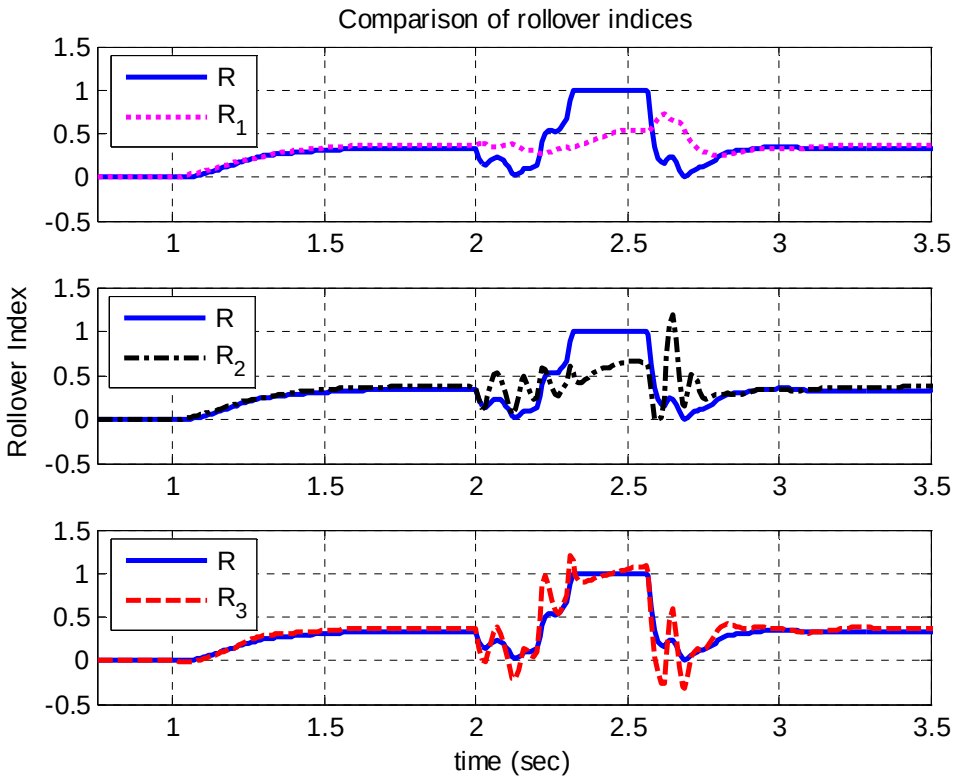

Figure 5.25: Rollover Indices with Step Steering Input (δ=1.2 deg.) and Road Bump (z_{ri}=0.15 m)

Figure5–24b and Figure5–25 show that if a vehicle experiences only lateral acceleration, then the rollover indices R_1, R_2, and R_3 can all be used to detect rollovers. However, if a rollover happens due to tripping from external inputs, all the results show that the rollover indices R_1 and R_2 fail to estimate the actual (unimplementable) rollover index. (Only lateral acceleration and roll angle measurements by themselves cannot predict tripped rollover.) The values of the rollover index R_3 are close to the value of the actual rollover index R in all cases. Therefore, the results show that the developed rollover index is able to predict both tripped and un-tripped rollovers very well.

5.8.5. Experimental Set Up

We use the scaled vehicle as described in section 5.7.

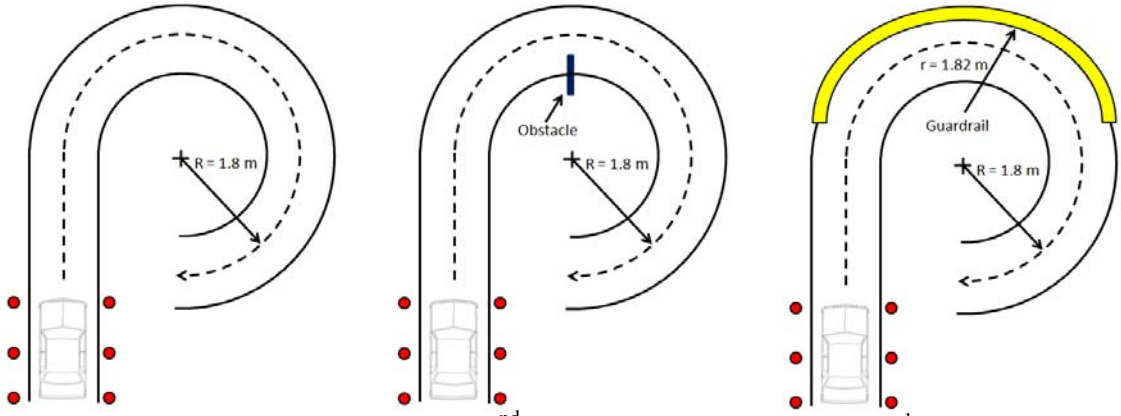

a) 1st experiment b) 2nd experiment c) 3rd experiment

Figure 5.26: The Scaled Vehicle Path

To evaluate the rollover index, the scaled vehicle speed and steering inputs are programmed in the microcontroller. So, the identical experiment can be repeated many times. For the first experiment, we set the vehicle to follow the path as shown in Figure5–26a at a speed of approximately 2.4 meter per second. In this case, the wheels of the scaled vehicle come close to lifting off from the ground.

For the second experiment, we put an obstacle on the route of the vehicle as shown in Figure5–26b. The size of the obstacle is 2.54 centimeters in height and 2.54 centimeters in width. Then, we set the vehicle to follow the path at a speed of approximately 2.4 meter per second. In this case, the right wheels of the scaled vehicle fully lift off.

For the third experiment, we want to evaluate the developed rollover index in the case that the vehicle is confronted with unknown lateral forces. We set a guardrail on the route of the vehicle as shown in Figure5–26c. The size of the guardrail is 3.9 centimeters in height and 1.82 meters in radius. Then, we set the vehicle to follow the path at a speed of approximately 2.4 meter per second. However, it is difficult to experimentally have only unknown lateral forces applied to the vehicle. When the vehicle strikes the guardrail, the front left wheel of the vehicle confronts with both unknown lateral forces and unknown vertical forces. Therefore, in this experiment, when the vehicle strikes the guardrail, the vehicle firstly leans toward the inside of the curve because of the vertical forces. After that, the vehicle leans back toward the outside of the curve and fully rolls over because of the lateral forces and lateral acceleration.

5.8.6. Experimental Results

The signals required for computing the new rollover index are the lateral acceleration, the left and right vertical accelerations of sprung mass and unsprung masses, and roll angle. Since the mass of unsprung masses of the scaled vehicle is very small, it is reasonable to neglect the left and right vertical accelerations of unsprung masses. Also, the road input is a bump. The roll angle can be assumed to be small for the scaled vehicle. (With the linear potentiometer, we can

approximate roll angle of the scaled vehicle. When the scaled vehicle rolls over, the roll angle seems to be less than 0.1 rad.) Then, the simplified rollover indices we examine are shown in equations (5.61) and (5.62).

$$R_4 = \frac{2m_s a_y h_R}{mgl_w} \tag{5.61}$$

$$R_5 = \frac{-\frac{2}{l_s^2}(I_{xx} + m_s h_R^2)(a_{zl} - a_{zr}) + \frac{2}{l_s} m_s a_y h_R}{mg} \tag{5.62}$$

The results of the experiments are shown in Figure5–27- Figure5–30. The longitudinal and lateral accelerations in all experiments are similar and of the same order because of the same setting in all experiments. For the first and second experiments, the left vertical accelerations are close to zero. However, the right vertical acceleration from the second experiment is larger than that from the first experiment.

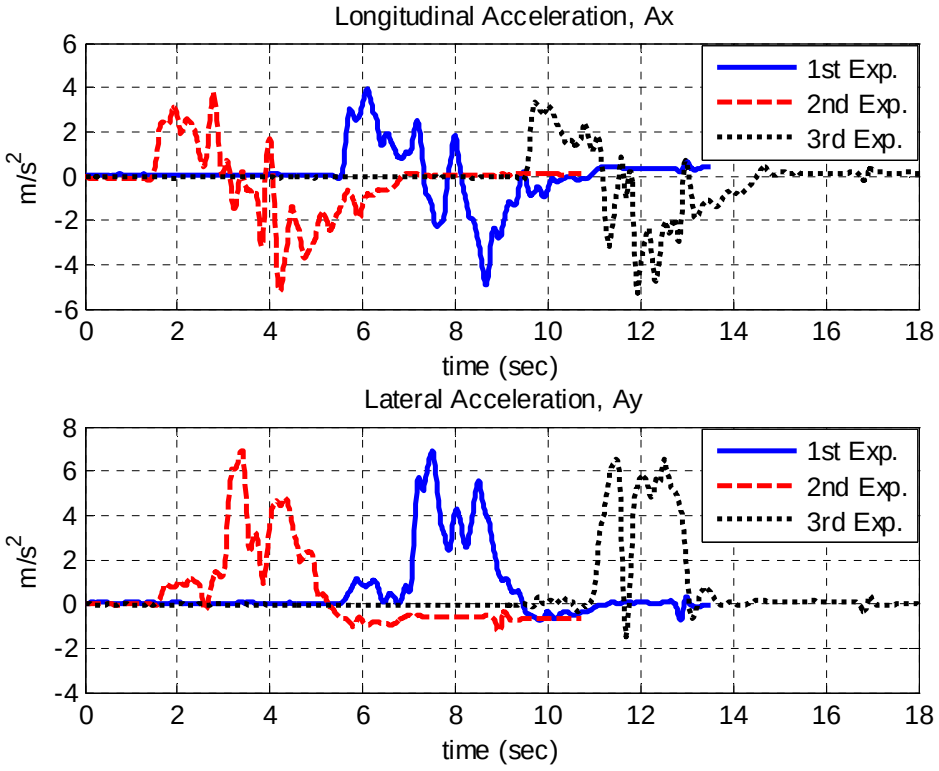

Figure 5.27: Longitudinal and Lateral Acceleration of the Scaled Vehicle

The left and right vertical accelerations of the third experiment are shown in Figure5–28When the vehicle strikes the guardrail during the time, $t \approx 11.4 - 11.7$ seconds, the vertical forces apply to the left side of the vehicle. This makes the left vertical acceleration larger than the right vertical acceleration. During the time, $t \approx 11.7 - 12$ seconds, the left vertical acceleration decreases and the right acceleration increases since the vehicle leans back toward the outside of the curve and fully rolls over after the time, $t > 12$ seconds. It should be noted that roll angle

during the time, $t \approx 12 - 13$ seconds, is very large. So the measurements during this period may not be accurate.

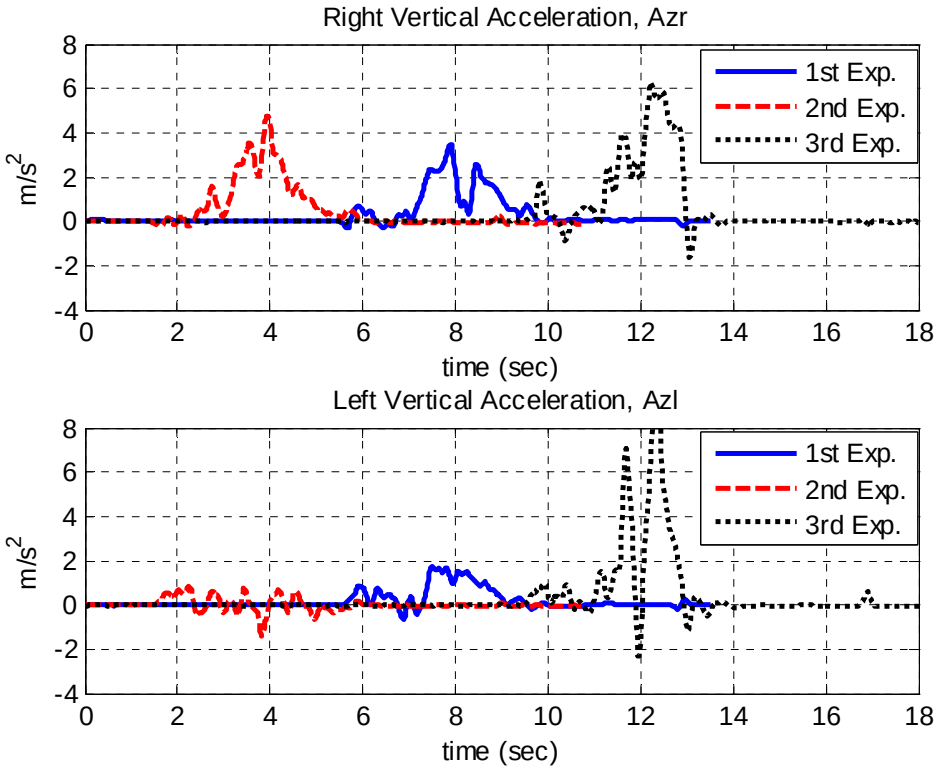

Figure 5.28: Right and Left Vertical Acceleration of the Scaled Vehicle

The first row of Figure5–29 shows the rollover indices from the first experiment. In this experiment, the external input is not applied to the vehicle. So, the difference of vertical accelerations is small. Then, the rollover indices from the equations (5.61) and (5.62) are almost the same. Both rollover indices show that the wheels of the vehicle are close to lift off.

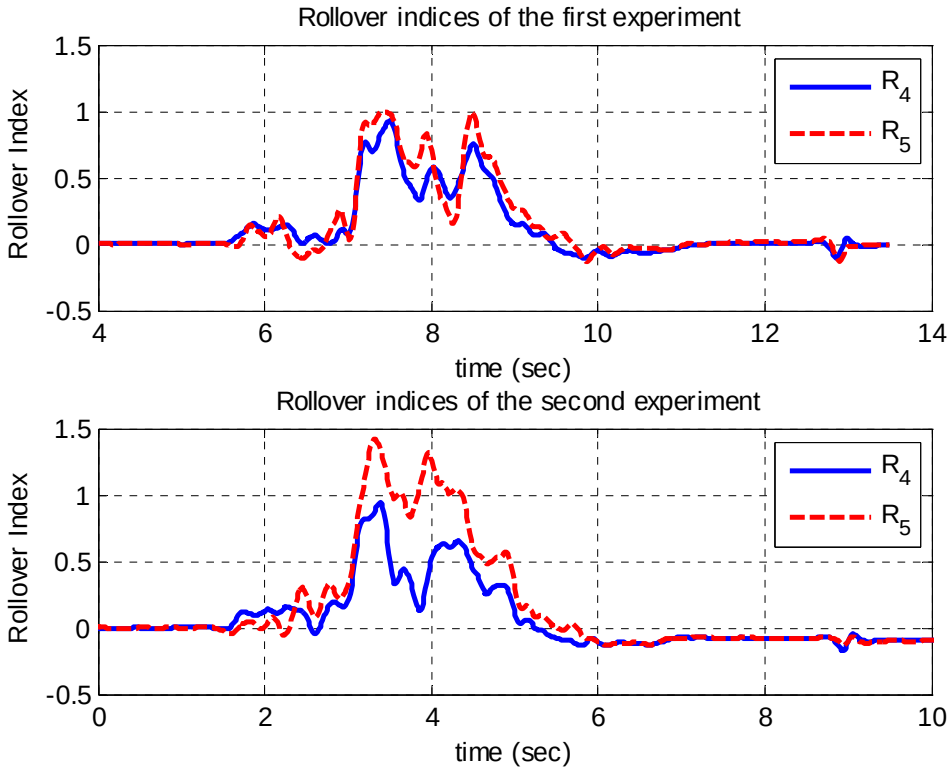

Figure 5.29: Comparison of Rollover Indices of the Scaled Vehicle.

Likewise, the second row of Figure5–29 shows the rollover indices from the second experiment. The scaled vehicle strike the obstacle and its right wheels lift off in this case. Thus, there is a difference of vertical accelerations. The traditional rollover index R_4 in equation (5.61) shows that the wheels of the vehicle come close to lift off. That fails to detect the wheel lift off condition. However, the new rollover index R_5 of equation (5.62) shows that the wheels of the vehicle do lift off. Therefore, the develop rollover index is able to detect both tripped and un-tripped rollovers.

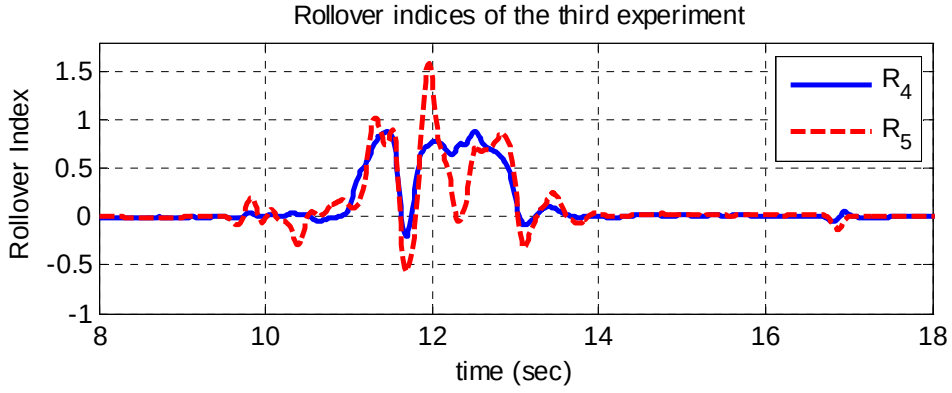

Figure 5.30: Comparison of Rollover Indices of the Third Experiment

Figure5–30 shows the rollover indices from the third experiment. In this case, the vehicle leans toward the inside of the curve. Then the vehicle leans back toward the outside of the curve and fully rolls over. The results show that the traditional rollover index R_4 fails to detect the wheel lift off condition. However, the new rollover index R_5 shows that the wheels of the vehicle do lift off. Therefore, the new rollover index can also handle unknown external lateral force inputs with the same algorithm.

Chapter 6. Feasibility of Rollover Prevention in Tripped Rollovers

A method for predicting an imminent rollover was developed in the previous chapters that worked for both tripped and untripped rollovers. This method was based on algorithms for unknown input estimation in nonlinear systems. The present chapter presents simulation results to show how the developed rollover prediction algorithm can be used to prevent tripped rollovers and thus protect the occupants.

Two types of rollover prevention systems will be evaluated in this chapter:

a) Automatic braking and individual wheel brake force control
b) Semi-active suspension control

These two types of actuation systems were chosen for evaluation, since they are currently available on cars sold in the market. Automatic braking and individual wheel brake torque control is widely available on passenger vehicles in the form of ABS and electronic stability control systems. Electronic stability control is mandated and required to be installed on all new passenger vehicles starting January 2012. Semi-active suspension control, based on the use of magneto-rheological shock absorbers, is available on some Cadillac and Corvette models [36].

While fully active suspensions and active steering would undoubtedly be of great value in rollover prevention, these systems are not yet available on vehicles sold in the market. Since the primary objective of this project is the development of algorithms to predict imminent rollover in the case of tripped rollovers, the feasibility evaluation of rollover prevention is restricted to systems already available in the market. The objective here is to show that rollovers that occur due to tripping can in many cases indeed be prevented if they are reliably predicted.

6.1. Control Systems

6.1.1. Rollover Prevention using Brake Torque Control

The individual wheel brake torque control system uses the estimated rollover index R to determine if intervention is required. When the vehicle is being driven straight and the rollover index threshold is exceeded, the intervention consists of slowing the vehicle down. When the vehicle is turning and the rollover index exceeds a threshold, the intervention consists of both slowing the vehicle and bounding its yaw rate using the electronic stability control system.

Brake torque algorithm during straight driving:

$$P_{bfr} = P_{bfl} = P_{brr} = P_{brl} = 0 \quad if\ |R| \le A_1\ and\ \left|a_y\right| \le B_1 \tag{6.1}$$

where $\boldsymbol{R}$ is rollover index, $\boldsymbol{a_y}$ is lateral acceleration, $\boldsymbol{A_1}$ and $\boldsymbol{B_1}$ are thresholds.

$$P_{bfr} = P_{bfl} = P_{brr} = P_{brl} = C(V_x) \quad if\ |R| > A_1\ and\ \left|a_y\right| \le B_1 \tag{6.2}$$

where C is the applied brake pressure and is chosen as a function of longitudinal velocity V_x.

The lateral acceleration a_y has a threshold B_1 which is used to determine if the vehicle is turning or being driven straight.

Brake torque algorithm during cornering:

The desired yaw rate is first computed using

$$\Psi_{des} = \begin{cases} f(\delta, V_x) & if\ |R| \le A_2\ , \text{and}\ \left|a_y\right| > B_1 \\ sign(\dot{\Psi}) \times D & if |R| > A_2\ , \left|\dot{\Psi}\right| \ge D, \text{and}\ \left|a_y\right| > B_1 \\ f(\delta, V_x) & if |R| > A_2\ , \left|\dot{\Psi}\right| < D, \text{and}\ \left|a_y\right| > B_1 \end{cases} \tag{6.3}$$

where $\dot{\Psi}$ is yaw rate, δ is steering angle, V_x is longitudinal velocity, A_2 is the threshold on the rollover index, and D is the bound on the yaw rate.

$$P_b = K \times \left(\dot{\Psi} - \dot{\Psi}_{des}\right) \tag{6.4}$$

where K is gain, P_b is brake pressure. If $|R| > A_2$ and $\left|a_y\right| > B_1$, then

$$P_{bfr} = P_{brr} = C(V_x) + |P_b|\ \ if\ P_b > 0 \tag{6.5}$$

or

$$P_{bfr} = P_{brr} = C(V_x)\ \ if\ P_b \le 0 \tag{6.6}$$

and

$$P_{bfl} = P_{brl} = C(V_x) + |P_b|\ \ if\ P_b < 0 \tag{6.7}$$

or

$$P_{bfl} = P_{brl} = C(V_x)\ \ if\ P_b \ge 0 \tag{6.8}$$

If $|R| \le A_2$ and $\left|a_y\right| > B_1$, then

$$P_{bfr} = P_{brr} = |P_b|\ \ if\ P_b > 0 \tag{6.9}$$

or

$$P_{bfr} = P_{brr} = 0\ \ if\ P_b \le 0 \tag{6.10}$$

and

$$P_{bfl} = P_{brl} = |P_b| \;\; if \; P_b < 0 \tag{6.11}$$

or

$$P_{bfl} = P_{brl} = 0 \;\; if \; P_b \geq 0 \tag{6.12}$$

The above control algorithm is not a rigorously developed optimal control law. It is used here merely to show that *an* active control system can prevent rollovers even in the case of tripping, provided a reliable algorithm for prediction of imminent rollover is available.

6.1.2. Rollover Prevention using Semi-Active Suspension

In the case of the semi-active suspension system, independent quarter-car suspension control is implemented at each of the four wheels of the vehicle. First, the desired force at each wheel is determined as

$$F_{des} = -k_{sky}\dot{z}_s \tag{6.13}$$

where k_{sky} is the sky-hook damping gain, $\dot{z}_s$ is the sprung mass velocity measured at that quarter car chassis location and F_{des} is the desired suspension force. A full-state feedback LQR based control law can also be used in place of the sky hook damping algorithm of equation (6.13).

Second, the real-time value of the damping coefficient for the shock-absorber is determined using the control algorithm

$$\begin{aligned} b_{semi} &= -\frac{F_{des}}{\dot{z}_s - \dot{z}_u} \;\; if \; F_{des}(\dot{z}_s - \dot{z}_u) < 0 \\ b_{semi} &= b_{max} \qquad if \; -\frac{F_{des}}{(\dot{z}_s - \dot{z}_u)} > b_{max} \end{aligned} \tag{6.14}$$

and

$$b_{semi} = 0 \;\; if \; F_{des}(\dot{z}_s - \dot{z}_u) \geq 0 \tag{6.15}$$

The semi-active suspension control algorithm above is based on reducing vibrations at each quarter car or wheel of the vehicle. It does not explicitly utilize the rollover index developed in this project for prediction of tripped rollovers. Thus the semi-active control system can be considered as an alternative or competitor to the system developed in this project that relies on rollover prediction based on unknown input estimation. The semi-active control algorithm proposed above is the most commonly used version of the control algorithm.

6.2. Simulations of Tripped Events during Straight Driving

In this section, the control algorithm described in the previous section and the rollover index developed in previous chapters will be evaluated in simulation. The industry standard vehicle

dynamics simulation software CARSIM will be used for this purpose. The vehicle model from CARSIM chosen for this simulation is a standard SUV. It should be noted that while CARSIM is a sophisticated complex model with many degrees of freedom, the estimation algorithm developed in the previous chapters is based on just three degrees of freedom. However, the estimation algorithm still works well in terms of its ability to predict wheel lift-off and vehicle rollover.

In the case of straight driving, we simulate the case that the SUV vehicle strikes a road bump on one side of the road. The road bump is shown on Figure 6–1 and schematically in Figure 6–2. The bump is applied to the right wheels of the vehicle. The magnitude of the bump is about 0.1 meters. The vehicle is set up to have vehicle speed of 95 kph (approximately 60 mph).

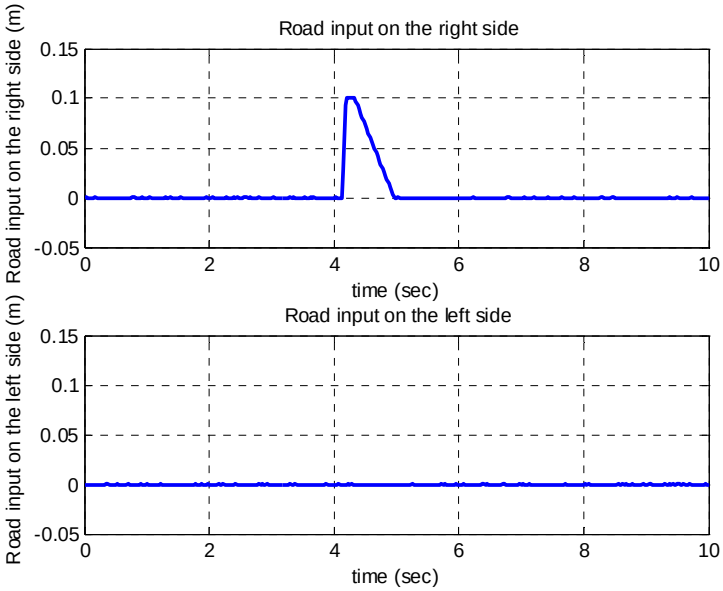

Figure 6.1: Road Inputs on the Right and Left Sides

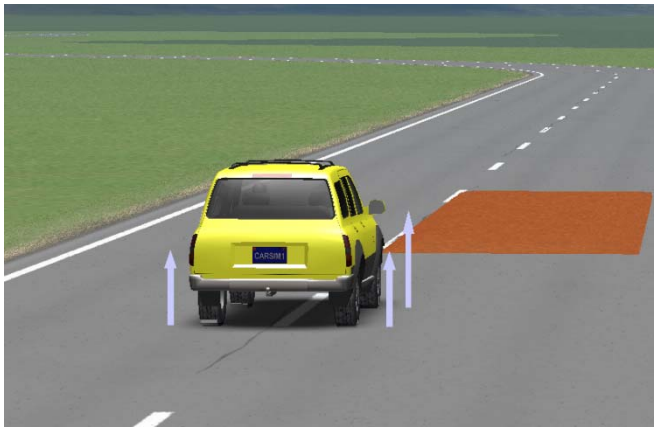

Figure 6.2: Vehicle Strikes a Bump during Driving Straight

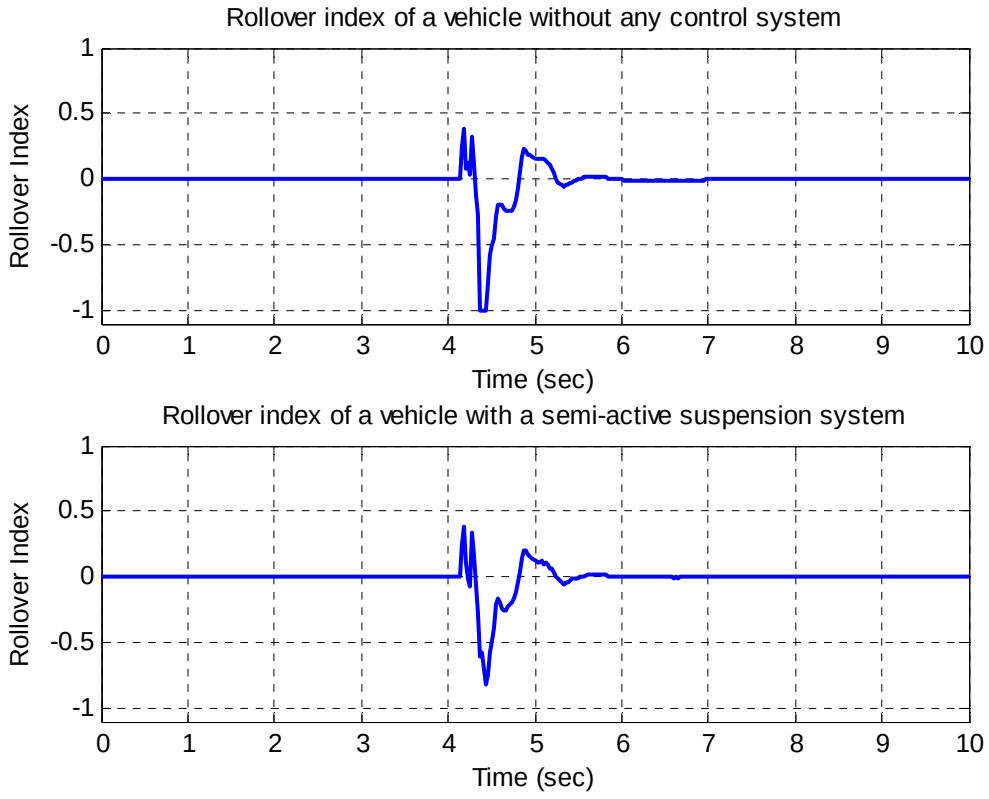

Figure 6.3: Rollover Indices without any Control System and with a Semi-Active Suspension

Figure 6–3 shows the value of the rollover index for this simulation scenario. The rollover index is computed using

$$R = \frac{F_{zr} - F_{z\ell}}{F_{zr} + F_{z\ell}} \tag{6.16}$$

where F_{zr} and $F_{z\ell}$ are the right and left tire forces which are available from the simulation program for plotting. It should be noted that when right tire force becomes zero and there is wheel lift-off, then $R = -1$.

As seen in the first row of Figure 6–3, without any control systems, when the vehicle strikes the bump, the right wheels of the vehicle lift off the road surface. The rollover index reaches a value of -1 and stays at this value for a few hundred milli-seconds. While the vehicle does not rollover, a larger bump or striking the same bump during a lane change or cornering maneuver, could indeed cause the vehicle to rollover.

The second row of Figure 6–3 shows the rollover index of a vehicle with the semi-active suspension system. The absolute value of rollover index in this case is less than 1. This means that the wheels of the vehicle do not lift off the road surface. The semi-active suspension system has the potential to prevent tripped rollovers, even though it does not explicitly use the rollover index estimation in its control algorithm.

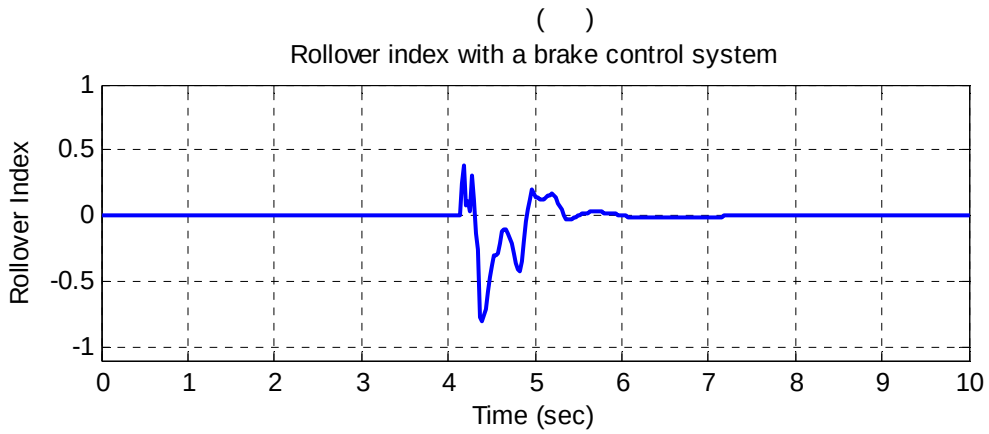

Figure 6.4: Rollover Index of a Vehicle with an Automatic Brake Torque Control System

Figure 6–4 shows the rollover index in the case where the active brake torque control system from section 6.1 is utilized. It can be seen that the absolute value of rollover index in this case is clearly less than 1. This means that the wheels of the vehicle do not lift off the road surface. The reason that brake action is effective is due to the fact that the road bump acts as a lower frequency excitation when the vehicle slows down, thereby considerably reducing the resulting sprung mass oscillation of the vehicle.

In summary, tripped rollovers can happen in the absence of rollover prevention systems when a vehicle strikes a bump during straight driving. The simulation results in this section showed that a semi-active suspension system and a vehicle with a brake torque control system can both be used to prevent tripped rollovers or reduce the propensity to rollover in this scenario.

6.3. Simulations of Tripped Events during Cornering

The same standard SUV car model in CARSIM will be used again for the simulations in this section. In this simulation scenario, the SUV vehicle will negotiate a curved road and strike road bumps during cornering. The curvature of the road is shown in Figure 6–5 and the road bump is shown in Figure 6–6. The road curves to the left, causing the vehicle to have a roll angle towards the right during cornering. The bump is applied to the left wheels of the vehicle. The bump would thus add to the roll angle due to cornering, increasing the propensity to rollover. The magnitude of the bump is about 0.07 meters. The vehicle is set up to have a longitudinal speed of 95 kph (approximately 60 mph). Figure 6–7 shows a schematic of the simulation scenario.

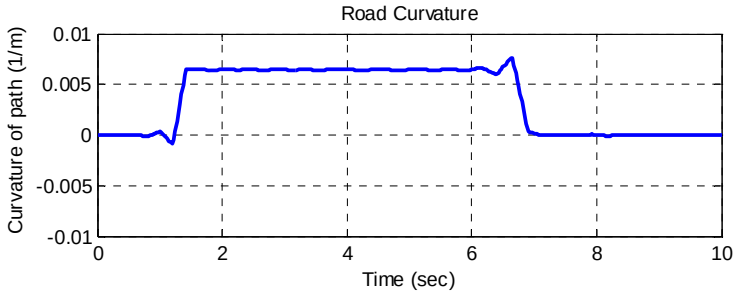

Figure 6.5: Road Curvature

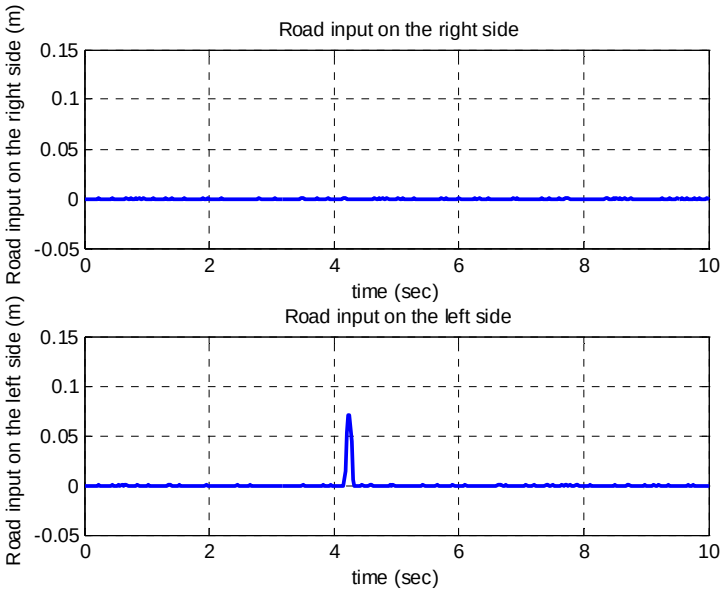

Figure 6.6: Road Inputs on the Right and Left Sides

Figure 6.7: Vehicle Strikes a Bump during Cornering

Without any control systems, when the passive vehicle travels over the bump on the road, the left wheels of the vehicle lift off the road surface. Figure 6–8 shows the rollover index of the vehicle, computed using the tire forces, as in equation (6.16). In this case when the left tire forces become zero, the rollover index R becomes equal to 1. It can be seen that the rollover index becomes equal to 1 and stays at that value for a few hundred milli-seconds. If the bump were larger or if the curvature were greater, or if the vehicle speed were higher, the vehicle could indeed rollover.

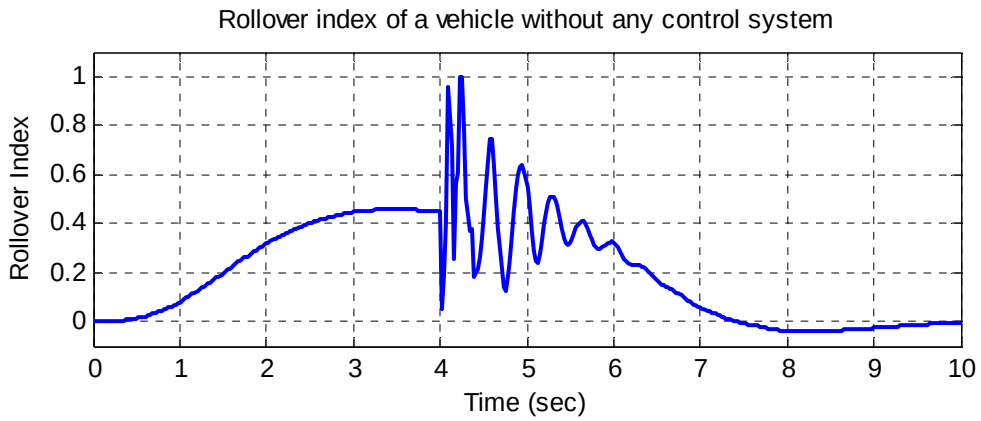

Figure 6.8: Rollover Index of a Vehicle without any Control System

Figure 6–9 shows the rollover index of the same vehicle when a semi-active suspension system is utilized. It can be seen that the rollover index is not much changed at all. The left wheels of the vehicle do lift off, in spite of the semi-active suspension system. Thus, the semi-active suspension system cannot prevent a rollover during the cornering and bump situation simulated in this scenario.

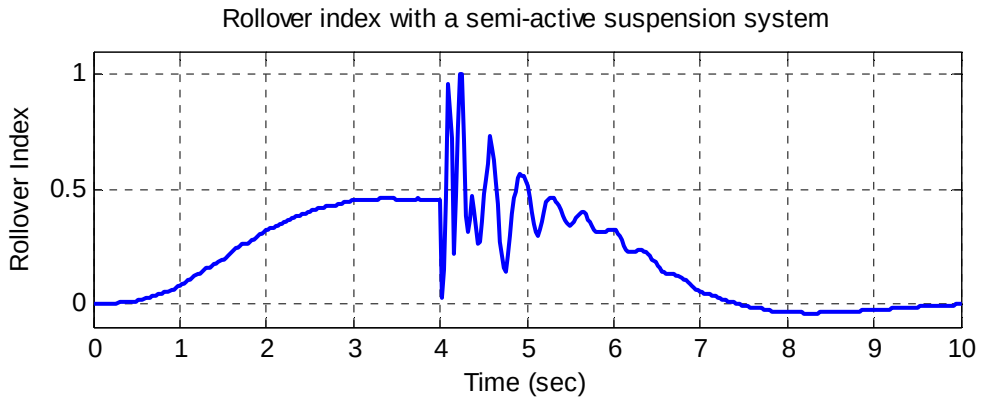

Figure 6.9: Rollover Index with a Semi-Active Suspension System

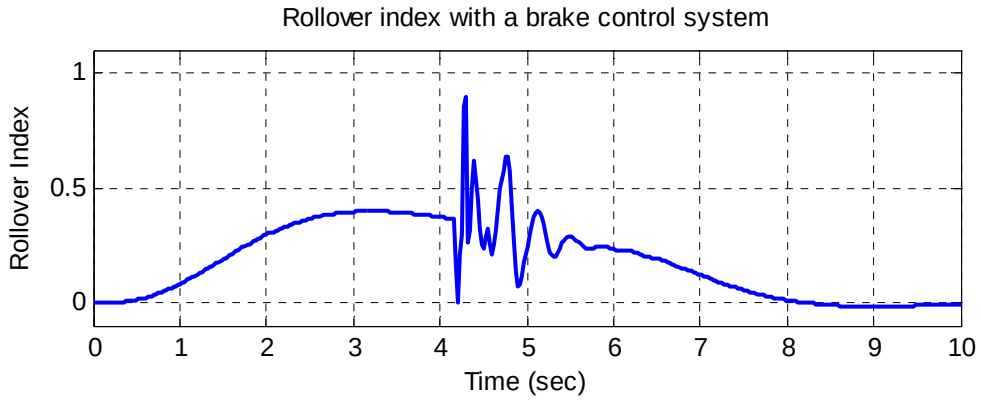

Figure 6.10: Rollover Index with a Brake Control System

Figure 6–10 shows the rollover index of the brake torque control system for the same simulation scenario. In this case, the rollover index is clearly reduced significantly and is below 1. Thus the left wheels do not lift off in this case.

The reason why the brake torque control system is more effective than the semi-active suspension system can be understood from the inability of the semi-active system to compensate for cornering maneuvers. The semi-active system does apply a suspension force designed to reduce sprung mass oscillations in response to the bump in the road. However, the brake torque control system is able to both reduce speed to counter the effects of the bump and also reduce yaw rate to counter the effects of cornering. Thus the brake torque control system is more effective at preventing wheel lift-off.

6.4. Conclusions

Rollover prevention during cornering in the absence of tripping has been previously investigated by several researchers and it has been established that reducing yaw rate and speed can reduce rollover propensity. However, in the case of tripping caused by external inputs, the rollover index currently used in literature cannot predict a rollover. It has also not been established in literature whether control systems using existing actuators can be effective at preventing rollovers when there is external tripping.

This chapter evaluated the feasibility of preventing rollover in the case of roll induced by tripping. Two types of actuation systems, namely active brake torque control and semi-active suspensions, were evaluated for this purpose. Both these actuation systems are currently available on vehicles sold in the market.

Simulations using CARSIM showed that the active brake torque system could be effective at preventing tripped rollovers during both straight driving and cornering. While the semi-active system could reduce rollover propensity due to external road bumps, it was not as effective as the brake torque control system in handling external road bumps during cornering.

Chapter 7. Conclusions

The increasing worldwide use of automobiles has brought about a dramatic increase in numbers of traffic accidents. In particular, vehicle rollovers are responsible for almost one-third of traffic fatalities in the U.S. While automotive companies have recently developed rollover prevention systems, these systems can only deal with untripped rollovers. A majority of actual vehicle rollovers are tripped rollovers and are not addressed by current systems.

In predicting rollover, a real-time variable called the rollover index is computed and describes how close the wheels of the vehicle are to lift-off. In the case of untripped rollovers, the rollover index can be reliably estimated using a lateral accelerometer and a roll angle sensor. However, in order to estimate the rollover index for tripped rollovers, one must estimate states in the presence of unknown road and external force inputs that act on the vehicle system. Due to the significant nonlinear roll dynamics in a vehicle, the design of the estimation algorithm for this application is challenging.

This project developed a new class of nonlinear observers to deal with nonlinear systems. The developed nonlinear observer design techniques utilize a bounded Jacobian approach in which the nonlinearity is assumed to have a globally (or locally) bounded Jacobian. The technique is based on a modified version of the mean value theorem and utilizes it to express the nonlinearity in the estimation error dynamics as a convex combination of known matrices with time varying coefficients. The observer gains are then obtained by solving linear matrix inequalities. The developed approach can enable observer design for a large class of differentiable nonlinear systems, including systems with a nonlinear function in the measurement equation.

The nonlinear observer technique was extended to address state estimation for an unknown inputs nonlinear system. The approach utilized here was to express the unknown inputs as a function of the measurements and states and to use the mean value theorem to express the nonlinear error dynamics as a convex combination of known matrices with time varying coefficients.

In order to predict and prevent vehicle rollovers in tripped and untripped situations, an algorithm to estimate rollover index was developed based on the developed theory for unknown input estimation in bounded Jacobian nonlinear systems. The algorithm was used to estimate vertical tire forces and predict tripped rollovers in situations involving road bumps, potholes, and unknown lateral force inputs. This estimation algorithm also provided estimation of the rollover index, roll angle, and state variables of the vehicle.

The developed estimation algorithm was then evaluated through simulations with industry standard software, CARSIM, and with experimental tests on a $1/8^{th}$ scaled vehicle. The simulation and experimental results showed that the developed algorithm can reliably predict imminent rollover for both tripped and untripped scenarios.

Finally, the value of the developed algorithm in actually preventing tripped rollovers was evaluated by simulations with CARSIM. The two commonly available actuation systems of semi-active suspensions and active brake torque control were used to prevent rollover based on

the new real-time rollover index. Simulations showed that the new rollover index can indeed play a vital role and that it is feasible to prevent rollovers even in tripped scenarios, if imminent rollover can be reliably predicted.

References

[1] National Highway Traffic Safety Administration (NHTSA), "Types of Rollovers," National Highway Traffic Safety Administration, Available: http://www.safercar.gov, accessed on 06/01/2011.

[2] A. Hac, T. Brown, and J. Martens, "Detection of Vehicle Rollover," *SAE International*, no. 0-7680-1319-4, 2004.

[3] Desmond N. Penny, "Rollover of Sport Utility Vehicles," *The Physics Teacher*, vol. 42, pp. 86, February 2004.

[4] B.C. Chen and H. Peng, "Rollover Warning for Articulated Heavy Vehicles Based on a Time-to-Rollover Metric," *Proceedings of the 1999 ASME International Congress and Exposition*, Knoxville, TN, November, 1999.

[5] J. Yoon, D. Kim, and K. Yi, "Design of a Rollover Index-Based Vehicle Stability Control Scheme," *Vehicle System Dynamics*, vol. 45, no. 5, pp. 459-479, May 2007.

[6] K. Yi, J. Yoon, and D. Kim, "Model-based Estimation of Vehicle Roll State for Detection of Impending Vehicle Rollover," *Proceedings of the 2007 American Control Conference*, New York, NY, July, 2007.

[7] Yang Hanlong and Liu Louis Yizhang, "A Robust Active Suspension Controller with Rollover Prevention," *Society of Automotive Engineers*, vol. 112, no. 6, pp. 992-997, 2003.

[8] D. Odenthal, T. Bunte, and J. Ackermann, "Nonlinear Steering and Braking Control for Vehcile Rollover Avoidance," *DLR Report*, German Aerospace Center, Institute of Robotics ans System Dynamics, Oberpfaenhofen, D-82230 Wessling, Germany.

[9] S. Solmaz, M.J. Corless, and R. Shorten, "A Methodology for the Design of Robust Rollover Prevention Controllers for Automotive Vehicles: Part 1 - Differential Braking," in *45th IEEE Conference on Decision and Control*, San Diego, CA, 2006, pp. 1739-1744.

[10] P.K. Sahoo and T. Riedel, *Mean Value Theorems and Functional Equations*, 1st ed.: World Scientific Publishing Company, Hackensack, NJ, 1999.

[11] K. Eriksson, D. Estep, and C. Johnson, *Applied Mathematics: Body and Soul*, 1st ed.: Springer Berlin Heidelberg, 2010.

[12] A. Zemouche, M. Boutayeb, and G.I. Bara, "Observer Design for Nonlinear Systems: An Approach Based on the Differential Mean Value Theorem," *Proceedings of the 44th IEEE Conference on Decision and Control, and the European Control Conference 2005*, Seville, Spain, 2005, pp. 12-15.

[13] G. Phanomchoeng and R. Rajamani, "The Bounded Jacobian Approach to Nonlinear Observer Design," *Proceedings of the 2010 American Control Conference*, Baltimore, MD, 2010.

[14] K. Vijayaraghaven, R. Rajamani, and and J. Bokor, "Quantitative Fault Estimation for a Class of Non-linear Systems," *International Journal of Control*, vol. 80, no. 1, pp. 64-67, January 2007.

[15] J. Lu, D. Messih, and A. Salib, "Roll Rate Based Stability Control-The Roll Stability Control System," in *Proceedings of the 20th Enhanced Safety of Vehicles Conference*, Lyon, France, 2007.

[16] C. Geng, L. Mostefai, M. Denaï, and Y. Hori, "Direct Yaw-Moment Control of an In-Wheel-Motored Electric Vehicle Based on Body Slip Angle Fuzzy Observer," *IEEE Transactions on Industrial Electronics*, vol. 56, no. 5, pp. 1411-1419, May 2009.

[17] C.R. Carlson and and J.C. Gerdes, "Optimal Rollover Prevention with Steer by Wire and Differential Braking," *ASME International Mechanical Engineering Congress and Exposition*, pp. 345-355, Washington DC, November 2003.

[18] S. Takano and M. Nagai, "Dynamic Control of Large Vehicles for Rollover Prevention," *IEEE IVEC*, pp. 85-89, 2001.

[19] M. Akar and J.C. Kalkkuhl, "Design and Evaluation of an Integrated Chassis Controller for Automated Vehicle Emulation," *IEEE Transactions on industrial Electronics*, vol. 56, no. 9, pp. 3571-3579, September 2009.

[20] Marie C. Walz, "Trends in the Static Stability Factor of Passenger Cars, Light Trucks, and Vans," National Highway Traffic Safety Administration, Washington, DC 20590, *NHTSA Technical Report DOT HS 809 868*, June 2005.

[21] P.J. Liu, S. Rakheja, and A.K.W. Ahmed, "Detection of Dynamic Roll Instability of Heavy Vehicles for Open-Loop Rollover Control," *Society of Automotive Engineers, Inc*, pp. 105-112, November 1997.

[22] R. Rajamani, *Vehicle Dynamics and Control*. New York: Springer Verlag, 2nd edition, 2012.

[23] S.N. Brennan, "Modeling and Control Issues Associated with Scaled Vehicles," University of Illinois at Urbana-Champaign, Thesis 1999.

[24] S. Brennan and A. Alleyne, "A Scaled Testbed for Vehicle Control: The IRS," *Proceedings of the 1999 IEEE*, Kohala Coast-lsland of Hawaii, HI, 1999, pp. 327 - 332.

[25] R.T. O'Brien, J.A. Piepmeier, P.C. Hoblet, S.R. Burns, and C.E. George, "Scale-Model Vehicle Analysis Using an Off-the-Shelf Scale-Model Testing Apparatus," in *Proceeding of the 2004 American Control Conference*, Boston, MA, 2004, pp. 3387 - 3392.

[26] S. Brennan and A. Alleyne, "Using a Scale Testbed: Controller Design and Evaluation," *IEEE Control Systems Magazine*, vol. 21, no. 3, pp. 15-26, June 2001.

[27] R. Verma, D. D. Vecchio, and H.K. Fathy, "Development of a Scaled Vehicle With Longitudinal Dynamics of an HMMWV for an ITS Testbed," *IEEE/ASME Transactions on Mechatronics*, vol. 13, no. 1, February 2008.

[28] S.J. Hallowell and L.R. Ray, "All-Wheel Driving Using Independent Torque Control of Each Wheel," in *Proceedings of the American Control Conference*, vol. 3, Denver, CO, 2003, pp. 2590-2595.

[29] W.E. Travis, R.J. Whitehead, D.M. Bevly, and G.T. Flowers, "Using Scaled Vehicles to Investigate the Influence of Various Properties on Rollover Propensity," in *Proceeding of the 2004 American Control Conference*, Boston, MA, 2004.

[30] A. Al-Sharif, "Design and Development of a Scaled Test Laboratory for the Study of ABS and other Active Vehicle Systems," The University of Texas at Austin, Thesis 2001.

[31] R. Whitehead, B. Clark, M. Breland, K. Lambert, D.M. Bevly, and G. Flowers, "Scaled Vehicle Electronic Stability," ESV International Collegiate Student Safety Technology Design Competition, North American Regional Review 2005.

[32] M. Polley and A.G. Alleyne, "Dimensionless Analysis of Tire Characteristics for Vehicle Dynamics Studies," in *Proceeding of the 2004 American Control Conference*, Boston, MA, 2004, pp. 3411 - 3416.

[33] F.M.White, *Fluid Mechanics*, 5th ed.: McGraw Hill International, Columbus, OH, 2003.

[34] D. Piyabongkarn, R. Rajamani, J. Grogg, and J. Lew, "Development and Experimental Evaluation of a Slip Angle Estimator for Vehicle Stability Control," *IEEE Transactions on Control Systems Technology*, vol. 17, no. 1, pp. 78-88, January 2009.

[35] R. Rajamani, D. Piyabongkarn, V. Tsourapas, and and J.Y. Lew, "Real-Time Estimation of Roll Angle and CG Hight for Active Rollover Preventioin Applications," in *American Control Conference*, St. Louis, MO, 2009.

[36] Emanuele Guglielmino, Tudor Sireteanu, Charles W. Stammers, Gheorghe Ghita, and Marius Giuclea, *Semi-active Suspension Control: Improved Vehicle Ride and Road Friendliness*, 1st, Ed.: Springer, New York, NY, 2008.